Search for quarks using a flash tube chamber

Saleh, A. J.

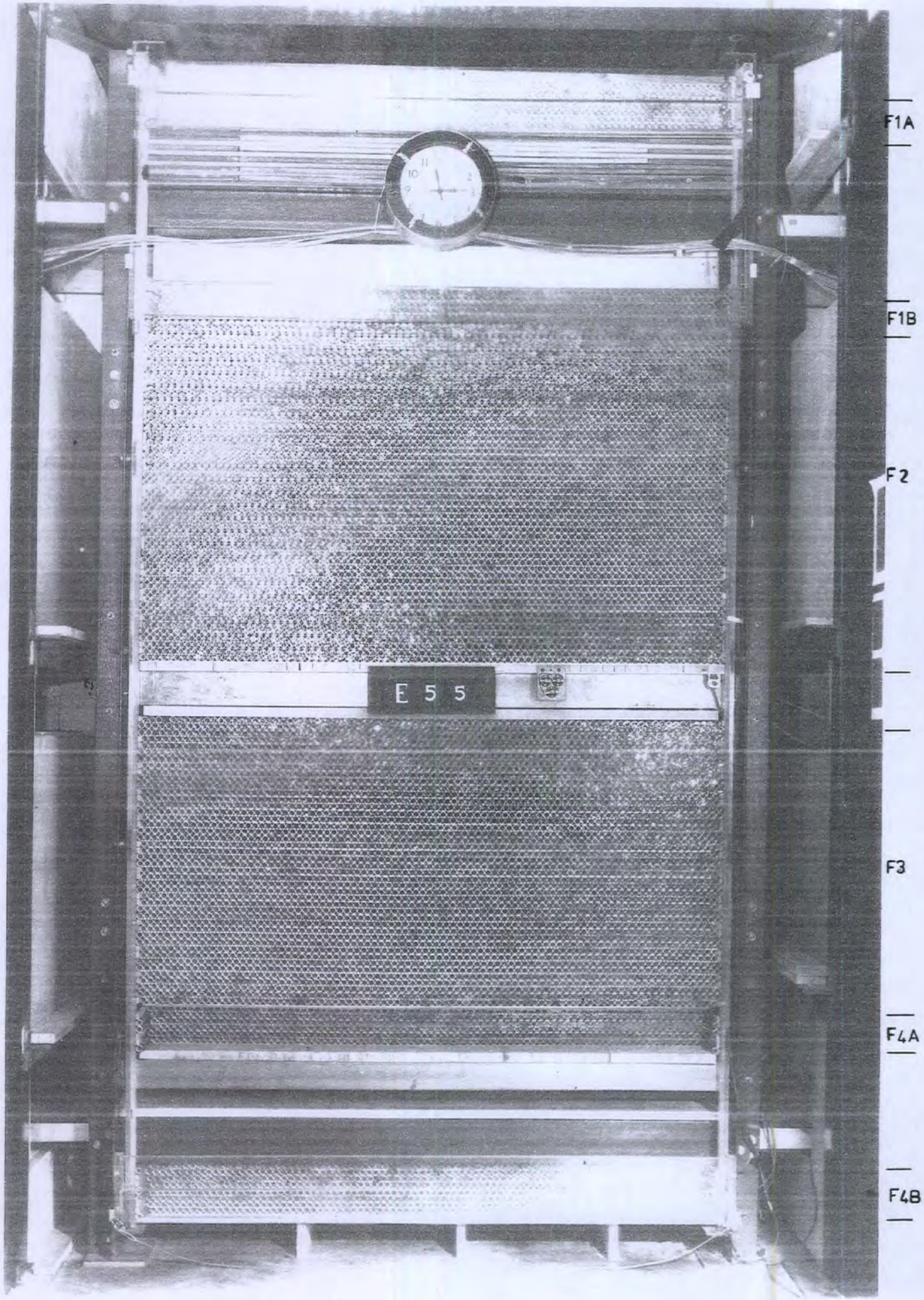

The flash tube chamber

SEARCH FOR QUARKS

USING A FLASH TUBE CHAMBER

by

A.J. Saleh, B.Sc.

A thesis submitted to the

University of Durham

for the

Degree of Master of Science.

August 1973.

CONTENTS

		Page
ABSTRACT		i
PREFACE		ii
CHAPTER 1	INTRODUCTION	
1.1.	The elementary particles and the quark model	1
1.2	Search for quarks in cosmic rays	4
1.3	The search for e/3 quarks close to extensive air shower cores.	6
CHAPTER 2	THE NEON FLASH TUBE CHAMBER	
2.1	The quark telescope	7
2.1.1	Design of the telescope	7
2.1.2	The neon flash tubes	7
2.1.3	The plastic scintillators	8
2.1.4	The liquid scintillators	9
2.2	Efficiency of the neon flash tube	9
2.2.1	Single particle trigger	9
2.2.2	The measurement of the efficiency-time delay curve.	10
2.2.3	The theory of the efficiency of neon flash tubes	10
2.3	The single particle calibration run	11
2.4	The air shower run	12
2.4.1	The air shower trigger	12
2.4.2	The position of the core and size of the shower	12
2.4.3	Variation of shower rate with barometric pressure	13
CHAPTER 3	EXTENSIVE AIR SHOWER EXPERIMENT TO SEARCH FOR QUARKS	
3.1	Introduction	14

		Page
3.2	Quark results	14
	3.2.1 Analysis of data	14
	3.2.2 Basic experimental data	15
3.3	Examination of quark candidates	16
	3.3.1 Background effect	16
	3.3.2 The angular separation of tracks	17
	3.3.3 Knock-on electron test	17
3.4	Discussion	18
3.5	The elastic collision of extensive air shower particles	20
	3.5.1 Introduction	20
	3.5.2 The basic results	20
	3.5.3 Conclusion	22
3.6	Mass determination of stopping cosmic ray particles in EAS	23
	3.6.1 Introduction	23
	3.6.2 Experimental technique	23
	3.6.3 The results	24
	3.6.4 Discussion	26
3.7	The neutral particles in EAS	27
3.8	The low energy particles in EAS	28
3.9	The recovery time of the neon flash tube	29
3.10	The angular distribution of accepted particles	31
CHAPTER 4	THE CHARACTERISTIC INTERACTIONS OF INCOHERENT PARTICLES IN COSMIC RAYS OBSERVED IN THE FLASH TUBE CHAMBER	
4.1	Introduction	32
4.2	Classification of the observed events	32
4.3	Knock-on electrons	34
4.4	The multiply scattered particles	37

page

4.5 The mass estimation of stopping incoherent particles 38

4.5.1 Introduction 38

4.5.2 The Mass distribution 38

4.5.3 Discussion 39

CHAPTER 5 CONCLUSION 40

ACKNOWLEDGEMENTS 42

REFERENCES 43

APPENDIX The Mass Ratio of Two Body Elastic Collisions in the Non-relativistic Approximation. 45

ABSTRACT

A large flash tube chamber has been used at Durham to search for e/3 charged particles (quarks) in extensive air showers where the local electron density is greater than $40m^{-2}$. The response of the detector to relativistic muons was measured and the equivalent characteristics for relativistic e/3 quarks calculated. The response for the more energetic muons in air showers was also measured. In a running time of 2,570 hours no definite quark tracks have been detected and the limit on the charge e/3 quark flux was set as:

$$I < 8.0 \ 10^{-11} \ cm^{-2} \ sec^{-1} \ st^{-1}.$$

No non relativistic heavy mass particles, irrespective of their charge, were detected in the chamber from measurements on two body elastic collisions of EAS particles with essentially free protons.

PREFACE

This thesis describes the work performed by the author in the physics department of the University of Durham while he was a research student under the supervision of Dr. F. Ashton. An experiment was performed to detect the e/3 charge particle (quark) in extensive air showers at sea level. Day-to-day running of the apparatus, analysis and the interpretation of the data have been the responsibility of the author, with the assistance of Mr. D.A. Cooper and Mr. A. Parvaresh. The preliminary result of a search for e/3 quarks has been published in J. Phys. A, (Ashton et al. 1973).

CHAPTER ONE

INTRODUCTION

1.1 The elementary particles and the quark model

Before 1930 all physical phenomena, ignoring the structure of atomic nuclei, were explained in terms of three elementary particles, the proton, electron and photon, interacting through two basic types of force, electromagnetic and gravitational. In 1932 the neutron was discovered and in order to account for the mass to charge ratio of the nuclei it was assumed they were composed of approximately equal numbers of protons and neutrons. The above picture was not complete because no explanation was given of how the protons and neutrons bind together inside atomic nuclei. To explain the stability of nuclei Yukawa in 1935, postulated the existence of a new nuclear force acting between nucleons in the nucleus which must be of a short range, and be some hundred times greater in strength than the Coulomb force to overcome the large Coulomb repulsion between protons. From the range of this force ($\sim 10^{-13}$ cm) he deduced that it was due to the virtual exchange of a particle between the nucleons which had a mass ~ 200 times that of the electron. This particle was subsequently discovered, the π-meson, by Lattes et al. 1947, in nuclear emulsion exposed to cosmic rays at mountain altitude.

Cosmic rays and later high energy accelerators soon showed a large number of particles to exist. The understanding and classification of these particles has become one of the major problems of nuclear physics.

Considerable advances in classification have been made by studying the conservation laws which govern particle interactions.

It has been found that the strong interaction particles (hadrons) are distinguished by two groups. Those with spin 0,1,2....etc in units of $\hbar$ and those with half-odd-integral spin $\frac{1}{2},\frac{3}{2}$,.... etc, the former are called mesons and the latter baryons.

In the strong interactions of the baryon group, for example, three conservation laws are obeyed:

The first: the conservation of electric charge 'Q', which is thought to be absolute.

The second: the conservation of baryonic charge 'B', to account for the abundance and stability of the proton.

The third: the conservation of hypercharge 'Y', to account for the associated production of the K-meson with Λ or Σhyprons in strong interactions.

The most successful model to explain these observed requlrities is based on the theories of unitary symmetry (su(3) etc) and the possible existence of three fundamental particles (p,n,λ)as proposed by Gell-Mann (1964) and by Zweig (1964).

These particles are called "quarks" (q) and this name was given by Gell-Mann and is now in general use. In this model three quarks make baryons (qqq) and a quark and antiquark make mesons ($q\bar{q}$), each will have baryon number (charge) B = $\frac{1}{3}$ and spin $\frac{1}{2}$.

The hypercharge has been defined by Y = S+B, Y = $\frac{1}{3}$ for p and n particles, and $-\frac{2}{3}$ for λ particle.

From the Gell-Mann, Nishijima relation:

$$Q = T_3 + \frac{B + S}{2} = T_3 + \frac{Y}{2}$$

the charge carried by these hypothetical particles (quarks) is deduced, the quantum numbers of quarks being given in table 1.1. The corresponding antiquarks have quantum numbers of opposite sign.

Table 1.1 Quantum numbers of quarks

Triplet particle	T_3	B	S	Y=B+S	$Q=T_3+Y/2$	Spin	Mass
p	$\frac{1}{2}$	$\frac{1}{3}$	0	$\frac{1}{3}$	$+\frac{2}{3}e$	$\frac{1}{2}\hbar$	M
n	$-\frac{1}{2}$	$\frac{1}{3}$	0	$\frac{1}{3}$	$-\frac{1}{3}e$	$\frac{1}{2}\hbar$	M
λ	0	$\frac{1}{3}$	-1	$-\frac{2}{3}$	$-\frac{1}{3}e$	$\frac{1}{2}\hbar$	M+146MeV/c^2 where M several GeV/c^2
$\bar{p}$	$-\frac{1}{2}$	$-\frac{1}{3}$	0	$-\frac{1}{3}$	$-\frac{2}{3}e$	$\frac{1}{2}\hbar$	M
$\bar{n}$	$\frac{1}{2}$	$-\frac{1}{3}$	0	$-\frac{1}{3}$	$+\frac{1}{3}e$	$\frac{1}{2}\hbar$	M
$\bar{\lambda}$	0	$-\frac{1}{3}$	+1	$\frac{2}{3}$	$+\frac{1}{3}e$	$\frac{1}{2}\hbar$	M+146 MeV/c^2

where: T_3 is the third component of isospin

B is the baryon number

S is the strangeness

Y is the hypercharge

Q is the electric charge.

The values of the charge of p,n,λ are $+\frac{2e}{3}$, $-\frac{e}{3}$, $-\frac{e}{3}$. Of these, the $+\frac{2e}{3}$ is expected to be stable while the -e/3 components are expected to have lifetimes of the order of minutes and about 10^{-10}sec. respectively against decay into the stable quark. According to Adair et al. (1964) the expected decay schemes are:

n-particle $q(-e/3) \rightarrow q(+2e/3) + e^- + \bar{\nu}_e \sim$ minutes.

λ-particle $q(-e/3) \rightarrow q(+2e/3) + \pi^- \sim 10^{-10}$sec.

It should be noted that although the simplest interpretation of the SU3 symmetry is that the fundamental triplet particles should carry

fractional charge it is possible that the basic triplet particles could have integral charge. In this case the predicted properties of the triplet particle is not unique and there are several possible representations, Lee (1965). Bacry et al. (1964) proposed the existence of two sets of triplet particles, t - trions and θ - trions, where all members have baryon number 1 and integral charge. The two triplets are distinquished by a new additive quantum number D and a generalisation of the Gell-Mann, Nishijima formula is required,

$$Q = T_3 + \tfrac{1}{2}Y + \tfrac{1}{3}D$$

Then t-trions and θ -trions are all possible triplets with charge $0, \pm 1$ such that $D > 0$.

However, the question remains whether the quark actually exists or whether it is just a useful mathematical model. The full details of the model are still not completely understood, Kokkedee (1969).

1.2 Search for quarks in Cosmic Rays

Since the theory of the quark was first produced a large number of experiments have been performed to search for quarks in cosmic rays and the progress made has been reviewed by Jones (1970, 1971) and Sitte (1970). All experiments which have attempted to detect the quark have so far been unsuccessful, and the flux limit obtained on the unaccompanied ($\lesssim 1 m^{-2}$) quark flux arriving at sea level by a number of workers is $< 10^{-10} cm^{-2} sec^{-1} st^{-1}$.

Experiments to search for quarks in air showers are less numerous and so far have produced conflicting results.

Some experiments have reported positive results from quark searches and these deserve careful attention. The Sydney group (Cairns et al. 1969; McCusker et al. 1969) have reported evidence for quarks with charge $2e/3$ being present close to the cores of extensive air showers initiated by primary cosmic rays of energy $> 4.10^{15}$ eV. The detectors

used by this group were four delayed-expansion cloud chambers each of 30 cm diameter and illuminated depth 5cm. Three of the chambers were shielded by 15cm lead while the fourth was unshielded. Air showers were selected by the coincidence of three small geiger counters. Four lightly ionising tracks were reported by Cairns et al (1969) after one years running time and a fifth lightly ionising track by McCusker et al (1969). The five quark candidates were obtained from the observation of $\sim$20,000 showers which were selected by a local electron density requirement of $>154 m^{-2}$. The flux of 2e/3 quarks obtained in this work was $\sim 5\ 10^{-10} cm^{-2} sec^{-1} st^{-1}$ at sea level.

The claim of the Sydney group that the events observed were genuine quarks was criticised by a number of authors (Wilson, 1970; Kiraly and Wolfendale, 1970; Adair and Kasha, 1969, Rahm and Sternheimer, 1969: Rahm and Louttit, 1970; Frauenfelder et al, 1970). The main point of criticism was that the Sydney group had not adequately demonstrated that the five events were well separated in ionisation density from the distribution due to plateau or minimum ionising charge e particles.

Chu et al (1970) claimed that from the observation of cosmic ray tracks occurring randomly in a bubble chamber, one track had a low ionisation as expected for a charge 2e/3 particle if the particle mass was <6.5 GeV/c^2 or a charge e/3 particle of mass (8.0 ± 3.0) GeV/c^2. However, this result has been criticised by Allison et al (1970).

Other searches in air shower cores depend on the fact that the large mass of the quark will cause it to be delayed by some nanoseconds with respect to the bulk of the shower particles. Experiments have been performed to search for delayed particles in air showers and

interesting results have been reported by Dardo et al (1972) working at 70mwe underground and Tonwar et al (1971) working at 2,150m above sea level.

Both groups find evidence which may be interpreted as indicating that a massive particle (10-20 GeV/c^2) has been detected and they claim definite signals at flux levels of 10^{-8} and 10^{-9} $cm^{-2}sec^{-1}st^{-1}$ respectively. If this interesting result is substantiated by further work that the signals observed are indeed due to heavy mass delayed particles it would seem certain they will be found to have integral charge and therefore they may possibly correspond to integral charge fundamental triplet particles.

1.3 The search for e/3 quarks close to the extensive air shower cores

An experiment has been constructed with the object of searching for relativistic e/3 quarks in extensive air showers (EAS). The principle of this experiment is essentially to select an air shower with core close to a flash tube chamber and to look forthe track efficiency which corresponds to the e/3 charged particle. This experiment has the advantage over other visual detectors, for example cloud chamber, of having a considerably larger sensitive volume.

The design of the experiment and the properties of neon flash tubes which have been used are given in chapter 2 and the quark search itself is discussed in chapter 3.

CHAPTER TWO

THE NEON FLASH TUBE CHAMBER

2.1 The Quark telescope

2.1.1 Design of the telescope

A large array of neon flash tubes has been constructed and used to search for quarks in extensive air showers.

Any search for quarks produced in extensive air showers (EAS) is influenced by the properties peculiar to quarks, namely the very high rest mass expected, and the fractional charge, predicted by theory.

To look for quarks in (EAS) one must be able to distinquish the quark of charge e/3 from charge e particles and select air showers with cores near the chamber and to absorb out the electronic component of EAS but allow muons, quarks etc. to penetrate and be observed. The chamber uses 10,478 flash tubes distributed in 124 layers, and shielded above with 15cm of lead absorber. Three liquid scintillators i.e. North (N), Middle (M), South (S), were used to select air showers and were placed above the lead as shown in figure 2.1. Two plastic scintillators A and B were positioned inside the chamber and were used to select single incoherent particles for calibration purposes. The chamber is situated in a tunnel of rectangular cross-section with 30cm thick barytes concrete walls. Also 15 cm of iron absorber was placed near the top of the chamber to assist in recognizing penetrating particles and also for indicating neutral nuclear active particles.

2.1.2 The neon flash tubes

The chamber uses flash tubes of internal diameter 1.58cm,

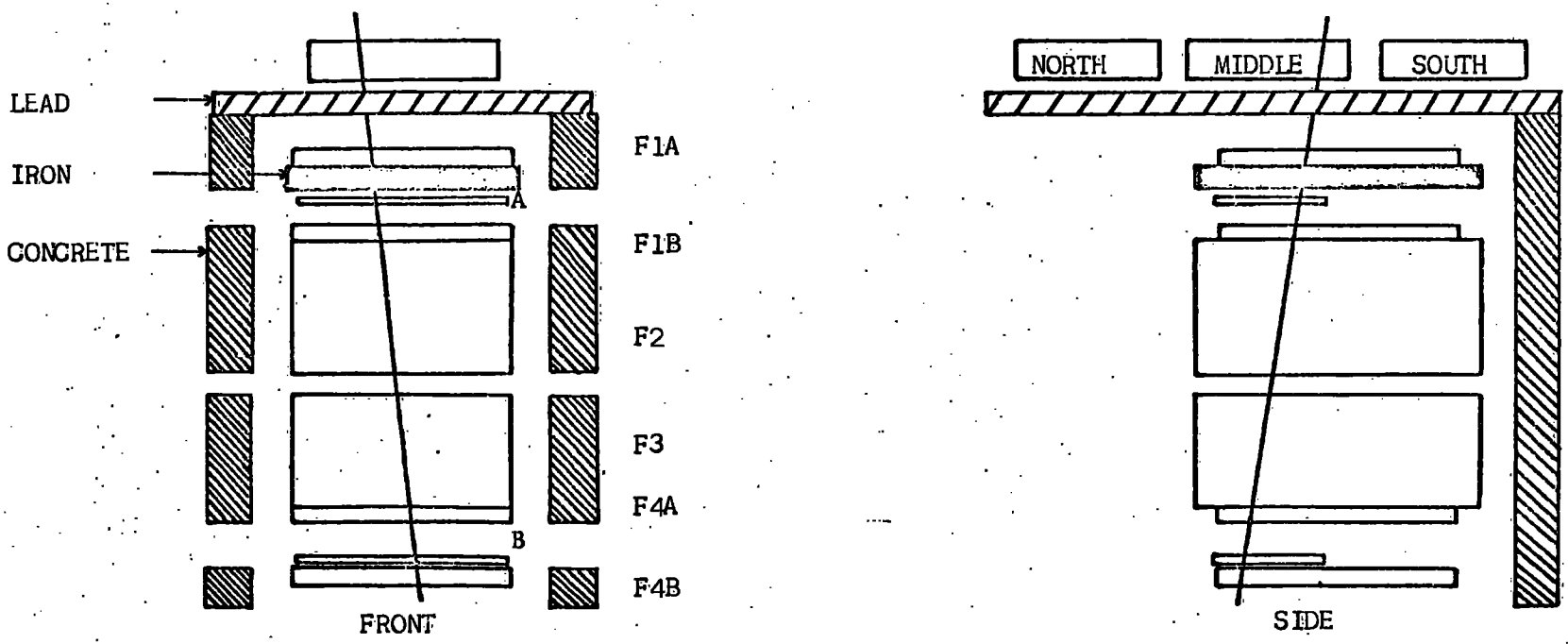

Figure 2.1 The flash tube chamber.

external diameter 1.78cm each filled with gas (98% Ne, 2% He) to a pressure of 60cm mercury and every flash tube is covered with a black polythene sleeve. Alternately , the layers contain 84 and 85 tubes stacked side by side and between every two layers there is a sheet of aluminium (0.122 cm thick). This covers the whole of the tubes.

The front view contains six blocks of tubes, F1A (8 layers) F1B (6 layers), F2 (52 layers), F3 (44 layers), F4A (6 layers) and F4B (8layers). There is a prism in front of each of F1A, F1B and F4B. The defining layers F1 and F4 are made shorter by 15cm at the front and back than in the blocks F2 and F3. The electrodes are connected alternately to earth and to a high voltage pulsing unit. The pulsing unit consists of a monostable and a thyristor to trigger a spark gap as shown in figure 2.2.ii. The capacitance of the flash tube stack was 0.0866μF.

2.1.3 The plastic scintillators

The plastic scintillation counters A and B (figure 2.1) were each of area 1.05m^2 and were used to select single muons traversing the chamber by a two fold coincidence. The phosphor of each counter was a large slab of 2inch thick NE 102A. The photomultipliers (Mullard 53 AVP) viewed the phosphor by light guides of solid perspex. A positive high tension was applied to each photomultiplier and negative output pulses were taken from the anode. The output pulses from each side of the phosphor were fed into an emitter follower, the outputs from these emitter followers were then added for each counter before feeding into the selection electronics figure 2.2.i.

Key: EF = emitter follower
A = Amplifier
D = Discriminator
Co = Coincidence
TH = Thyristor Unit
F/T= Flash tube chamber
F.O = Fan out
G = 1 minute delay generator
C.S = cycling system
M/S = mono stable
P.G.= pulse generator

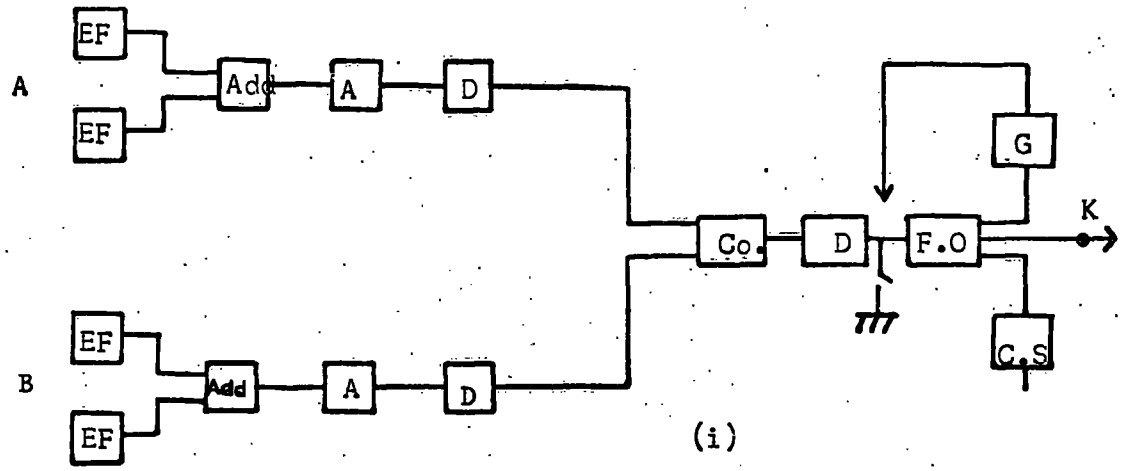

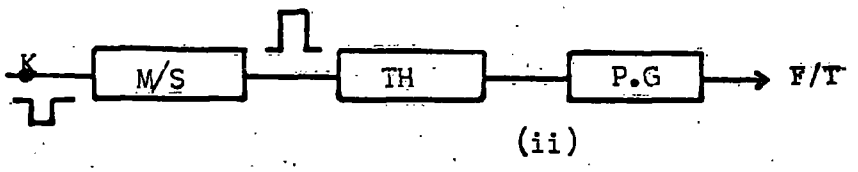

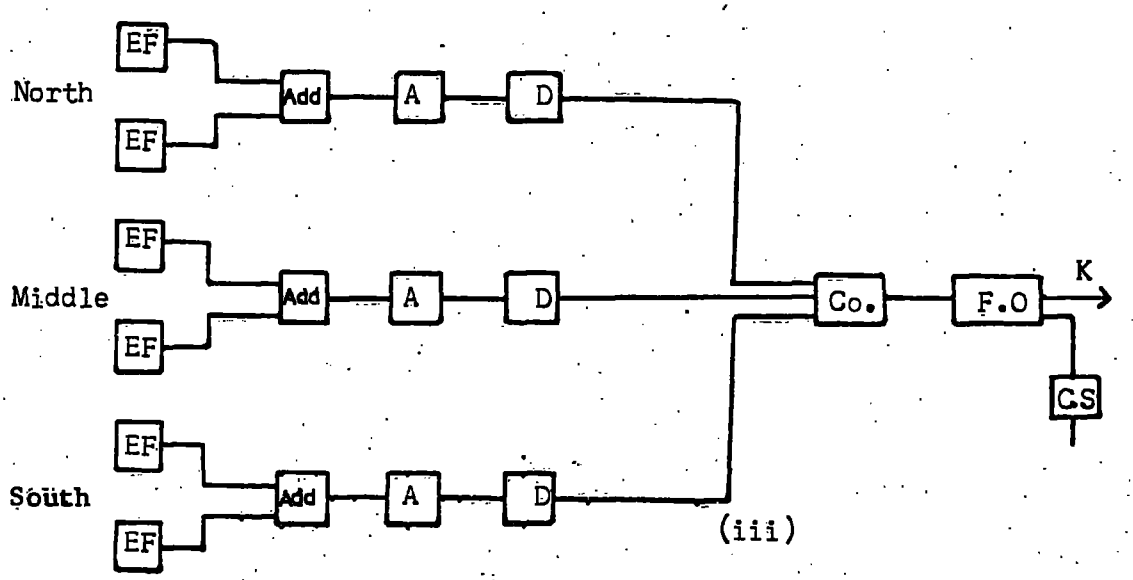

Figure 2.2 Block diagram of the electronics used in the flash tube chamber.
(i) two fold coincidence (plastic scintillators).
(ii) High voltage pulsing unit.
(iii) Three fold coincidence (liquid scintillators).

2.1.4 The Liquid Scintillators

Three large area ($1.24 m^2$) liquid scintillators were used to select extensive air showers. The construction of these counters has been described by Ashton et al 1965. Each scintillator employed two photomultipliers (EMI 9583B) viewing the phosphor through rectangular holes in the light quide mirrors. A positive high tension was applied to each photomultiplier and negative pulses were taken from the anode and were each fed into a separate emitter follower head unit. The output pulses from these head Units were then added for each counter before feeding into the selection electronics figure 2.2.iii.

2.2 Efficiency of the Neon Flash Tube

2.2.1 Single particle trigger

A single muon can be selected by a two-fold coincidence between the plastic scintillators A and B. The rate of the single particles through the telescope was measured to be $(11.5 \pm 0.4) sec^{-1}$ compared with 12 sec^{-1} calculated from 1.05 m^2 scintillator area and the 250 cm distance between the centre of A and B. Due to this high rate, an anti-coincidence gate was used which basically paralysed the electronics for 300 msec after one particle had passed the telescope. The pulse from the coincidence between A and B was fed firstly through the anti-coincidence gate and then allowed to trigger the spark gap applying the high voltage pulse to the flash tubes and to start the cycling system. In the mean time the paralysed electronics gave time to wind on the camera and allows the high voltage capacitor to get charged. Approximately this cycle takes 7 seconds to make the experiment sensitive again.

2.2.2 The measurement of the efficiency-time delay curve

As with many particle detectors the flash-tube relies for its operation on the ionisation left by an ionising particle. In view of the fact that its sensitivity to the ionisation can be varied by varying the time delay between the passage of the particle and the application of the high voltage pulse to the chamber. The most important characteristic for the present application is the efficiency-time delay variation. The efficiency is measured in practice by counting the number of tubes flashed in successive layers along the length of the track. Measurements of the number of flashes along the track in F_2+F 3 were taken for various time delays and are shown in figure 2.3. The means of these distributions were plotted on the efficiency-time delay curve figure 2.4.

The time delay used to operate the chamber was 20μs, because it gave a good separation between the distribution of the number of flashes on a track for e and e/3 particles respectively.

2.2.3 The theory of the efficiency of neon flash tubes

Lloyd (1960) has produced universal curves for the expected variation of efficiency with time delay $\frac{Dt}{a^2}$ in terms of the parameter af_1Q_1, where D, is the diffusion coefficient of a thermal electron in neon at the relevent pressure, a is the tube radius, f_1 is the average probability that a single electron is capable of producing a flash when a high voltage pulse is applied and Q is the average number of initial electrons produced per unit length in the neon gas.

He gives a plot of expected efficiency against Dt/a^2 where

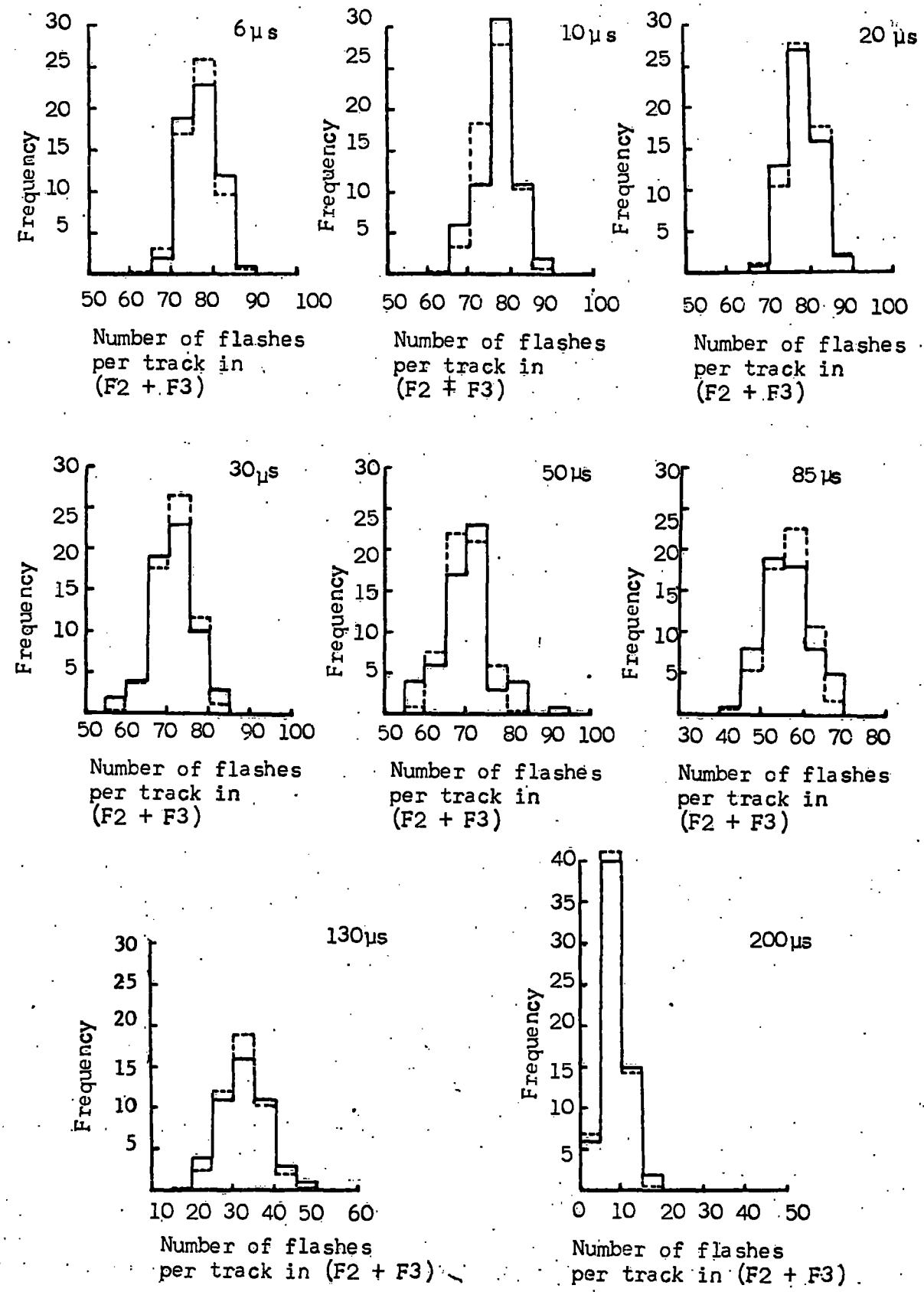

Figure 2.3 The distribution of the number of flashes along the track in F2 and F3 for various time delays. (The dotted curves represent a binomial fit).

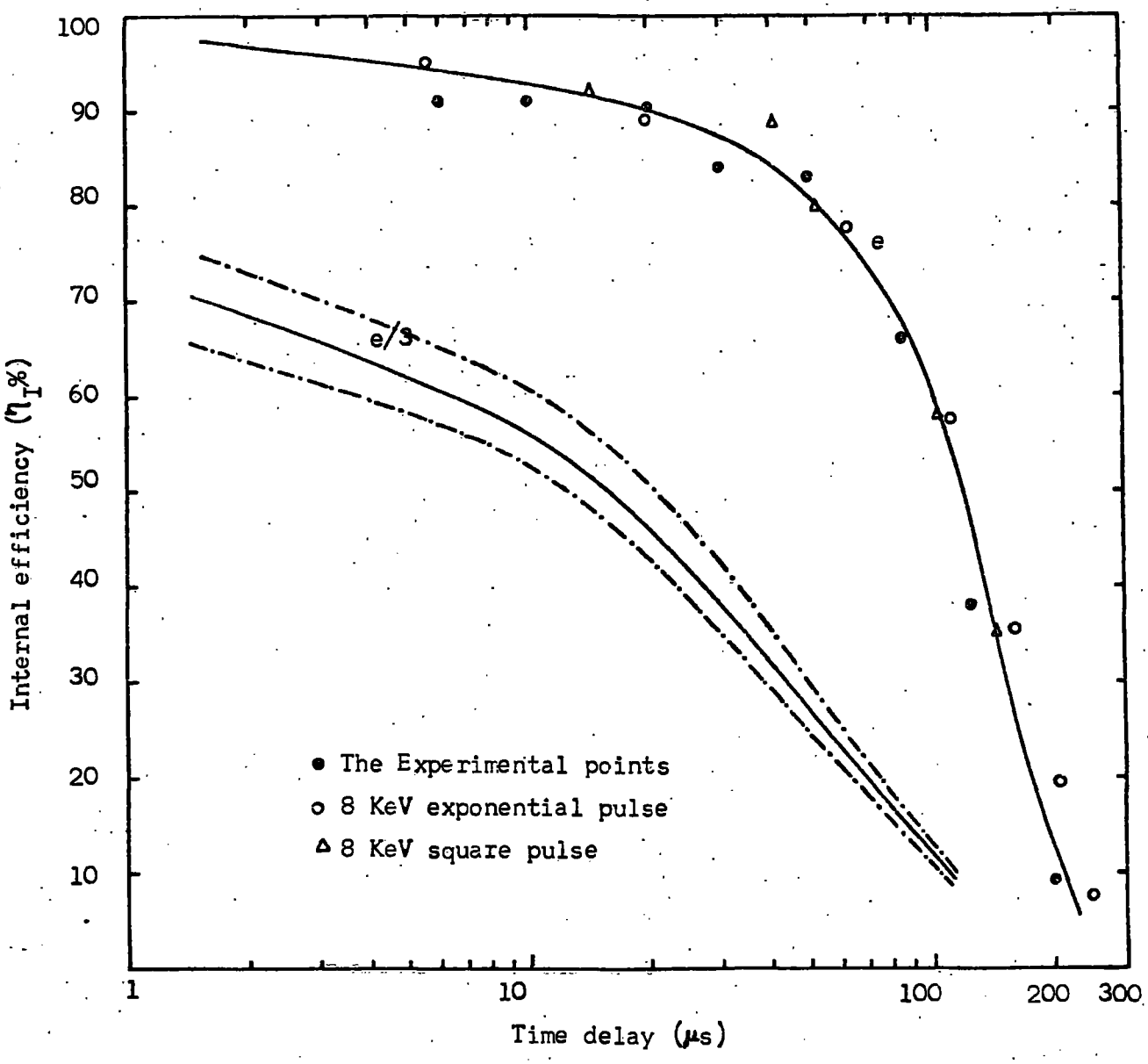

Figure 2.4. The variation of internal efficiency with time delay. The curve through the experimental points has $af_1Q_1 = 9$ and the expected curve for e/3 quarks has $af_1Q_1 = (1.0 \pm 0.1)$.

$Dt/a^2 < 0.2$ with af_1Q_1 as parameter.

For time delays so long that Dt/a^2 exceeds 0.2, the efficiency depends only on $af_1Q_1 \exp(-\beta_1^2 Dt/a^2)$ and a universal curve has been produced for all af_1Q_1.

A curve with $af_1Q_1 = (9\pm1)$ has been found to give the best fit to the measurements for single muons with charge e, figure 2.4.

The fall-off of the efficiency-time delay curve arises from the loss of the initial electrons by diffusion to the walls of the glass tube in the time interval between the passage of the particle and the application of the high voltage pulse to the chamber. The process has been studied empirically by Coxell and Wolfendale (1960).

Also shown in figure 2.4 is the efficiency-time delay curve expected for e/3 quarks. This has been calculated from the curve for unit charge using the Lloyd theory. Since f_1 is independent of the number of electrons present, so that the theory should be applicable to a quark as it is to a muon provided that Q is multiplied by the square of the quark charge e/3. The expected efficiency-time delay curve for e/3 quarks having the same value of $\gamma = E/mc^2$ (Lorentz factor), as the single muons is thus given by Lloyd curve with $af_1Q_1 = (\frac{1}{9}) \times (9\pm1) = (1.0 \pm 0.1)$.

2.3 The single particle calibration run

The distribution of the number of tubes flashed along the track for 1,046 particles was measured at 20μs time delay and is shown in figure 2.5. The mean number of flashed tubes along the track of a single particle (muon) passing through the chamber is 74.77 ± 0.14 with standard deviation of the distribution of $\sigma = 4.6$. The median momentum of muons producing calibration triggers is 2.1 GeV/c, at the centre of F2 and F3. Later, another calibration run

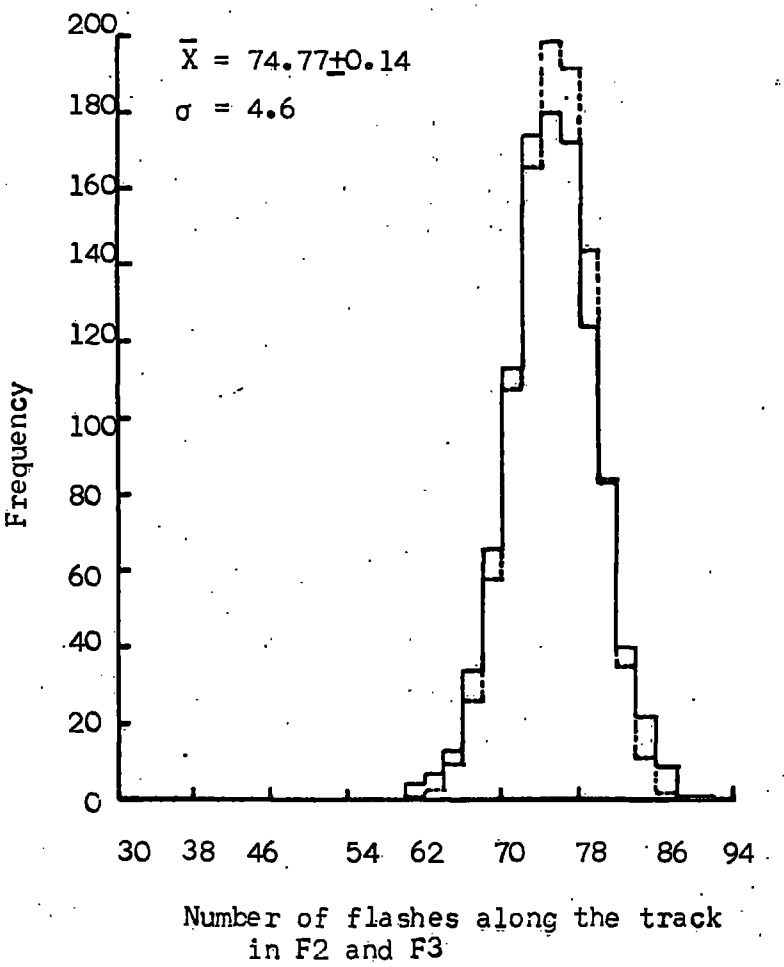

Figure 2.5 The frequency distribution of the number of flashed tubes along the track in F2 and F3 for 1,046 single muons. (The dotted curve represents a binomial fit).

was made so that the total number of single particles observed in the chamber is 5,283.

2.4 The Air Shower Run

2.4.1 The air shower trigger

Air showers were selected by a threefold coincidence between the liquid scintillators, N, M and s, as shown in figure 2.1. The discriminator threshold on each scintillator corresponded to an electron density of greater than $40m^{-2}$. With this master selection, the trigger rate was 4.4 showers per hour and the minimum shower energy to produce a trigger was 3×10^{14}eV.

2.4.2 The position of the core and Size of the shower

The range of the shower size that trigger the selection system, vary from small showers whose axes fall close to the chamber, to large showers whose axes fall a long distance away. The distribution of shower size and core distance have been calculated for EAS which produce local electron density of $> 40m^{-2}$. The calculations have been carried out numerically using the accepted values of the number spectrum and lateral distribution of electrons and nuclear active particle at sea level given by Cocconi (1961).

For muons the analytical expression for the lateral distribution given by Greisen (1960) has been used,

$$\Delta_\mu (N_e, r) = 18 \left[\frac{N_e}{10^6}\right]^{\frac{3}{4}} r^{-\frac{3}{4}} (1 + r/320)^{-2.5} \quad m^{-2}$$

where N_e is the electrons size and r is the radial distance in metres.

The result obtained by Cooper and Parvaresh (private communication) is shown in figure 2.6 and figure 2.7. From figure 2.6 and figure 2.7 it can be seen that the median electron shower size producing a local density $> 40m^{-2}$ is $4.5\ 10^5$ particles and the median core distance of

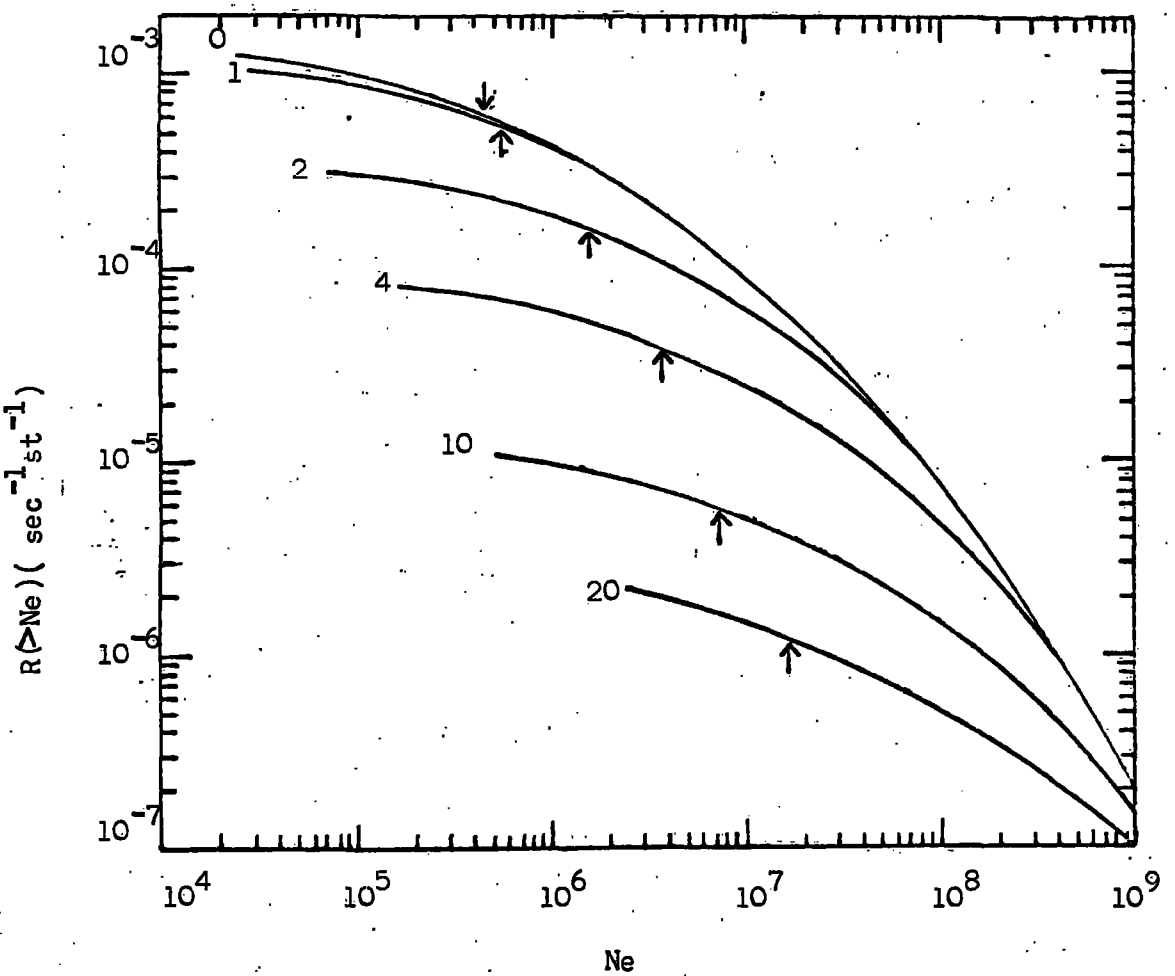

Figure 2.6 The rate of EAS of electron size > Ne producing a local electron density > $40m^{-2}$ associated with different minimum muon densities. Median shower sizes are shown by arrows and the number attached to the curves indicate $\Delta\mu\ m^{-2}$. Each curve starts at the minimum shower size to produce $\Delta_e > 40m^{-2}$ together with the indicated $\Delta\mu$.

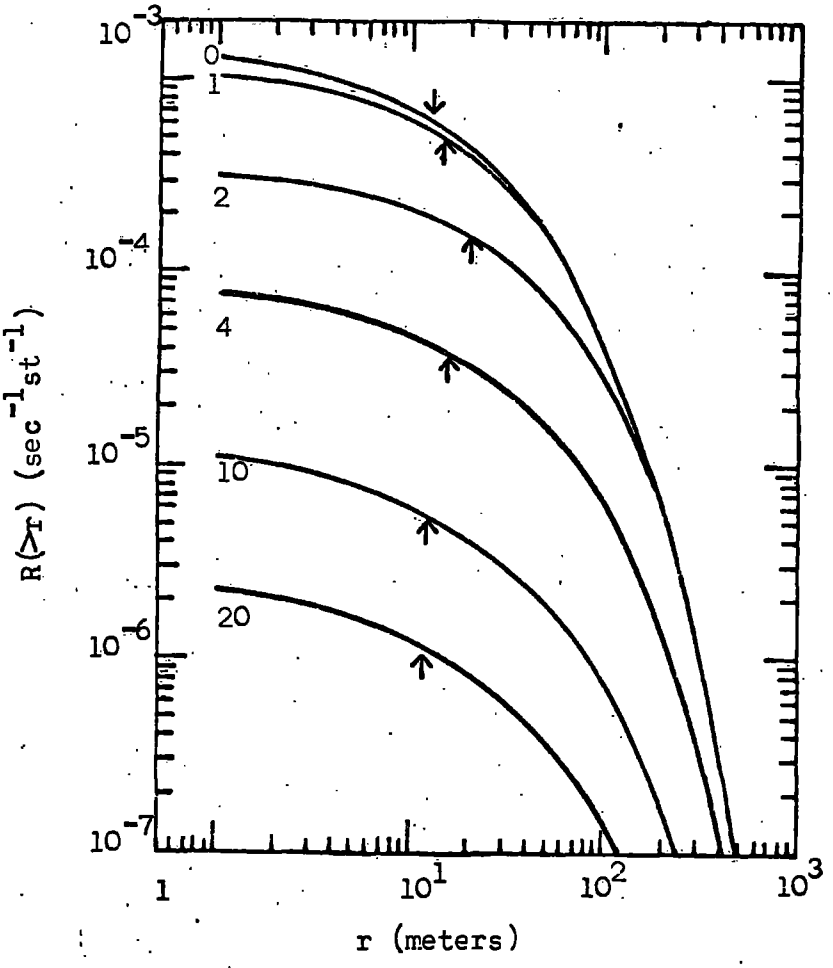

Figure 2.7 The rate of EAS which produce a local electron density $>40m^{-2}$ and whose cores fall at a distance $>r$ meters from the detector. Median core distances are shown by arrows and the numbers attached to the curves indicate $\Delta\mu\, m^{-2}$.

of the shower producing such triggers is 12 meter with a median shower energy 3.5×10^{15} eV.

2.4.3 Variation of shower rate with barometric pressure

The variation in the rate of showers of a given size with barometric pressure is of interest because it affords a measurement of the attenuation of the showers in the atmosphere. The variation is shown in figure 2.8. The solid line is the fit using the weighted least squares method. The pressure reading of the barometer used was systematically 12.5mm Hg higher than the true pressure. The value of the barometric coefficient has been evaluated as $(11.6 \pm 0.86)\%\ cm^{-1}$ Hg from figure 2.8. The triggering shower size has been found approximately to be $(10^5 - 10^6)$ particles by using the relation between the barometric coefficient and shower size which has been given by Galbraith (1958).

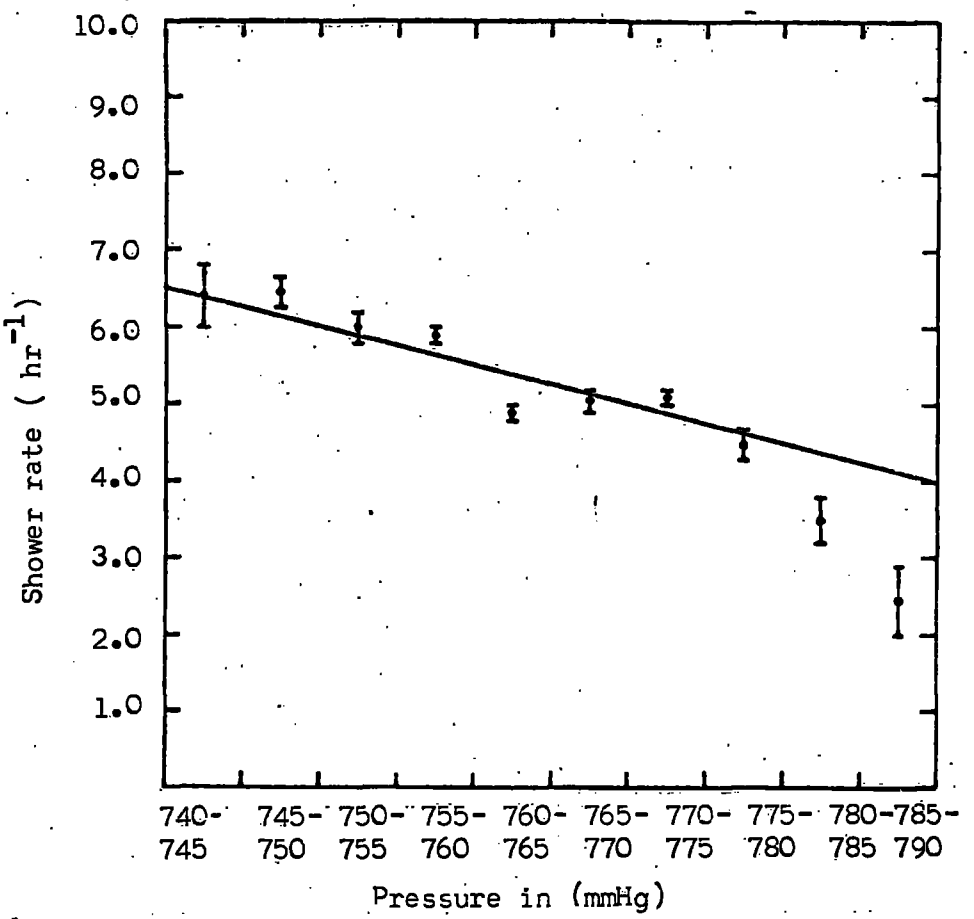

Figure 2.8 The variation of shower rate with atmosphere pressure.

CHAPTER THREE

Extensive air shower experiment to search for quarks

3.1 Introduction

Since Gell-Mann (1964) and Zweig (1964) predicted the existance of fractionally charged particles (quarks), many experiments have been carried out in an attempt to detect these particles among secondary cosmic rays. The main area in which the search has taken place are at the accelerators and in the cosmic radiation, and as yet none has proved successful. The flash tube chamber which has been described in chapter two was used to look for quarks in EAS close to the core. Briefly, a fractional charge e/3 quark is expected to have significantly fewer flashes along its track than a charge e particle and this property is looked for in the quark search.

3.2 Quark results

3.2.1 Analysis of data

Analysis of individual events was achieved by projection of the extensive air shower run films on the scanning tables. All the films have been scanned carefully and the events classified. The selection criteria for measurable events from the film were based solely on the flash tube information.

The number of flashes was counted for trays F2 and F3 and the angle of the track to the vertical was measured and a small scale diagram of each event was drawn. All the interesting events observed in the chamber were recorded, drawn and studied. The tracks with F2 + F3 > 60 flash tubes were only measured in the scanning if they had at least one shower track of length greater

than 60cm in the chamber and were parallel to it, to $\pm 5^{o}$ and produced at least one flash in each of the defining layers F1 and F4. All the tracks with F2 + F3 in the range 20-60 were measured irrespective of the angle they made to shower tracks in a picture.

3.2.2. Basic experimental data

The summary of the basic experimental data referring to the E-series films measurement is shown in table 3.1. All this data was obtained using a local electron density of $>40m^{-2}$ as a master trigger.

Film Numbers	Running time (hr)	Total no of photographs	Total number of measurable photographs	Percentage of photos that give at least one measurable track (%)	Total number of measurable tracks.
E1-E69	2,570hrs	12,057	2,753	23%	4,501

Table 3.1 Basic experimental data

The frequency distribution of the number of measurable tracks per photograph is shown in table 3.2.

The frequency distribution of the number of flashes in F2 + F3 for 4501 measured tracks in the chamber is shown in figure 3.1. The mean number of flashes along the track for shower particles passing through the chamber is 78.11 $\pm$ 0.07 and the standard deviation on the distribution is 4.73. The expected number of flashes for minimum and plateau ionizing charge e particles and quarks of charge e/3 and 2e/3 are shown in figure 3.1 by arrows, the small bars indicate the uncertainty in the position of the arrow and the large bars the expected standard deviation of the distribution. It is clear from this figure that the chamber should register the passage of quarks with charge e/3 but those with charge 2e/3 will not be distinguished

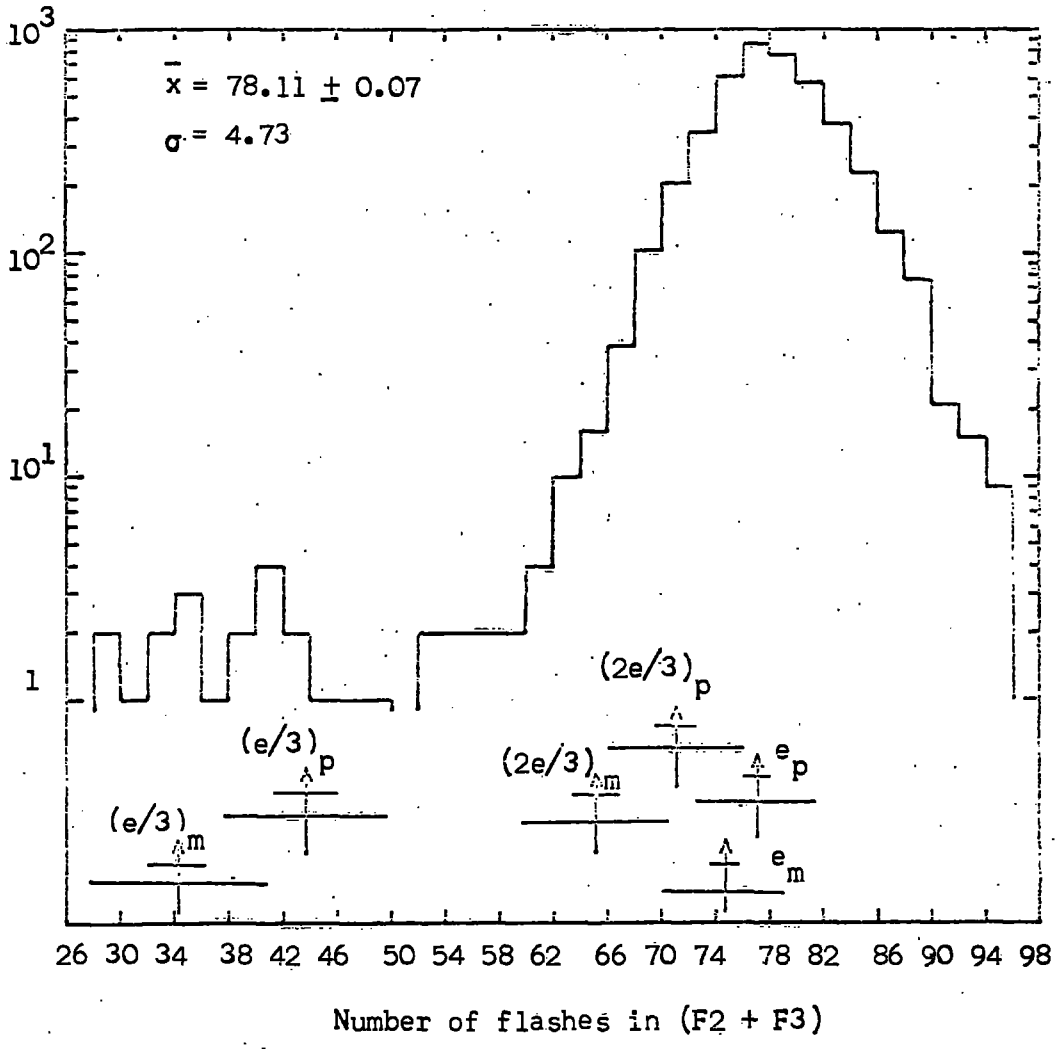

Figure 3.1. The frequency distribution of number of flashes in F2 and F3 for 4,501 measurable EAS tracks in the chamber. Events in range (20-60) have measured irrespective of the angle of other shower tracks.

from charge e particles and the quarks are expected to have a value of F2 + F3 in the range 28-50 flashes. As can be seen from figure 3.1, 20 tracks with F2 + F3 in the region 28-50 were observed during the running time 2,570 hours. A small scale diagram for each of these 20 events is shown in figure 3.2 (a-e). No events were observed with F2 + F3 in the range 20-26.

Number of measurable tracks per photograph, n	Number of photographs, N	N x n
1	1604	1604
2	758	1516
3	254	762
4	84	336
5	42	210
6	7	42
7	3	21
8	0	0
9	0	0
10	1	10
SUM	2,753	4,501

Table 3.2: The frequency distribution of the number of triggers N having n measurable tracks.

3.3 Examination of the Quark Candidates.

3.3.1 Background effect

From the measured efficiency-time delay curve shown in figure 2.4 the tracks with F2 + F3 in the range 28 - 50 could be produced by incoherent muons which traversed the chamber in the period 103μs to 144μs preceding the air shower trigger. Also from the same curve it can be shown that the distribution of F2 + F3 for incoherent muon tracks should be flat over the range 28 - 50 flashes. The rate

Figure 3.2 (a-e) Flash tube diagrams of the 20 quark candidate events observed in EAS runs (E1 - E69). Each event is indicated by the film (E) and event number.

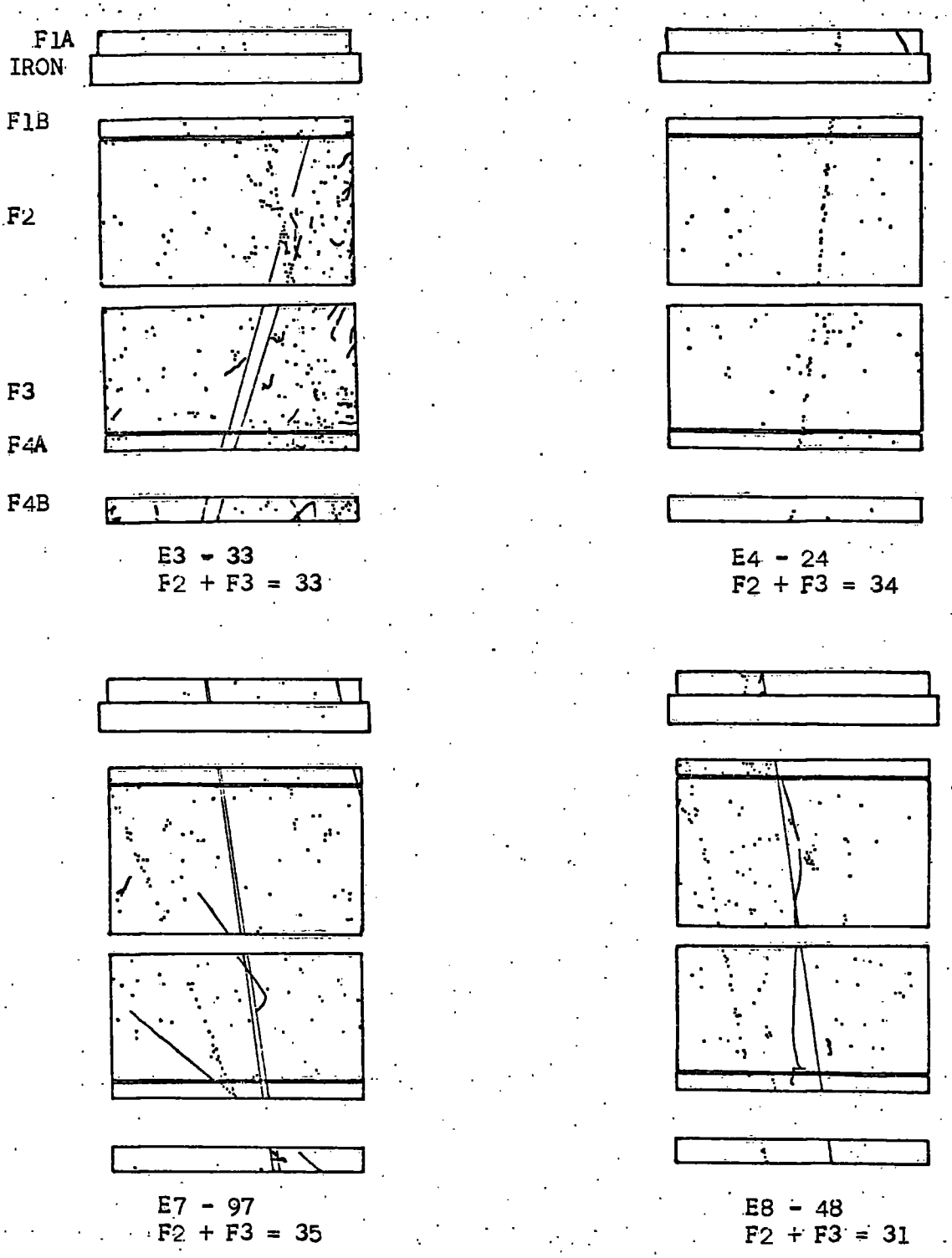

Figure 3.2 (a) The quark candidates

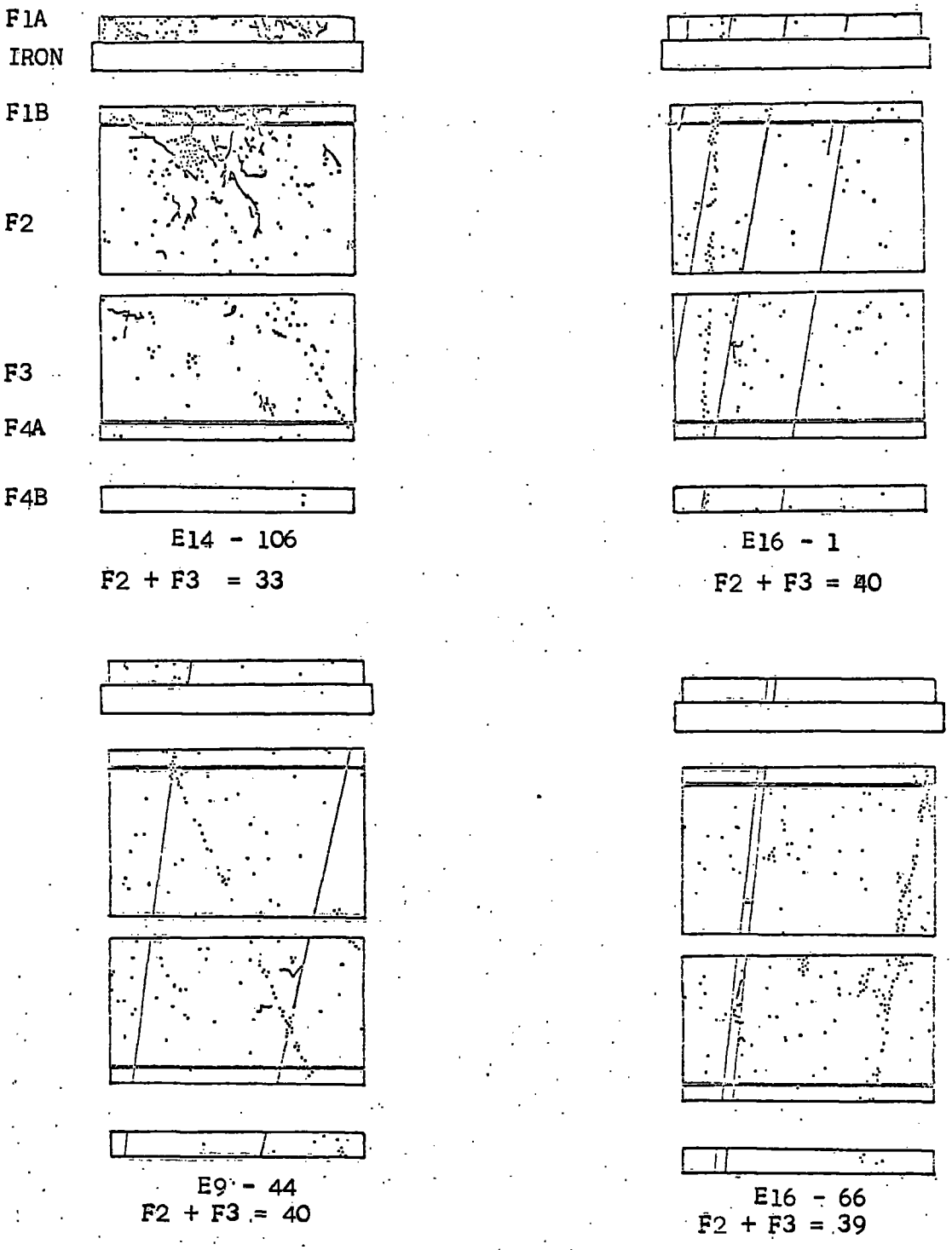

Figure 3.2 (b) The quark candidates

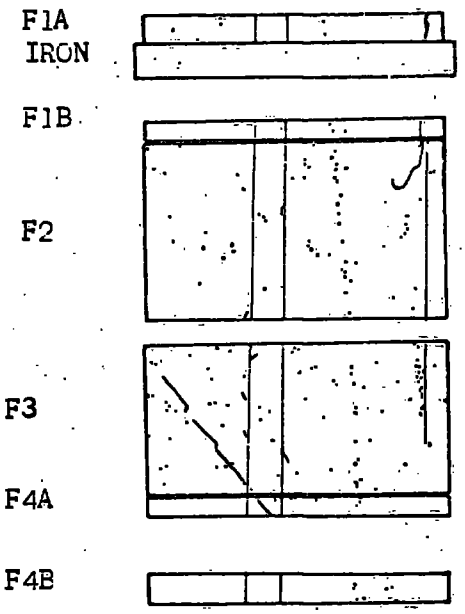

E19 - 45
F2 + F3 = 28

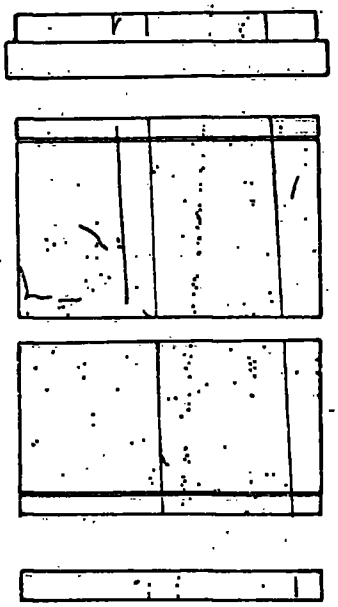

E34 - 117
F2 + F3 = 38

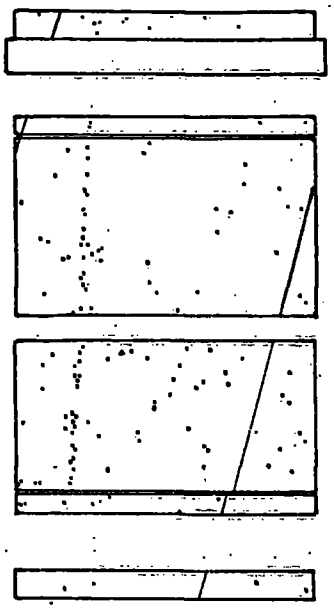

F26 - 162
E2 + E3 = 36

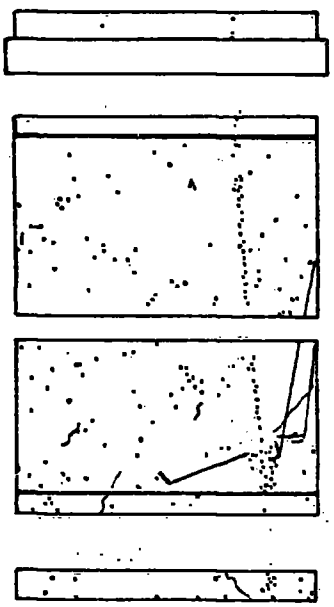

E41 - 51
F2 + F3 = 45

Figure 3.2 (c) The quark candidates

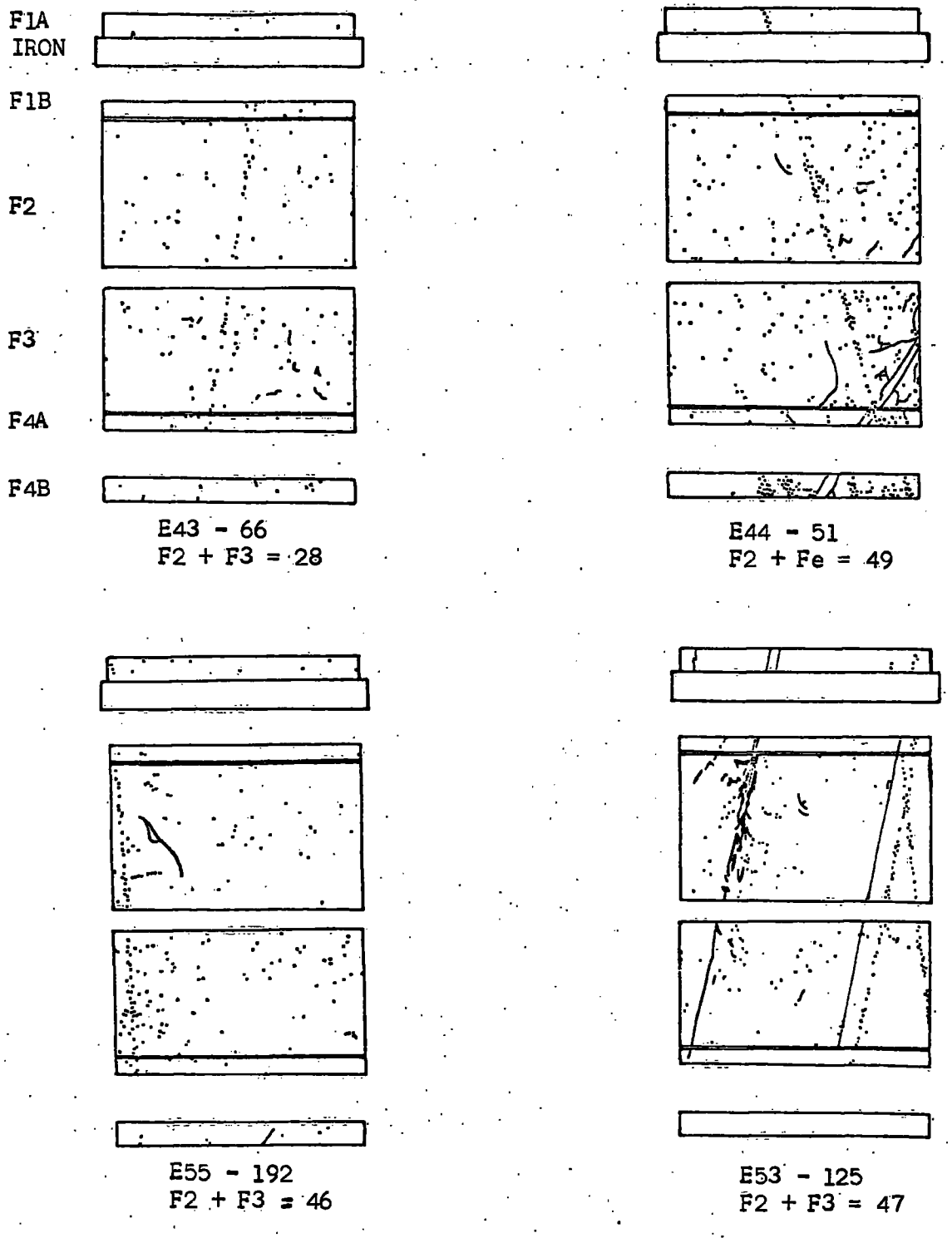

Figure 3.2. (d) The quark candidates

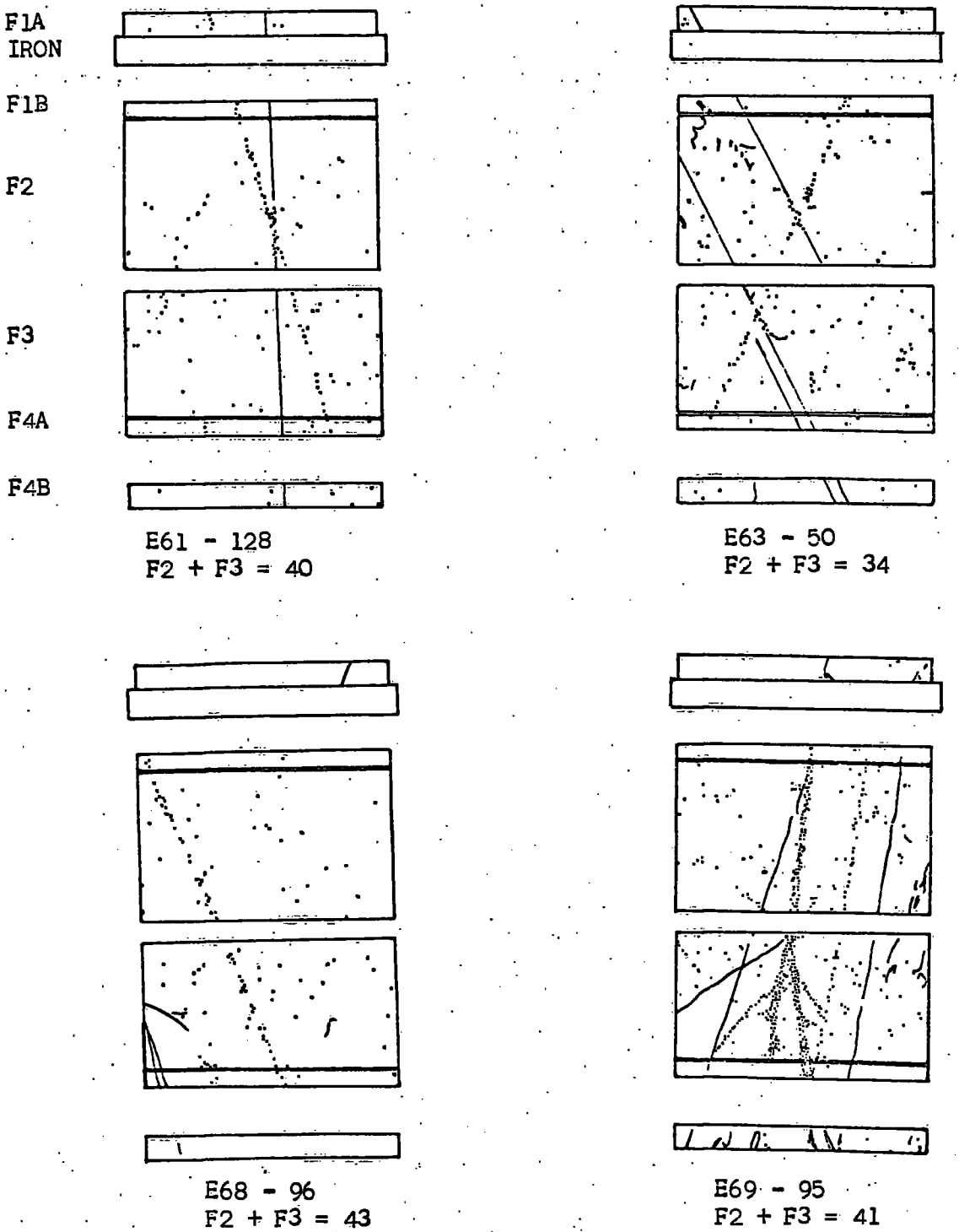

Figure 3.2. (e) The quark candidates

of the incoherent muons through the chamber sensitive volume was 104.2 sec^{-1} and the total time available for incoherent muon tracks to simulate quarks is 0.154 sec. Thus the expected number of the incoherent muons simulating quarks with F2 + F3 in the range 28-50 was calculated as 16. This should be compared with the observed number of tracks of 20 with F2 + F3 in the range 28-50 indicating rough agreement, which may not rule out the presence of a few genuine quarks.

3.3.2 The angular separation of tracks

An experimental test was done on these quark candidates in which to identify the possible quarks. It was assumed that the quark tracks should be essentially parallel to shower tracks and a limit of $\pm 5^{o}$ has been imposed. The 20 tracks which have been observed with F2 + F3 in the range 20-50 reduced to 6.0 and this should be compared with an expected number of incoherent muons of 2.2 . Figure 3.3 shows the same distribution which has been produced in figure 3.1 except that only tracks with F2 + F3 in the range 20 - 60 are plotted if they are parallel to shower tracks within $\pm 5^{o}$.

3.3.3 The knock-on electron test.

The second experimental test that can be applied is an examination of the number of knock-on electrons (δ-rays) produced by the particles. The 6 tracks, quark candidates, have been examined carefully and in detail for the occurrence of extra flashes due to knock-on electrons, a knock-on being defined as two adjacent flashes occurring in one layer of flash tubes. The mean number of knock-on electrons (KO's) on the 14 non parallel quark candidate tracks which were taken to be due to incoherent muons was found to

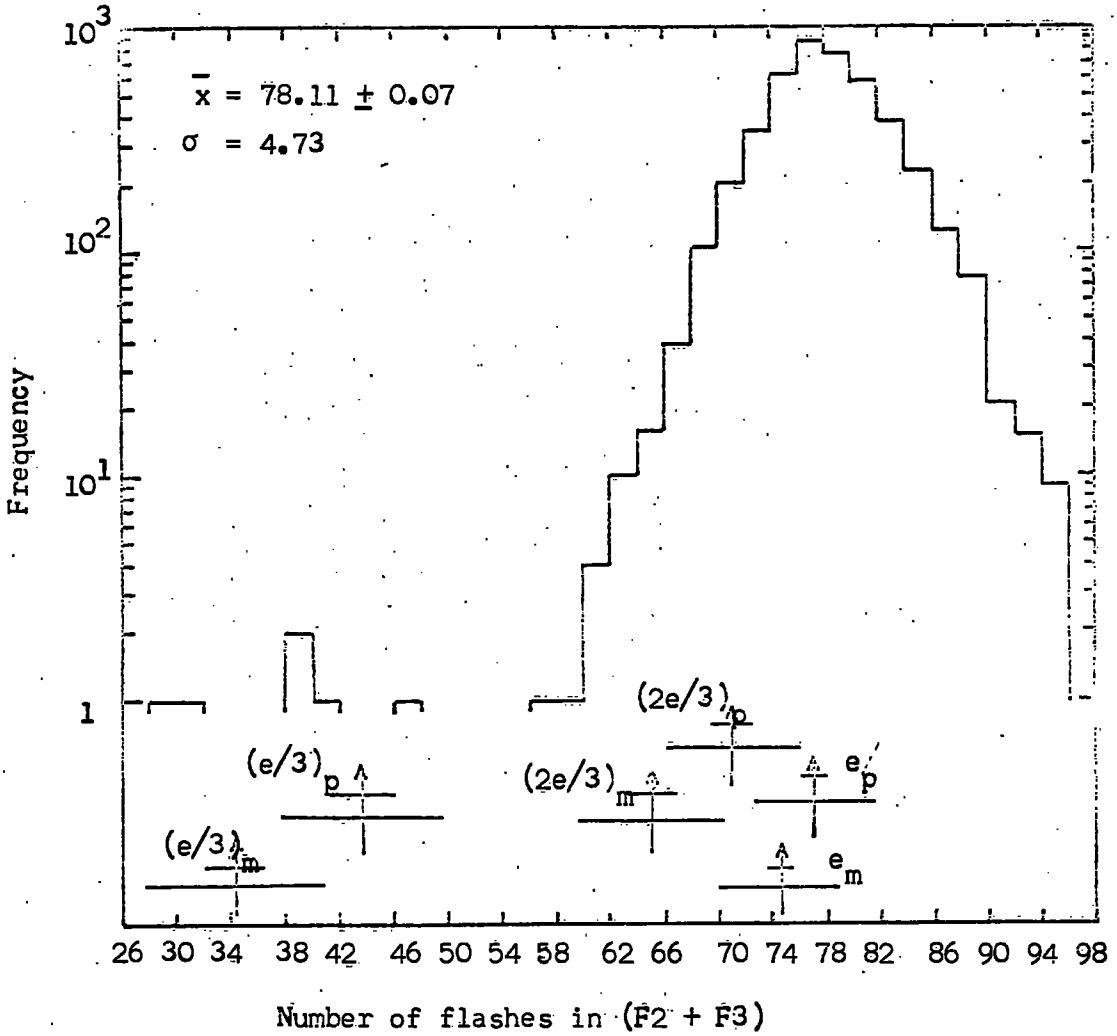

Figure 3.3 The frequency distribution of number of flashes in F2 and F3 for 4501 measurable EAS tracks in the chamber. Events with range (20-60) are plotted if they are parallel ($\pm 5^{o}$) to shower tracks.

be 1.79 and three of these tracks had no KO's along it. We expected the quark with charge e/3 would produce 1/9th the number of KO's that a charge particle e muon would produce. According to this the quark track should be virtually free of knock-on electrons. Of the 6 quark candidates, two have no observable KO's. The expected number of the incoherent muons simulating quarks, will be $2.2 \times \frac{3}{14} = 0.47$.

This should be compared with the observed number of two tracks which satisfy all above criteria. The basic information of these 6 events is given in table 3.3. The event E19-45 which shows a possible e/3 quark track is shown in plate 3.1.

3.4 Discussion

This experiment is therefore quite capable of detecting e/3 charge particles (but not quarks with 2e/3 charge) close to air shower cores and in observing 12,057 of these showers, two tracks were observed in the expected quark region and both were consistent with zero knock-on electron flashes associated with them. The most likely interpretation is that they are background incoherent muon tracks but it is possible that they are genuine quarks. The probability of observing two pseudoquarks is therefore 8%. Based on two possible events the upper limit to the flux of e/3 quarks in air showers where the electron density is $> 40 m^{-2}$ is less than $1.4\ 10^{-11}$ $cm^{-2}\ sec^{-1} st^{-1}$. This limit is calculated using an aperture of $1.57 m^2 st$ (defined by the middle of F1B and the middle of F4A shown in figure 2.1) and neglects the loss of quark due to inelastic interactions in the chamber material. Assuming a quark-nucleon inelastic cross section of $\frac{1}{3}$ the nucleon-nucleon inelastic cross section, the probability of a quark traversing the chamber without interacting has been calculated

Event	(F2 + F3) for quark candidate	No. of shower tracks in picture excluding quark candidate	Angle quark candidate tracks makes to other shower tracks	No. of KO's on track (i.e pairs of adjacent flashes)
E8-48	31	1	3^{o}	1
E16-66	39	2	4^{o}	7
E19-45	28	3	5^{o}	0
E34-117	38	3	5^{o}	0
E53-125	47	2	0^{o}	1
E69-95	41	2	0^{o}	1

Table 3.3: Details of the 6 events shown in fig 3.3 as quark candidates and appearing with (F2 + F3) in the range (28 - 50) flashes.

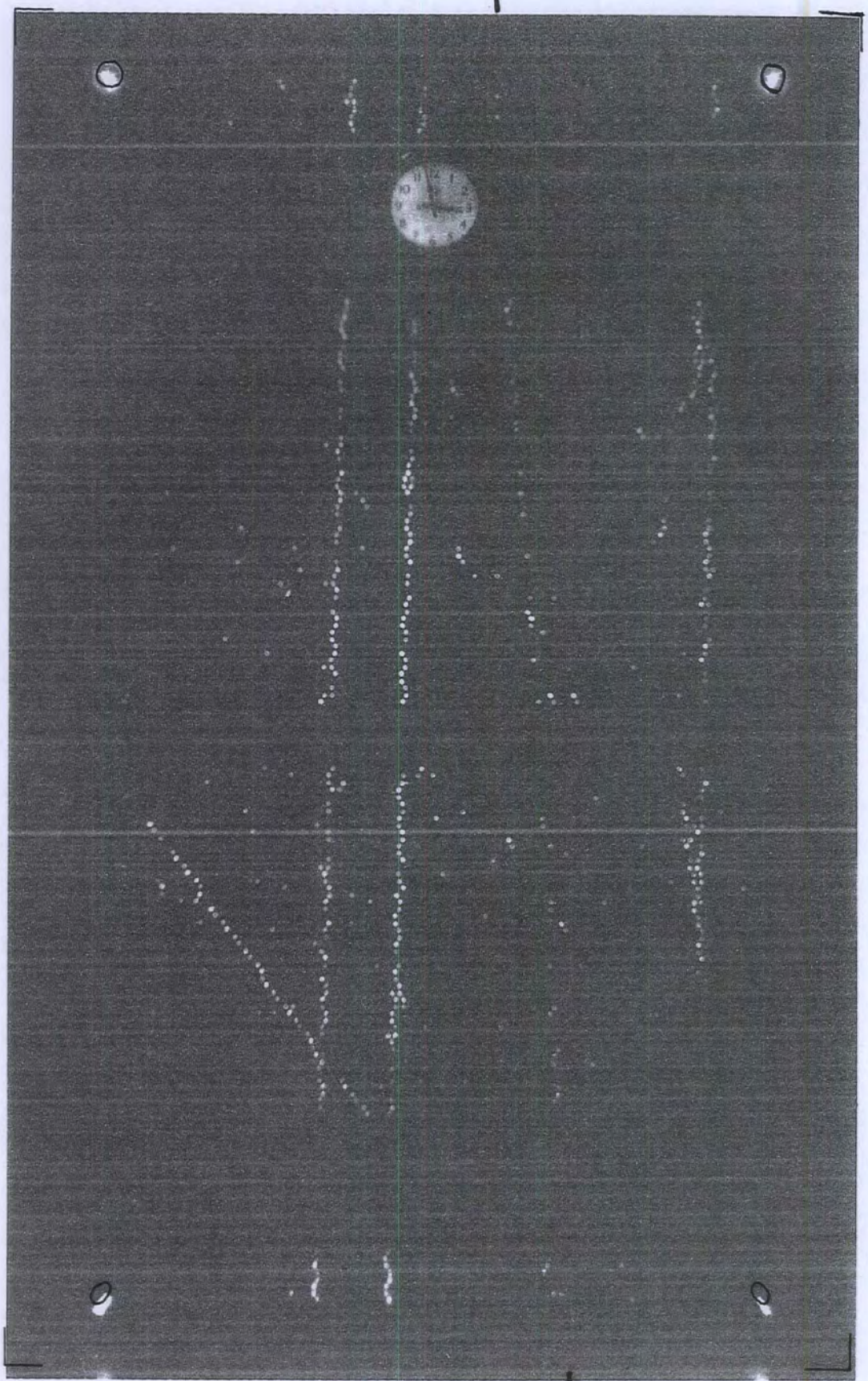

Plate 3.1 Event (E19-45)

A possible e/3 quark is indicated

to be 0.165. Taking this effect into account raises the upper limit quoted above to $< 8.0. 10^{-11} cm^{-2} sec^{-1} st^{-1}$.

3.5 The Elastic Collision of Extensive Air Shower Particles

3.5.1 Introduction

The main interest in this problem is concerned with the equation of the existance of fundamental triplet particles carrying integral charge and a new quantum number Bacry et al. 1964, Han and Nambu. 1965, Lee, T.D., 1965. The experimental problem of detecting heavy mass ($>10 M_p$) integral charge particles is more difficult than detecting particles with fractional charge as their ionising power is no longer a unique signature for them. In fact it is necessary to measure their mass in some way to uniquely identify them and the method discussed below provides one possible way of doing this.

A collision between two particles in which energy and momentum are conserved is called elastic collision. Consider a particle of mass M scattered through an angle θ in an elastic collision with a proton (Mass Mp) and suppose the proton recoils making an angle ϕ with respect to the incident particle direction. In the non-relativistic approximation the ratio M/M_p depends only on θ and ϕ and is given by:

$$M/M_p = 2 \left[\frac{\sin \phi \cos \theta}{\sin \theta} + \cos \phi - \frac{\sin \phi}{\sin \theta} \right] \left[\frac{\sin \phi}{\sin \theta} \right]$$

Thus if non-relativistic elastic collisions of extensive air shower particles on protons are detected experimentally, the above equation provides a method of determining their mass distribution.

3.5.2 The Basic results

Scanning the films has revealed 84 events showing EAS particles scattered through an angle $> 4^{\circ}$ in elastic collisions with protons. It is believed that these collisions represent essentially free collisions with peripheral protons in glass nuclei (mainly S_i^{28} and

O^{16}) as no evidence for low energy evaporation protons is seen at the scattering vertex. The analysis was carried out using the expression given in section 3.5.1 assuming the smallest angle corresponds to the scattering particles and the largest angle to the recoil proton. The value of M/M_p was evaluated for each event and the frequency distribution of these events is shown, figure 3.4. It is seen that it has a most probable value 1.35 M/M_p suggesting that most of the collisions observed are proton-proton at such an energy ($\sim$600MeV) that the non relativistic approximation is beginning to breakdown. The type of collision is shown in plate 3.2. This event E50-18 shows two successive elastic scatters for a particle emerging from a local interaction in lead. The mass ratio calculated in the first collision and the second are 1.9, 1.5 respectively. The scatter plot of opening angle $(\theta + \phi)$ as a function of M/M_p is shown in figure 3.5, and it is seen that $(\theta + \phi)$ is close to 90° for M/M_p close to 1.0 as is expected for p-p collisions.

The relation between the scattering angle θ and the recoil angle ϕ was plotted for different primary energies, and recoil energies using the Oxford Kinematical Tables (Volumes 1 and 2, 1961). The fitting of the measured θ and ϕ on the above plots is shown in figure 3.6 for pp collisions and figure 3.7 for π p collisions. The solid curves shows the different primary energies and the dashed line shows the different recoil energies. In pp collision the maximum scattering angle is 45° but the curves for different primary energies (see figure 3.6) have been reversed only for θ and ϕ. It can be seen from figure 3.6 also that all the measured points fitted well and the points outside the 100 MeV primary energy curve have a low mass ratio and these might be due to μp or πp collisions.

It could be explained that the increase in the width of the mass distribution shown in figure 3.4 for high mass ratios is due to

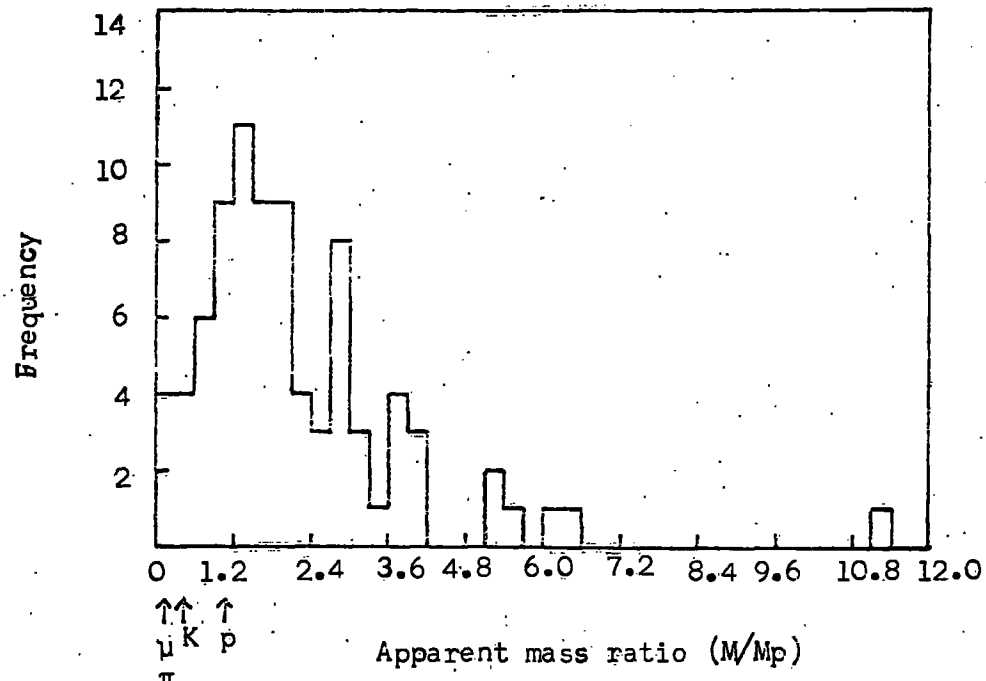

Figure 3.4 The mass distribution for 84 elastic scatters of EAS particles on protons observed in the flash tube chamber

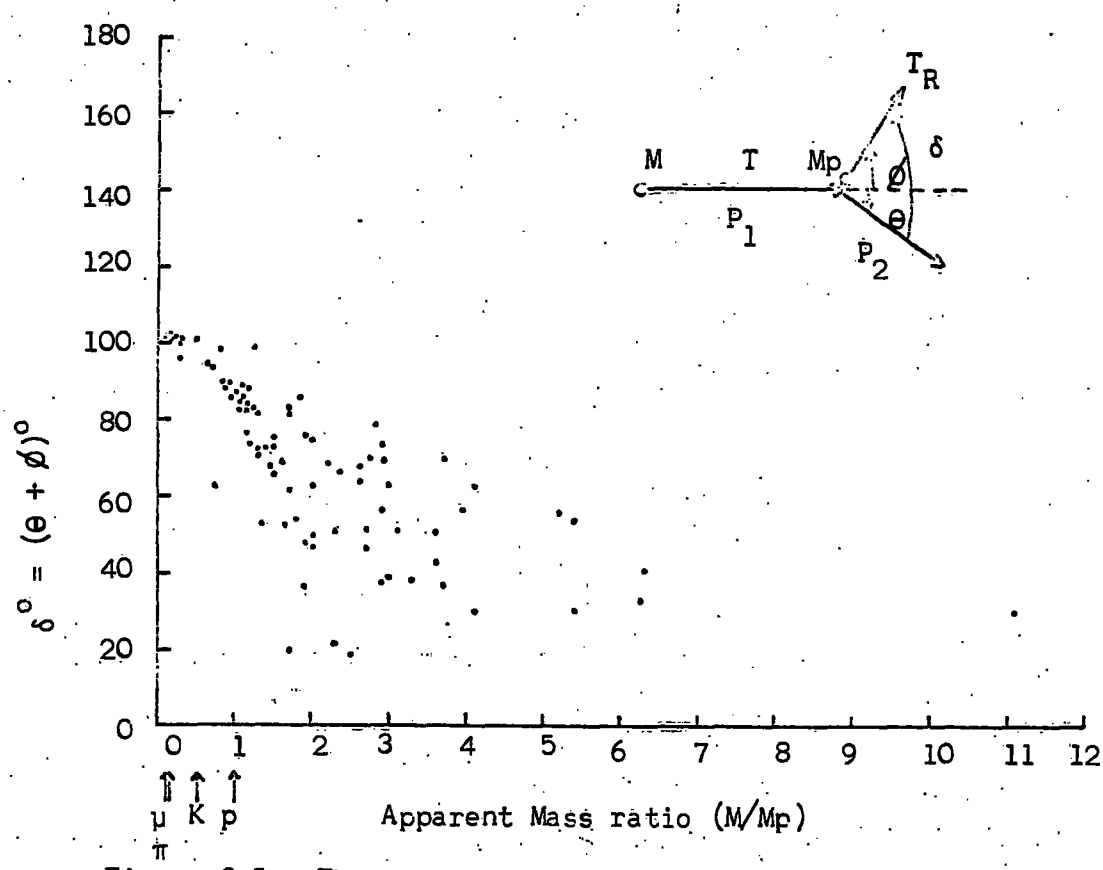

Figure 3.5 The scatter plot showing the correlation between the opening angle $\theta + \phi$ as a function of mass ratio.

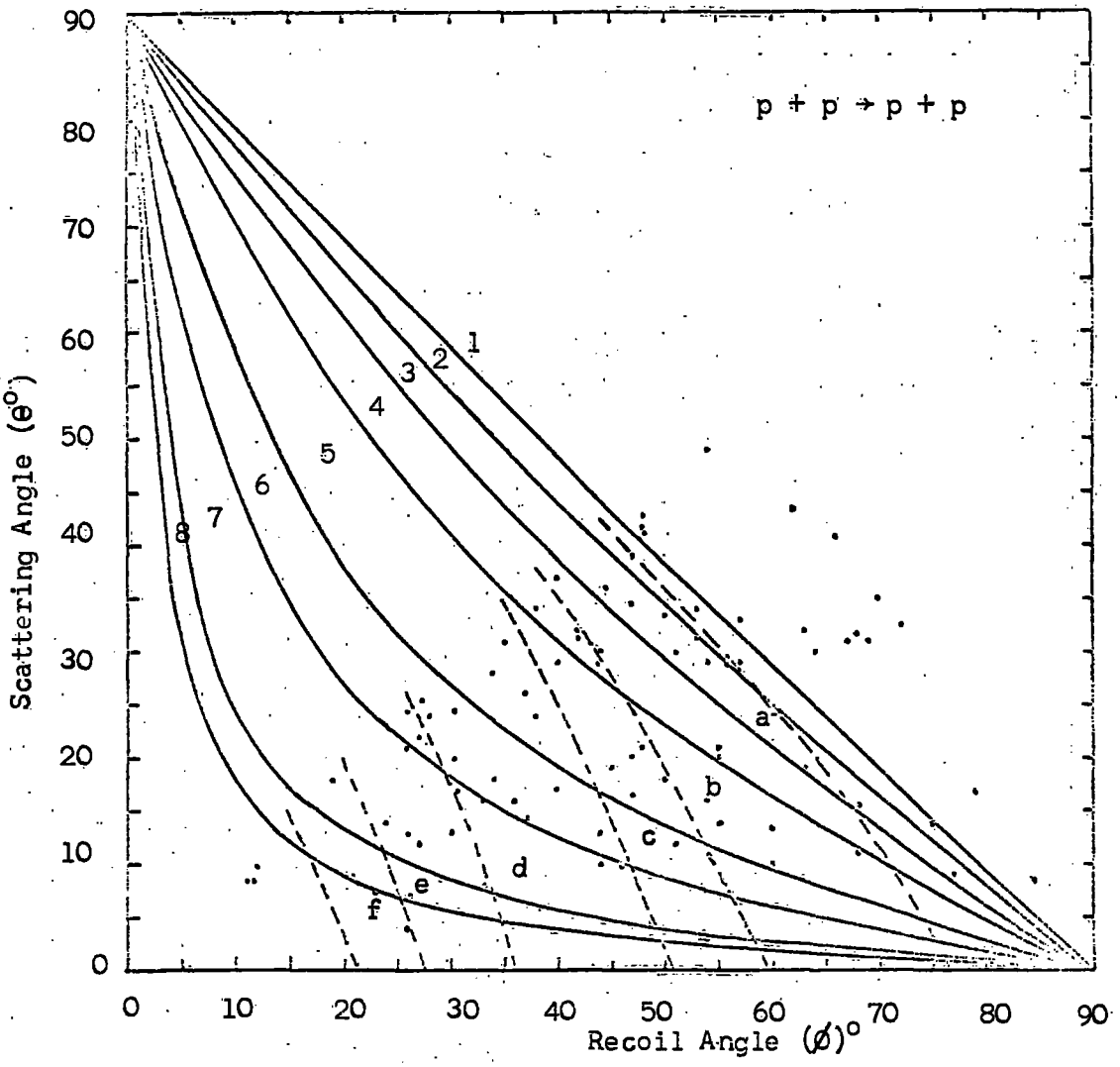

Figure 3.6 The scatter plot for measured scattering angle θ and recoil angle Ø. curves (1-8) shows different Kinetic energies of a primary proton T (MeV). Curves (a-f) shows different kinetic energies for a recoil proton T_R(MeV).

1	T = 100 MeV	a	T_R = 100 MeV
2	T = 400 MeV	b	T_R = 600 MeV
3	T = 900 MeV	c	T_R = 1000 MeV
4	T = 1800 MeV	d	T_R = 3000 MeV
5	T = 4500 MeV	e	T_R = 6000 MeV
6	T = 8000 MeV	f	T_R = 12000 MeV
7	T = 20000 MeV		
8	T = 30000 MeV		

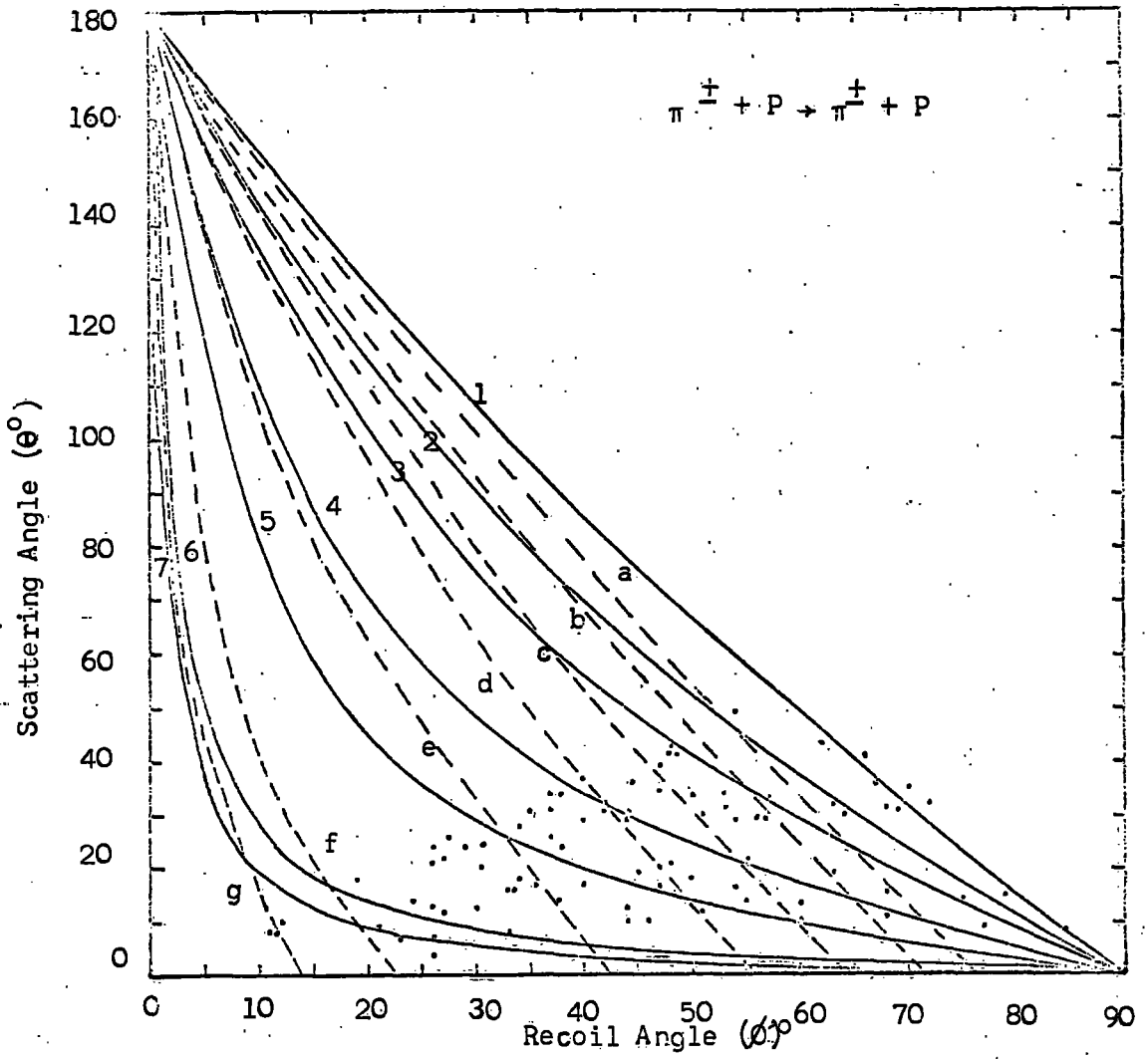

Figure 3.7 The scatter plot for measured scattering angle θ and recoil angle ϕ. Curves (1-8) show a different Kinetic energies for a primary pion T(MeV). Curves (a-g) show different kinetic energies for a recoil proton T_R(MeV).

1 T = 100 MeV
2 T = 500 MeV
3 T = 1000 MeV
4 T = 2500 MeV
5 T = 5000 MeV
6 T = 10000 MeV
7 T = 20000 MeV
8 T = 30000 MeV

a T_R = 100 MeV
b T_R = 200 MeV
c T_R = 400 MeV
d T_R = 800 MeV
e T_R = 2000 MeV
f T_R = 10000 MeV
g T_R = 20000 MeV

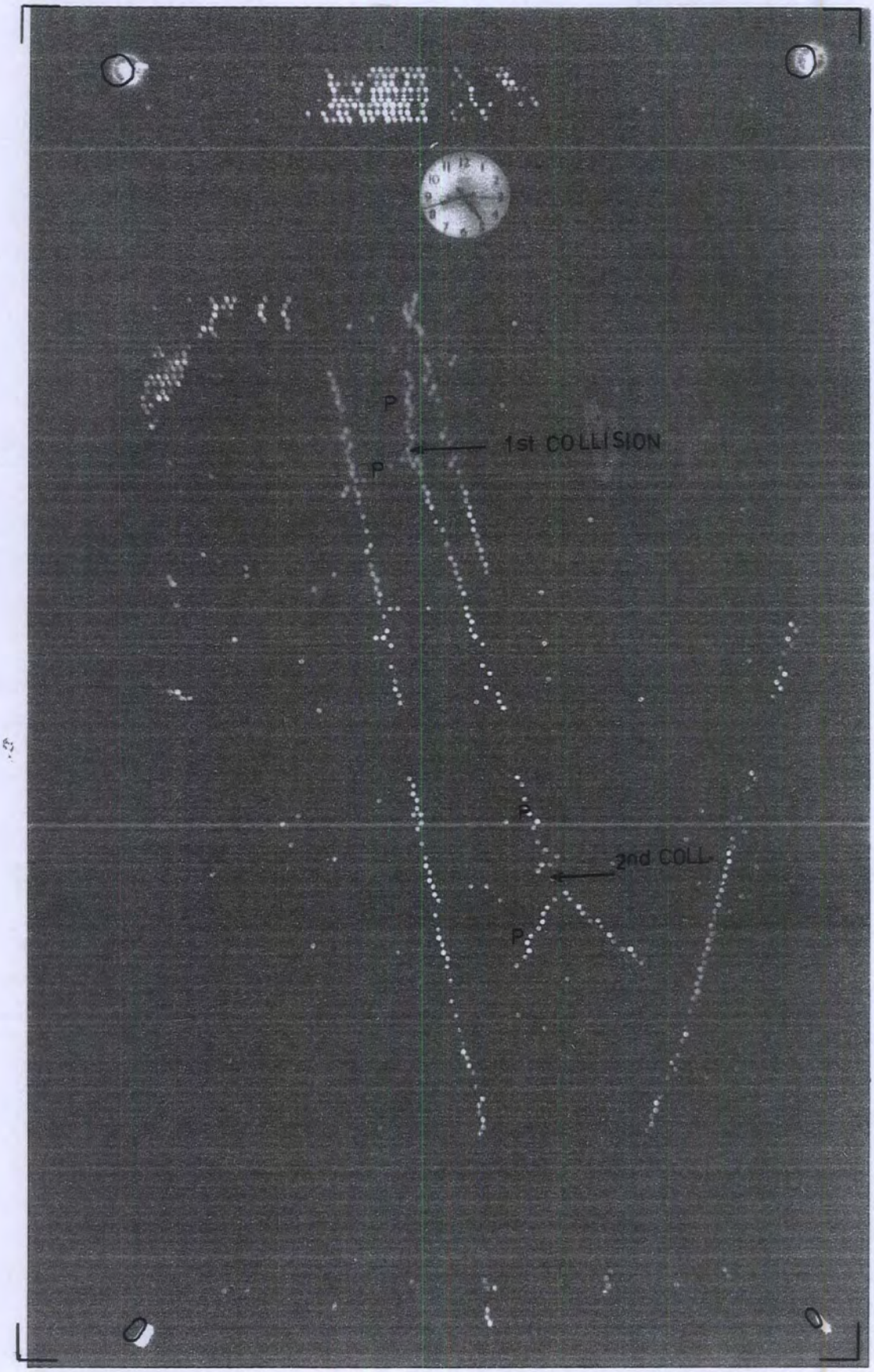

Plate 3.2 Event (E50-18)

Example of an EAS particle undergoing 2 successive elastic collisions on protons. The analysis described in the text shows the EAS particle to be a proton.

relativistic primary particles which begin to break down the non-relativistic approximation. The relation between the mass ratio (M/M_p) and the Kinetic energy of the primary particle for pp collision and π p collision is shown in figure 3.8 and figure 3.9.

It shows that M/M_p increases rapidly with the increase of the primary energy.

A single event E50-23 at high apparent mass, M/M_p = 11.1, was observed as a heavy mass candidate particle. The most likely interpretation is that it is due to a primary proton having energy $\sim$20 GeV and scattering through a small angle. This is shown in plate 3.3. It could also be explained that the increase in the width of the mass distribution is due to the error involved in using projected angles rather than true spatial angles. The heavy mass candidate has a geometry such that the plane of the scattered particle and recoil proton could be at a maximum angle of 70° to the axis of the flash tubes. Taking this to be so means that the spatial value of θ and ϕ are $\sim$3 times the measured projected value. Using these extreme values to find M/M_p gives M/M_p = 1.15 which is consistent with a pp collision.

3.5.3 Conclusion

Obviously the measurements should be repeated using a chamber constructed of alternate layers of crossed flash tubes so that true spatial angle of elastic scatters can be measured. In this case the test that the incident track, scattered track and recoil proton all lie in one plane could be used as an additional identification test for elastic scatters on essentially free protons.

Basing the result on one possible event the present result shows that the flux of heavy mass particles (irrespective of their charge) with $\beta < 0.8$ in regions of EAS of electron density $> 40 m^{-2}$ is $< 3.3\ 10^{-12}$ $cm^{-2} sec^{-1} st^{-1}$. This limit refers to particles capable of penetrating

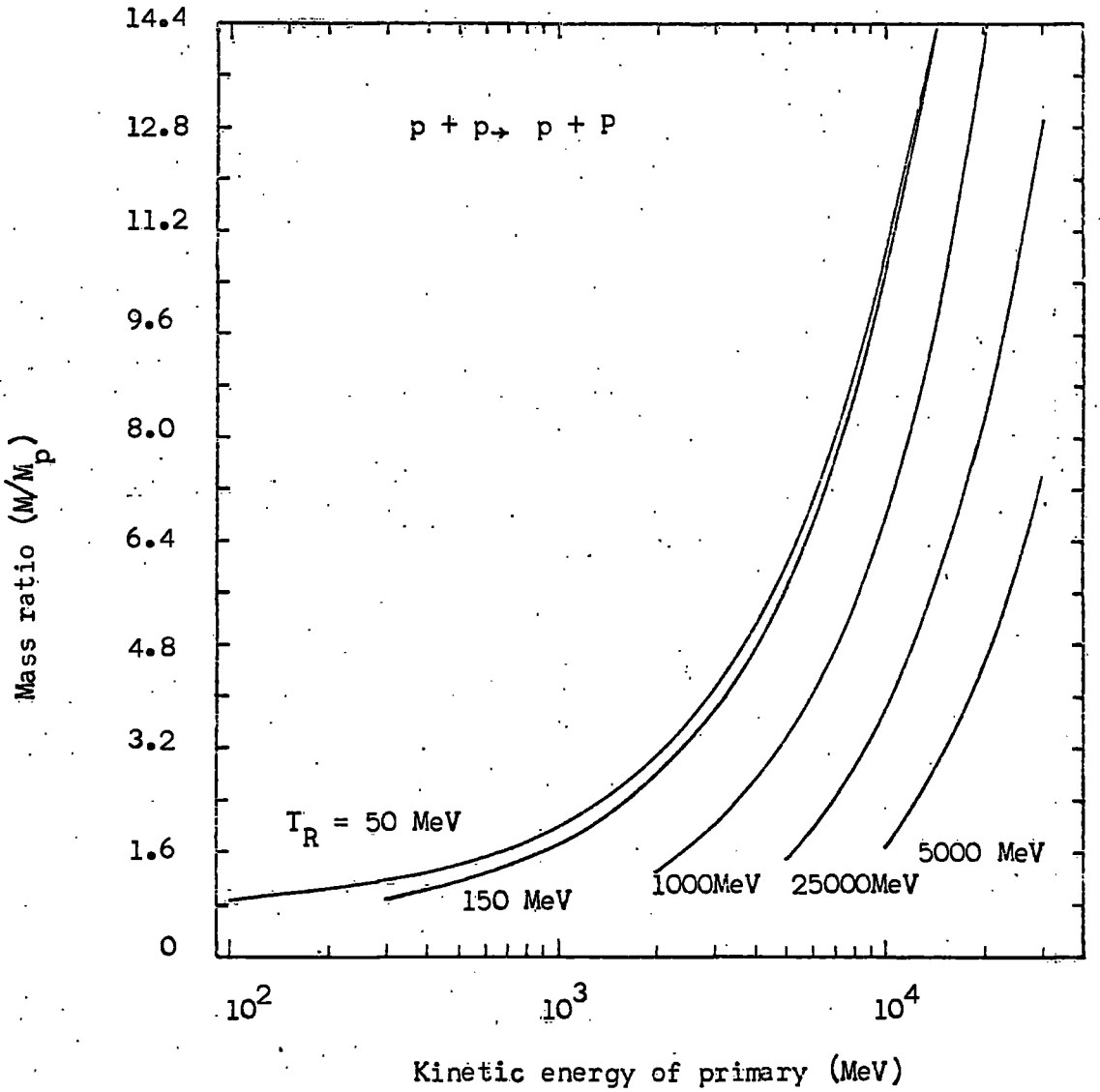

Figure 3.8 M/M_p - Kinetic energy of primary proton relation, for different recoil proton energies T_R(MeV).

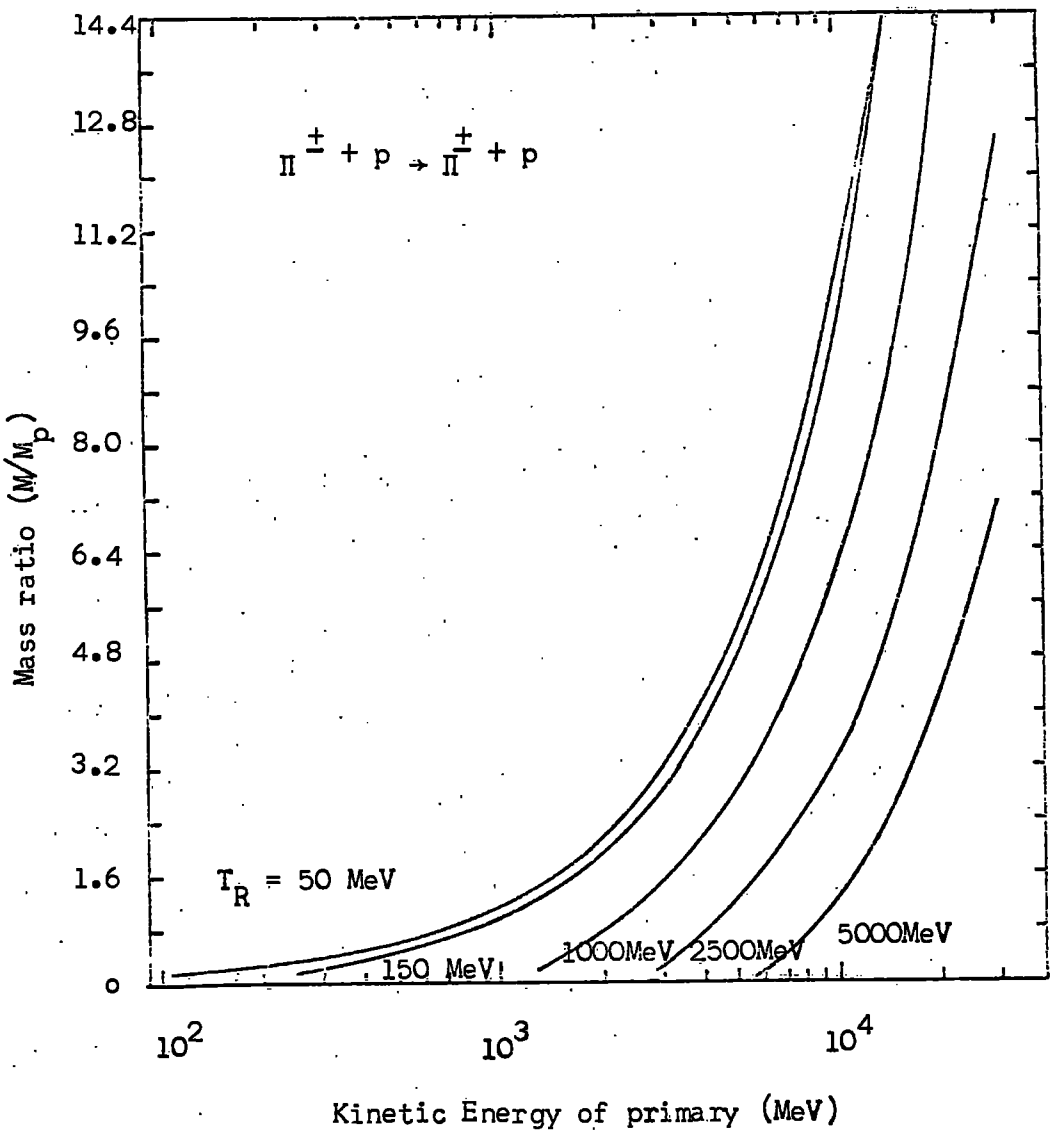

Figure 3.9 M/M_p - Kinetic energy of primary pion relation, for different recoil proton energies T_R(MeV).

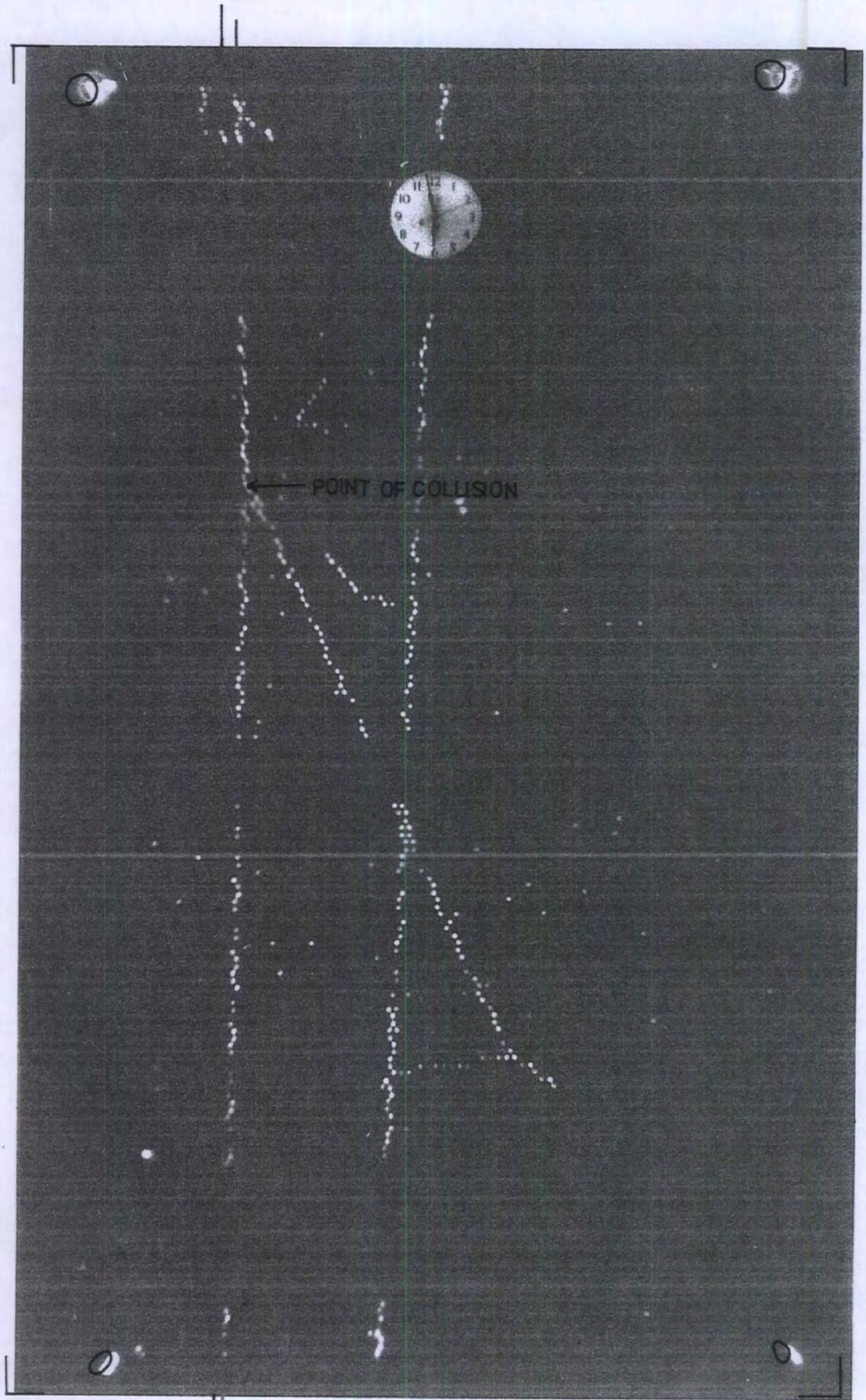

Plate 3.3 Event E50-23

A possible heavy mass particle indicated

15cm of lead, 15cm of iron and producing elastic collision on proton in ~ 15cm glass.

3.6 Mass determination of stopping cosmic ray particles in EAS

3.6.1 Introduction

This method provides another possible way to measure the mass of heavy particles having integral charge and is discussed below.

Suppose the measured root mean square (rms) angle of scattering of a particle with residual range R is $\langle\theta\rangle$. If the rms angle of scattering is determined from sampling the scattering in elements of path of length t radiation lengths ($t \ll R$), $p\beta c$ can be found from (Rossi 1952).

$$\langle\theta\rangle = \frac{K\, t^{\frac{1}{2}}}{p\beta c} \quad , \text{ where } K = 21 \text{ MeV}$$

The rest mass of a particle can be determined from the residual range measurement R and the $p\beta c$ determination.

Low energy particles lose kinetic energy only by ionisation in travelling to the end of their range for which

$$-\frac{dE}{dx} = \frac{1}{\beta^2} f(\beta)$$

This equation is independent of the mass of the ionising particle. Writing $E = Mc^2(\gamma - 1)$ and integrating, the range of a particle of rest mass Mc^2 can be shown to be $R = AMc^2F(\beta)$, where A is a constant, Using these results gives

$$\frac{R}{p\beta c} = \frac{AMc^2F(\beta)}{\gamma Mc^2\beta^2} = \phi(\beta)$$

This expression is independent of the particle mass and depends only on β.

3.6.2 Experimental technique

The trajectory of all the stopping particles is observed to be ~~closely~~ approximately circular except very close to the end of its range. For a

chord of length ℓ (ℓ is the line joining the points where the trajectory started in a circular path to the stopping point.) the angular deflection of the trajectory is related to the sagitta by $\Delta = \ell/8\,\theta$. Where Δ is the maximum perpendicular distance from the chord to the scattered trajectory. By measuring Δ and ℓ experimentally the value of θ is found.

Using the maximum track length available to do this the resulting value of θ is identified with $\langle\theta\rangle$ and $p\beta c$ was found from:

$$\langle\theta\rangle = \frac{1}{\sqrt{2}} \quad \frac{K\, t^{\frac{1}{2}}}{p\beta c} \qquad (K = 21 \text{ MeV})$$

where $t = 3.28$, the amount of material contained in F2 and F3 in radiation lengths. The factor $1/\sqrt{2}$ accounts for the fact that projected angles rather than spatial angles are measured. The residual range associated with this value of $p\beta c$ is taken from the mid point of the trajectory over which the sagitta is measured to the stopping point. Using the measured value of the range R and the momentum $p\beta c$ the value of β can be found from the universal curve shown in figure 3.10 which is independent of the mass of the particle. This curve has been calculated for an aluminium absorber, (note that the curve is closely valid for glass which has a similar average Z and A to aluminium), using the range - energy tables of Serre (1967).

Once β is measured, the mass can be found

$$Mc^2 = \frac{(p\beta c)(1-\beta^2)^{\frac{1}{2}}}{\beta^2}$$

3.6.3 The results

The types of decay events which have been observed in regions of extensive air showers of a local electron density $> 40 m^{-2}$ are shown in plates 3.4, 3.5 and 3.6 and their frequency of occurrence

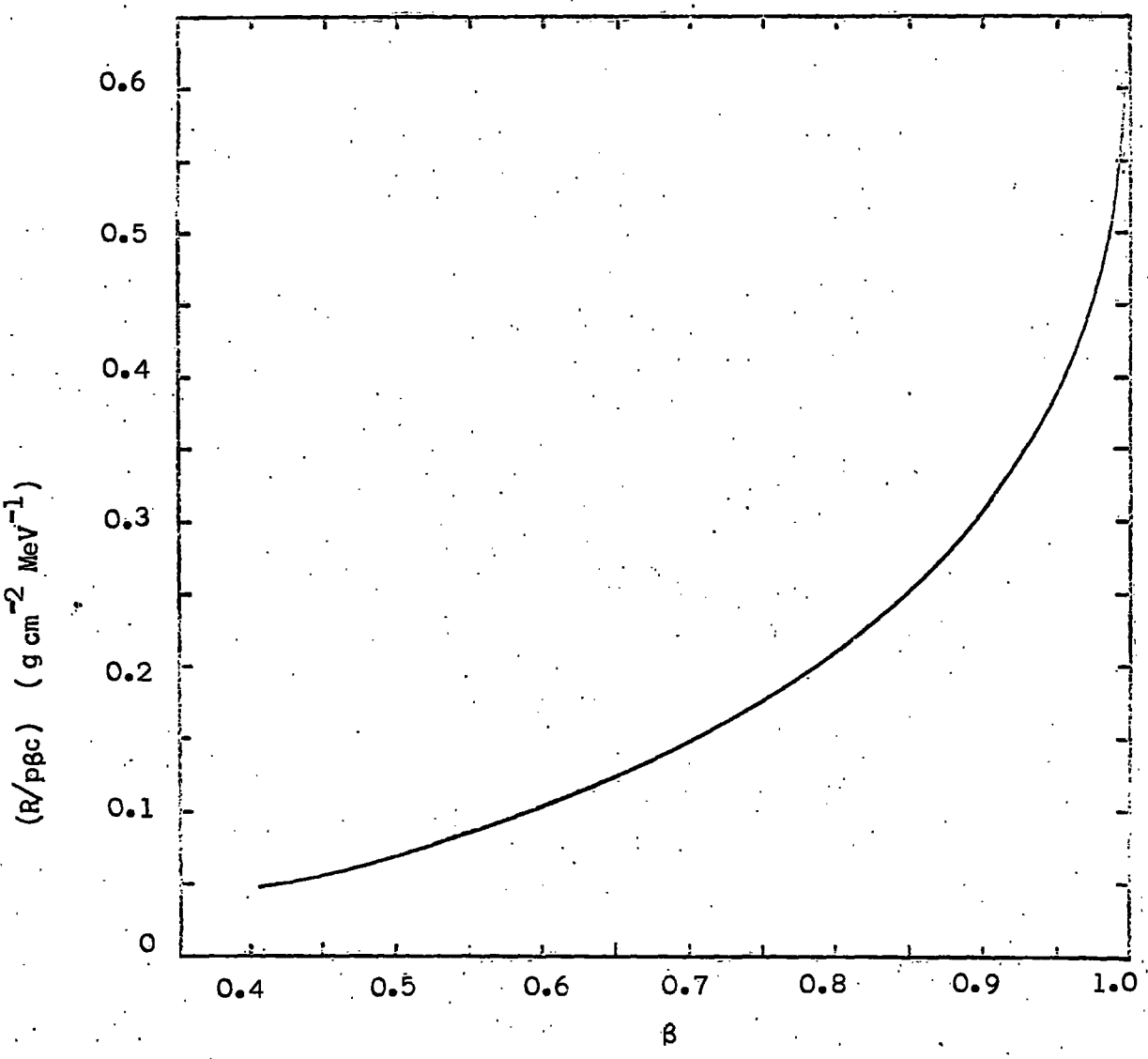

Figure 3.10 $\frac{R}{p\beta c}$ - β curve calculated for aluminium
(The curve is valid for any particle rest mass and also closely valid for glass which has a similar average Z and A to aluminium.)

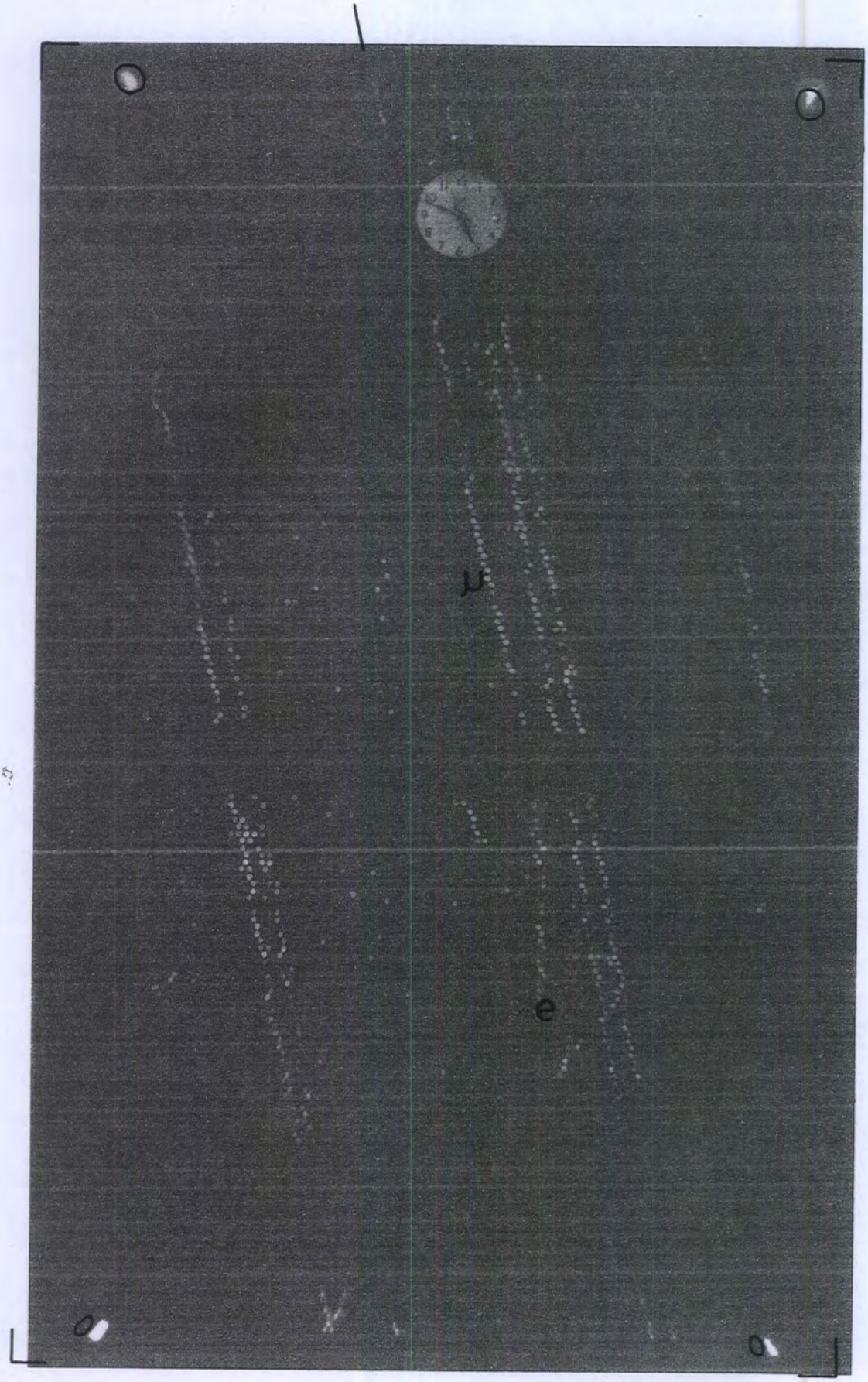

Plate 3.4 Event (E33-155)

Type 1. Possible μe decay or $\pi \mu e$ decay

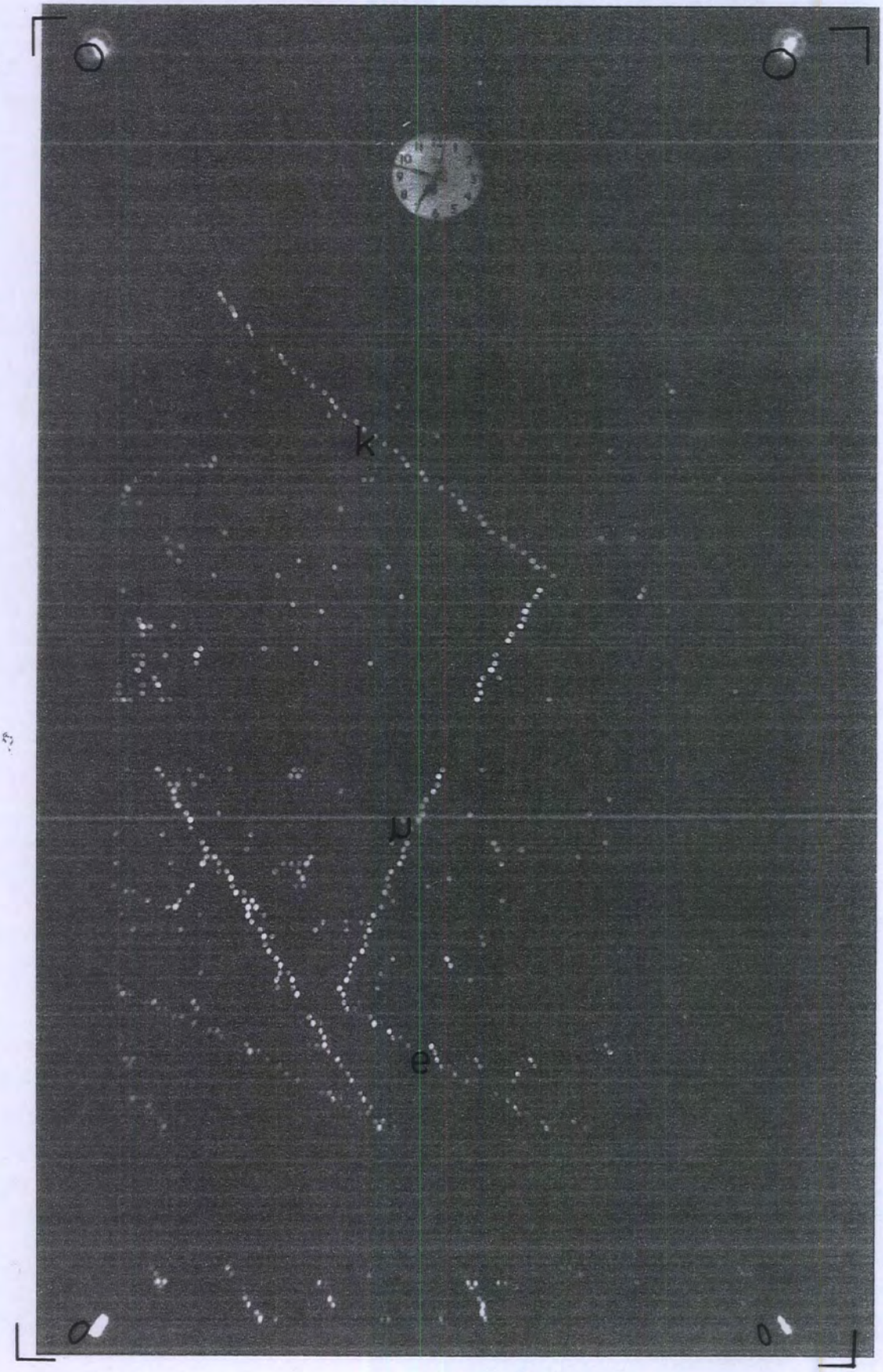

Plate 3.5 Event (E24-204)

Type 2. K →μ→ e decay.

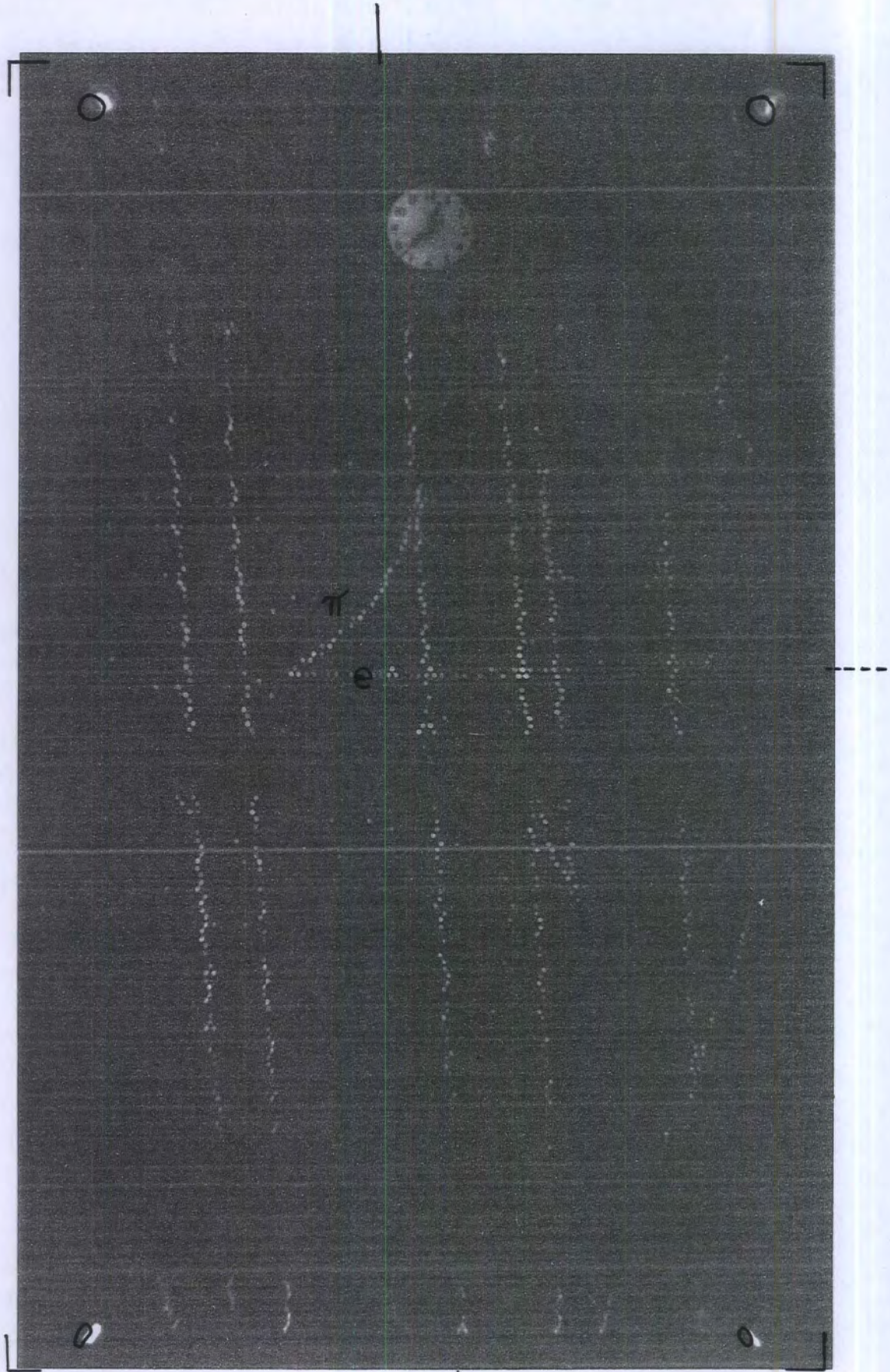

Plate 3.6

Event (E30-72)

Type 3. Electroproduction of a pion by a muon or decay of a heavy mass particle.

in the sample of 12,057 photos is shown in table 3.4. The scatter plot of the range R as a function of the momentum $p\beta c$ is shown, figure 3.11. The curves of muons, pions, kaons and protons are calculated from Serre tables (1967). The curves for 10 electron masses and 10 proton masses are calculated from, Rossi (1952). It can be seen, from figure 3.11 that the maximum value of $p\beta c$ measurable in this work was 710 MeV and this corresponds to a sagitta (Δ) cm measurement (precision 1 cm) for the trajectory from the top of F2 to the bottom of F3.

Event type	Description	Number of events observed	(%) of photos showing events type
1	Multiply scattered particle produces 1 (or 2)(or 3) charged secondaries	200 (24) (9) Total=233	1.7% (0.2%) (0.08%)
2	$K \rightarrow \mu \rightarrow e$ decay signature	2	0.02%
3	Electroproduction of a pion by a muon, or decay of a heavy mass particle	1	0.01%

Table 3.4 The observed frequency of occurrence of decay events in a sample of 12,057 photos.

The rest mass of each primary particle was estimated by measuring multiple scattering and residual range and the resulting mass distribution for 233 primary particles decays in the chamber and produced secondaries is shown in figure 3.12. In this figure also the mass distribution of 140 particles (from 233) entering the chamber parallel to the shower tracks and the mass distribution of 93 particles (from 233) emerging from a local interaction in the 15cm lead or 15 cm iron absorber. The following values of density ρ and

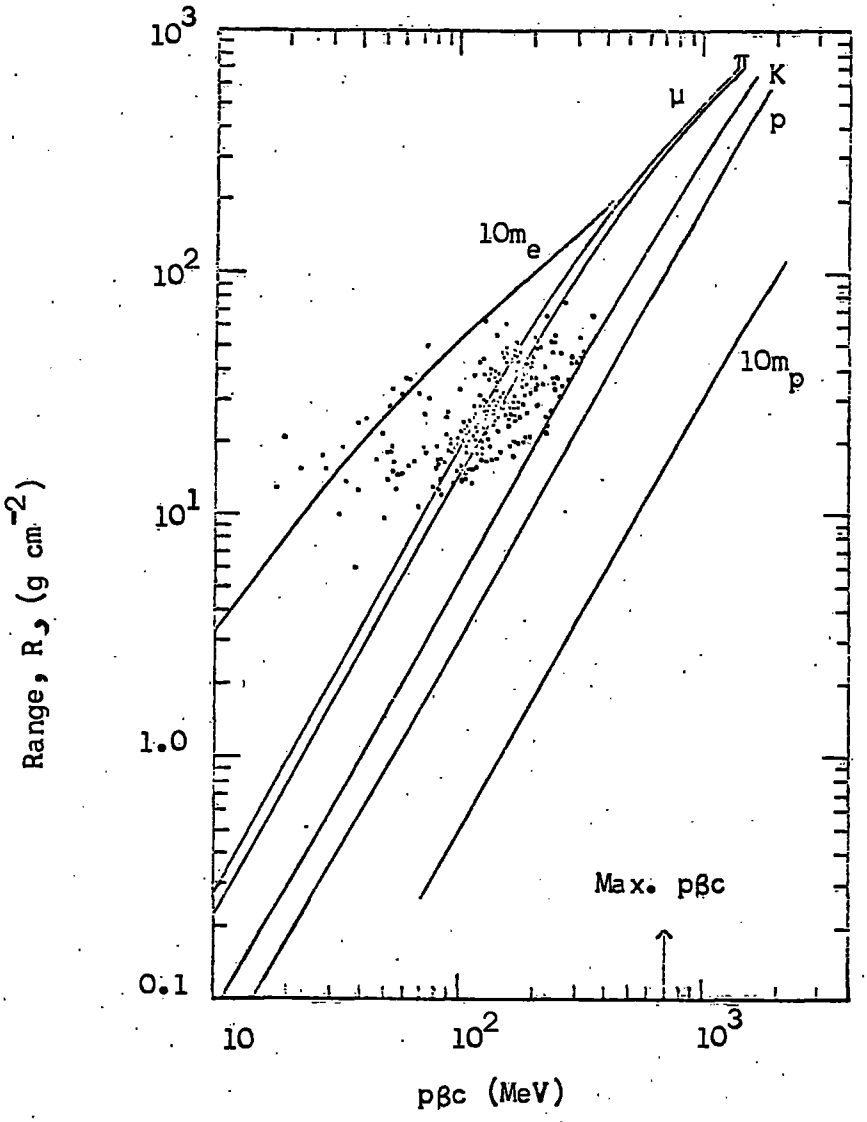

Figure 3.11. The scatter plot of Range - pβc of 233 stopping particles in EAS observed in flash tube chamber.

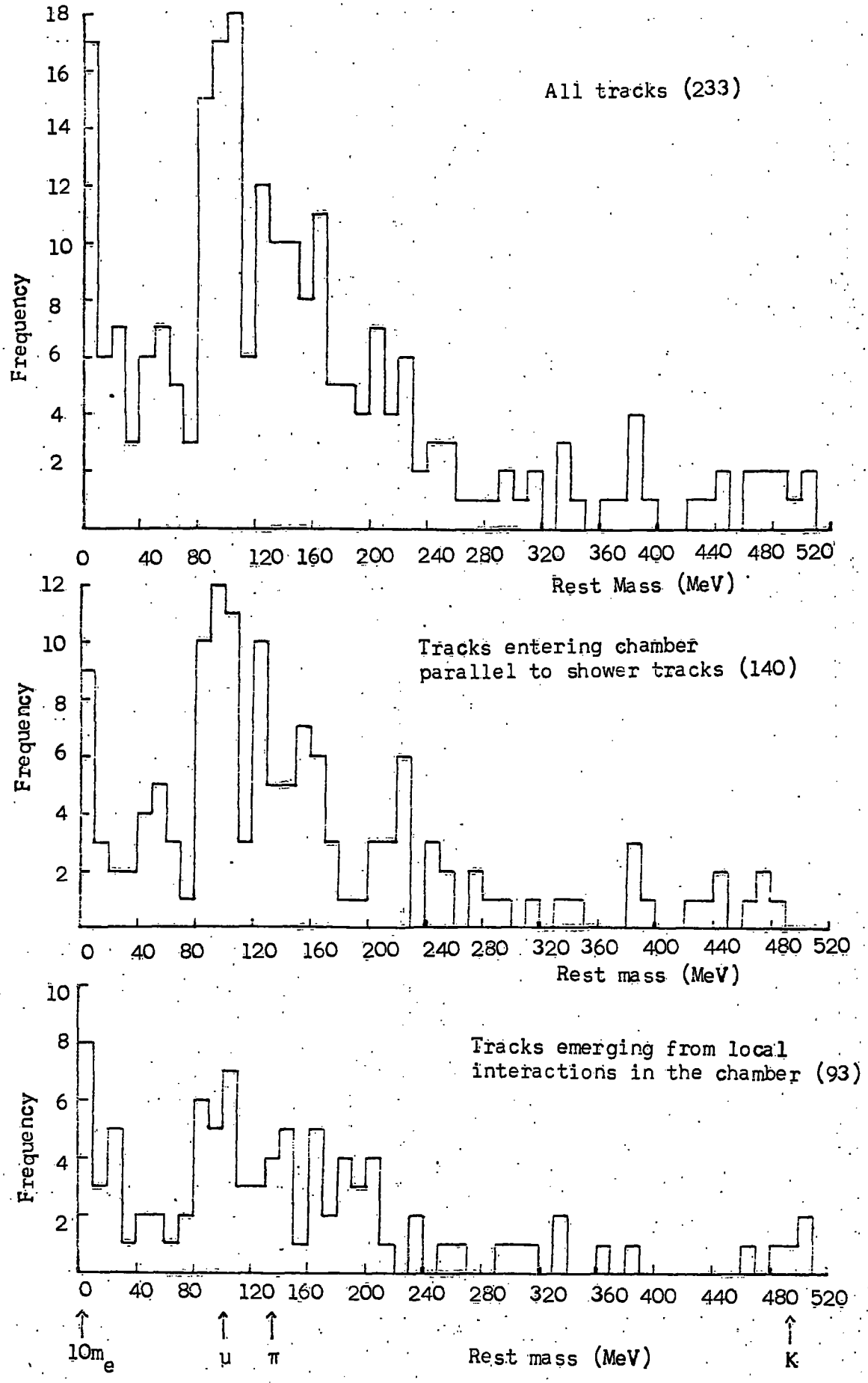

Figure 3.12 The mass distribution of the stopping EAS particles.

radiation length x_o were used in the calculation:
glass (ρ = 2.5 g cm^{-3}, x_o = 28.4 g cm^{-2}), aluminium (ρ =2.7 g cm^{-3}, x_o = 26.3 g cm^{-2}).

3.6.4 Discussion

The result from the mass distribution shows that most of the decays observed in the chamber were muons, pions and a few kaons.

No heavy mass particle (>10Mp) has been observed using this method, because the minimum sagitta (Δ) which can be measured in this technique on the chamber is 1 cm and this gives a mass particle ν (> m_p) which have a maximum pβc = 710 MeV in the middle of F2 and F3.

The low mass values (<10m_e) are probably due to π^+ mesons which suffer nuclear as well as Coulomb scattering and this effect would underestimate p βc and give spuriously low mass values. The most likely interpretation for the events of type 1 (plate 3.4) which show a single secondary charged decay particle are either μe or $\pi\mu$ e decays. The muon from pion decay at rest has a range 1 flash tube, this corresponding to 4 MeV muon kinetic energy, and the muon would not be resolved. The type 1 events showing 2 chargedsecondaries are presumably not decays but it could be $K^- + n \rightarrow \pi^- + \Lambda (\rightarrow p + \pi^-)$ in which the recoil proton is not observed. The type 1 events showing 3 charged secondaries could be kaon decays, e.g. $K^{\pm} \rightarrow \pi^{\pm} \pi^- \pi^+$ with branching ratio 6%.

Two events of type 2 (plate 3.5) were observed and these are consistent with kaon decay as $K \rightarrow \mu\nu$ with branching ratio 64% followed by muon decay as $\mu \rightarrow e \nu_e \nu_\mu$. The range of the muon from kaon decay at rest is 68 g m^{-2}, this corresponding to 153 MeV muon kinetic energy.

One event only of type 3 has been found, and this is of particular interest as such an event signature would be produced by $M_1^+ \rightarrow M_2 + \pi^+$

where M_1 and M_2 are heavy mass particles. The more likely explanation of this event is electroproduction of a pion by a muon ($\mu p \rightarrow \mu\, n\pi^+$). It can be seen from the event (plate 3.6) that the pion stopped in the chamber after undergoing multiple scattering and the decay electron from muon decay is observed to cross the chamber horizontally. As explained above the muon from $\pi\mu$ decay at rest would not be observed.

3.7 The neutral particles in EAS

The decay and interaction of a number of neutral particles in regions of EAS have been observed and an attempt has been made to interpret the observarions in terms of known elementary particles. Scanning the films showed 65 events in which a neutral primary particle produced two charged secondary particles. This type of event is shown in plate 3.7, the direction of the neutral particle being parallel to the shower direction.

The visible kinetic energies of the secondary particles were calculated assuming their ionisation loss was 2 MeV/g cm^{-2}. The scatter plot of the opening angle between the two charged secondary particles emerging from neutral particle decay or interaction versus the sum of the visible kinetic energy of the secondary particles has been shown in figure 3.13.

The theoretical curves are drawn for comparison and refer to the rms angle $\langle\theta\rangle$ between the trajectory of a secondary electron (muon) of energy E' and that of the primary photon of energy E in the electron (muon) pair production process where $\langle\theta\rangle$ is given by an expression of the form:

$$\langle\theta^2\rangle_{av}^{\frac{1}{2}} = q'(E,E',Z)\ \frac{mc^2}{E}\ \ln\left(\frac{E}{mc^2}\right)$$

where mc^2 is the mass of the electron (muon) and the function $q'(E,E',Z)$ is the order of unity (Rossi, 1952).

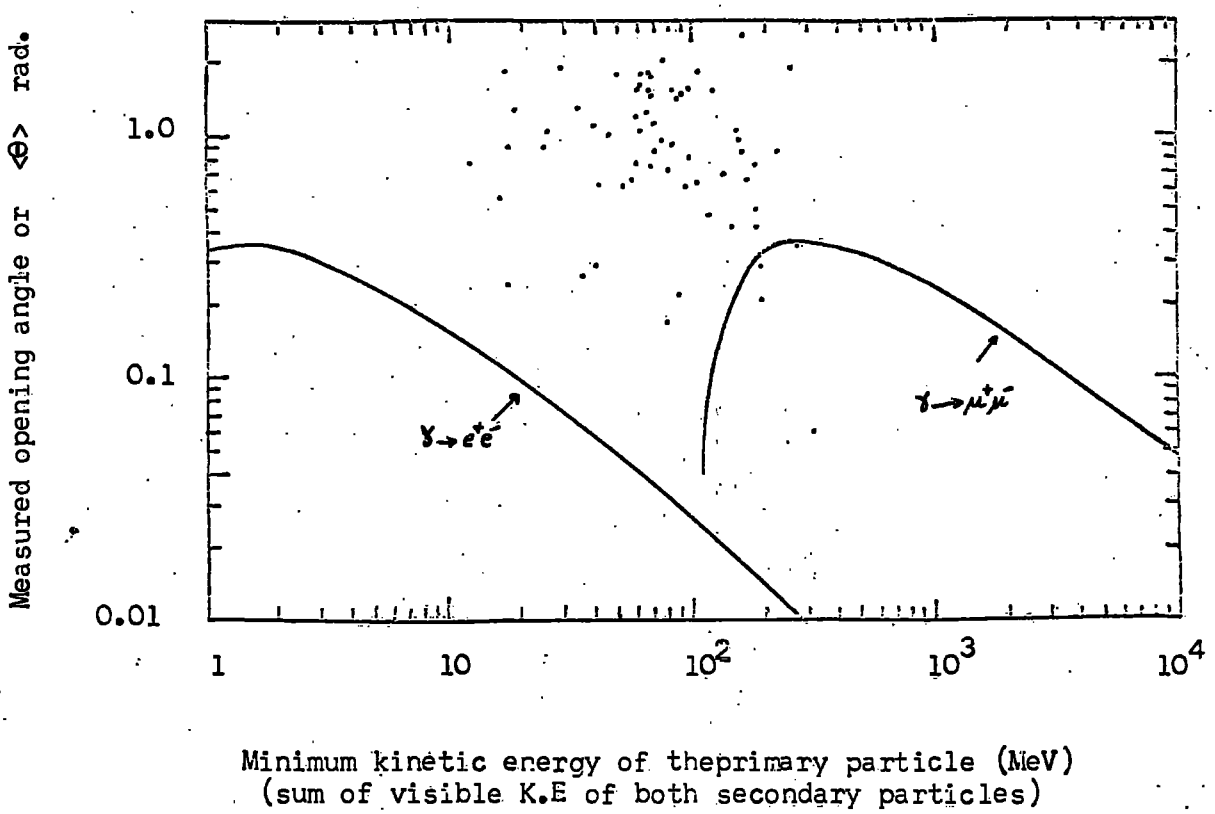

Figure 3.13. The scatter plot of 65 neutral particle events showing the correlation between the opening angle and the minimum kinetic energy (K.E) of the primary.

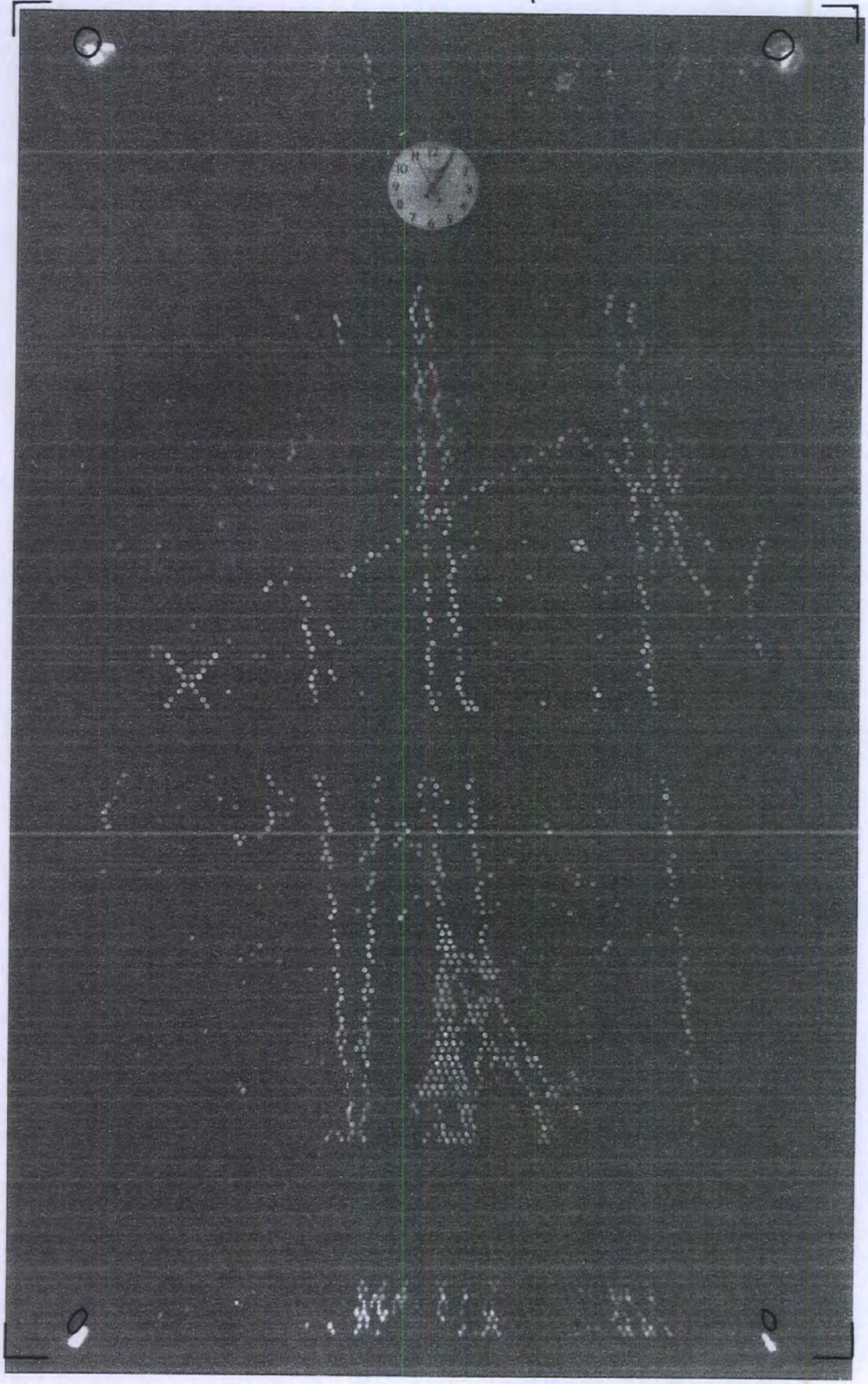

Plate 3.7 Event (E54-141)

Neutral particle decay in same shower direction

It could be explained, that the events with opening angle close to 90^{o} are produced by low energy neutrons ($\sim$1 GeV) which knock on a proton which then collides with a proton in the same nucleus so that two charged secondaries are observed with the characteristic non-relativistic pp elastic scattering opening angle of 90^{o}. However the events with smaller opening angles may well be neutral kaon decay to two charged pions.

A comparison has been made between the prong number frequencies produced by low energy (multiple scattered) charged (see table 3.4 section 3.6.3) and neutral primary particles. Table 3.5 shows the data obtained from scanning 12,057 photos.

Number of prongs	Charged primary particle	Neutral primary particle
1	200	Not measurable
2	24	65
3	9	3
4	0	8
5	0	2

Table 3.5. Comparison between the prong number distributions produced by charged and neutral primary particles.

3.8 The low energy particles in EAS

From scanning the films, 57 low energy EAS particles were found showing a multiple scattering shape in traversing F2 and F3 through the chamber in the same direction as the other shower tracks. The sagitta ($\Delta > 1$ cm) was measured as a maximum perpendicular distance from the chord formed by the line joining the points where the trajectory crossed the top of F2 and the bottom of F3 to the scattered trajectory figure 3.14.

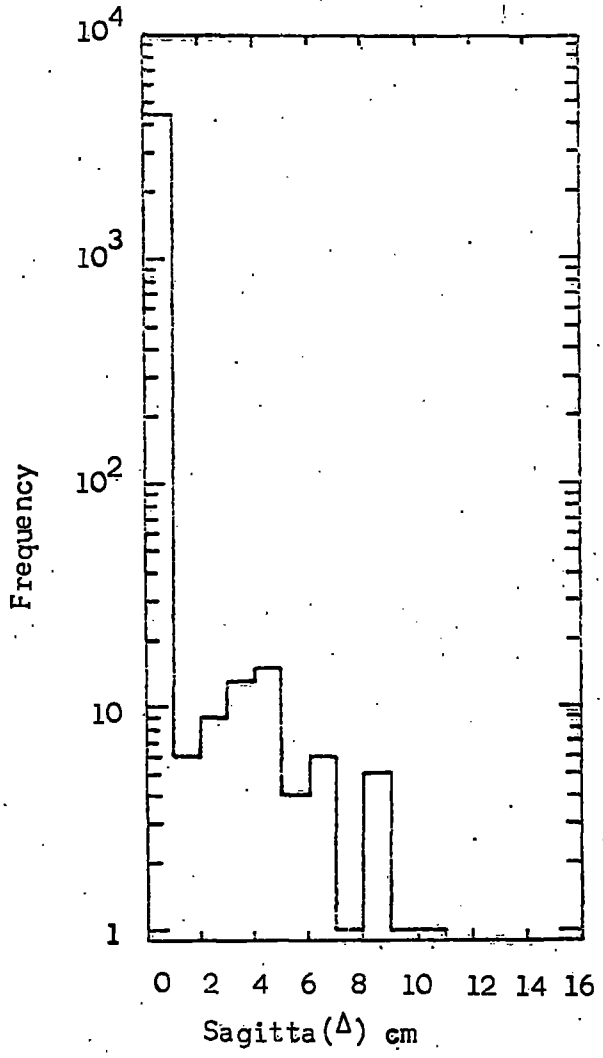

Figure 3.14. The scattering distribution for 4501 measurable tracks in EAS through the chamber.

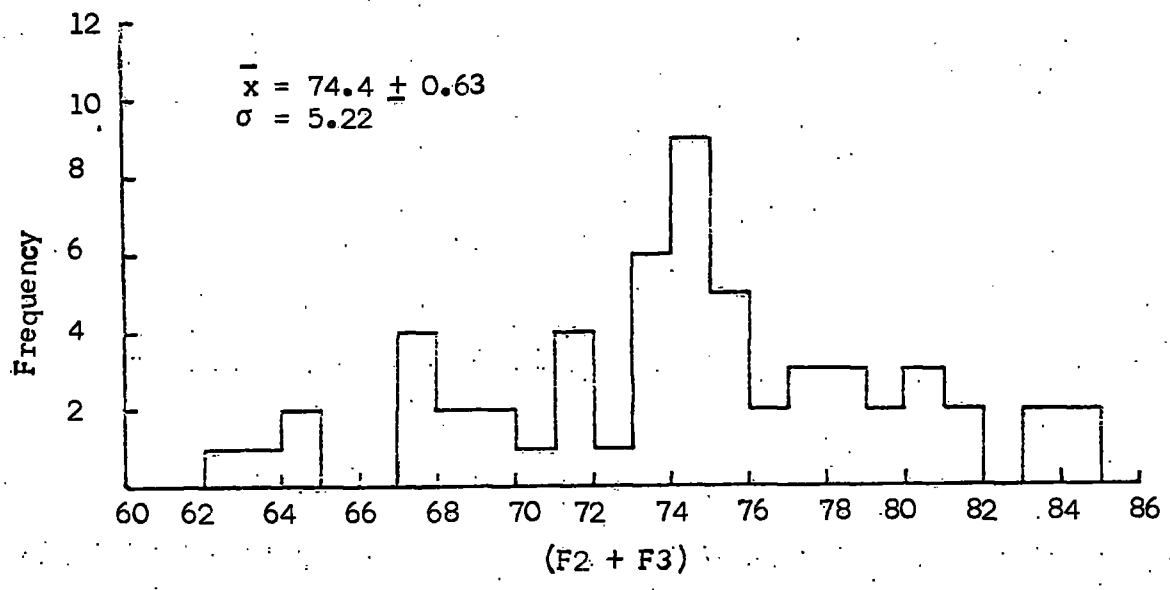

Figure 3.15. The frequency distribution of the number of flashes in F2 and F3 for 57 multiple scattering EAS tracks.

Particles of low velocity lose energy by ionisation only and the rate of energy loss by a particle of charge (Ze) in material of atomic number Z can be written as (Rossi, 1952):

$$-\frac{dE}{dx} = \frac{2C\, m_e G^2 Z^2}{\beta^2} \left[\ln \left(\frac{4\, m_e^2\, C^4\, \beta^4}{(1-\beta^2)^2\, I(Z)} \right) - 2\beta^2 \right]$$

where I(Z) is the average ionisation potential and C = 0.150 Z/A cm^2/g.

The number of flashes in F2 and F3 were counted for each multiply scattered EAS track and the distribution of the number of flashes in F2 and F3 for 57 tracks is shown, figure 3.15.

One can expect that these might be due to low energy background incoherent muons which are multiply scattered in traversing the chamber. 12% multiply scattered tracks with sagitta ($\Delta > 1$ cm) have been observed from a sample of 5,283 incoherent muons passing through the chamber.

Calculation shows that the expected number of the multiply scattered background tracks parallel ($\pm 5^\circ$) to the shower direction and in the region F2 + F3 between 60-77 flashes was 16. This figure is to be compared with observed number of 40 in the same range. Thus these results suggest that most of the particles in an air shower core are on the plateau of the ionisation curve. Some, however, may be on the minimum of the curve.

3.9 The recovery time of the neon flash tubes

A number of events were observed in which a dense shower caused flashes in most of the tubes and this was followed later by an event showing low efficiency muon tracks.

The interesting point in this problem is that, the efficiencies of these muons is similar to the efficiencies which can be caused by fractional charge particles (quarks). When a single relativistic

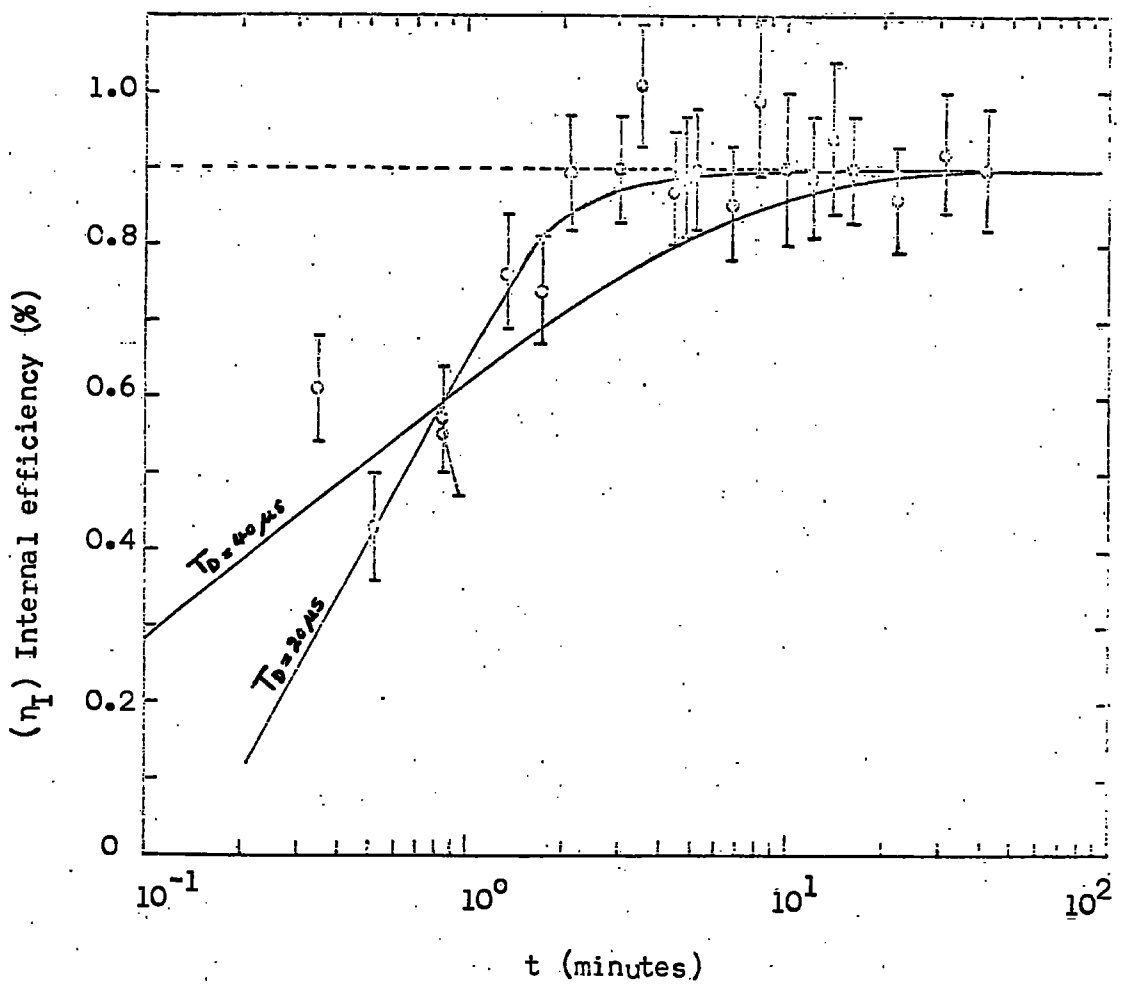

Figure 3.16 Reduction of efficiency due to remnant clearing field.

particle traverses a tube some ion pairs are produced along its track and during the application of the high voltage pulse the electrons are accelerated towards the positive electrode and multiplication produces breakdown. Photons cause the discharge to be propagated rapidly along the full length of the tube. The positive ions move more slowly towards the negative electrode and, if the applied pulse is long enough, some will reach the wall. After the cessation of the pulse there will be many electrons and positive ions adhering to the glass and it is considered that it is these which are mainly responsible for a remnant clearing field. The magnitude of this field will fall with time because of neutralization of electrons by positive neon ions from the gas and conduction of electrons along the inside surface of the glass to neutralize those positive ions which reached the wall during the pulse.

The efficiency of these muons was measured, with the result shown in figure 3.16. In this figure the internal efficiency (η_I) is given, that is, the layer efficiency (i.e. the number of tubes flashed along the length of the track divided by a number of layers) multiplied by the mean separation of the tube centres and divided by internal diameter.

The curve for T_D= 40μs has been given by Ashton et al (1971), and a comparison is made between this and the present experimental data E1-E69 for T_D = 20μs.

It can be seen that for T_D = 20μs a flash tube has a recovery time to full efficiency of $\sim$ 3 minutes. The time for each event was recorded andthe distribution of time separation of the shower events in films E1-E16 was drawn, figure 3.17. The mean time separation is given by $y = y_o e^{-t/\tau}$. τ was found equal to 17.8 minutes. The rate of the shower corresponds to the value of (τ) is 3.4 hrs^{-1} and the straight line was drawn to give a best fit to the measured events.

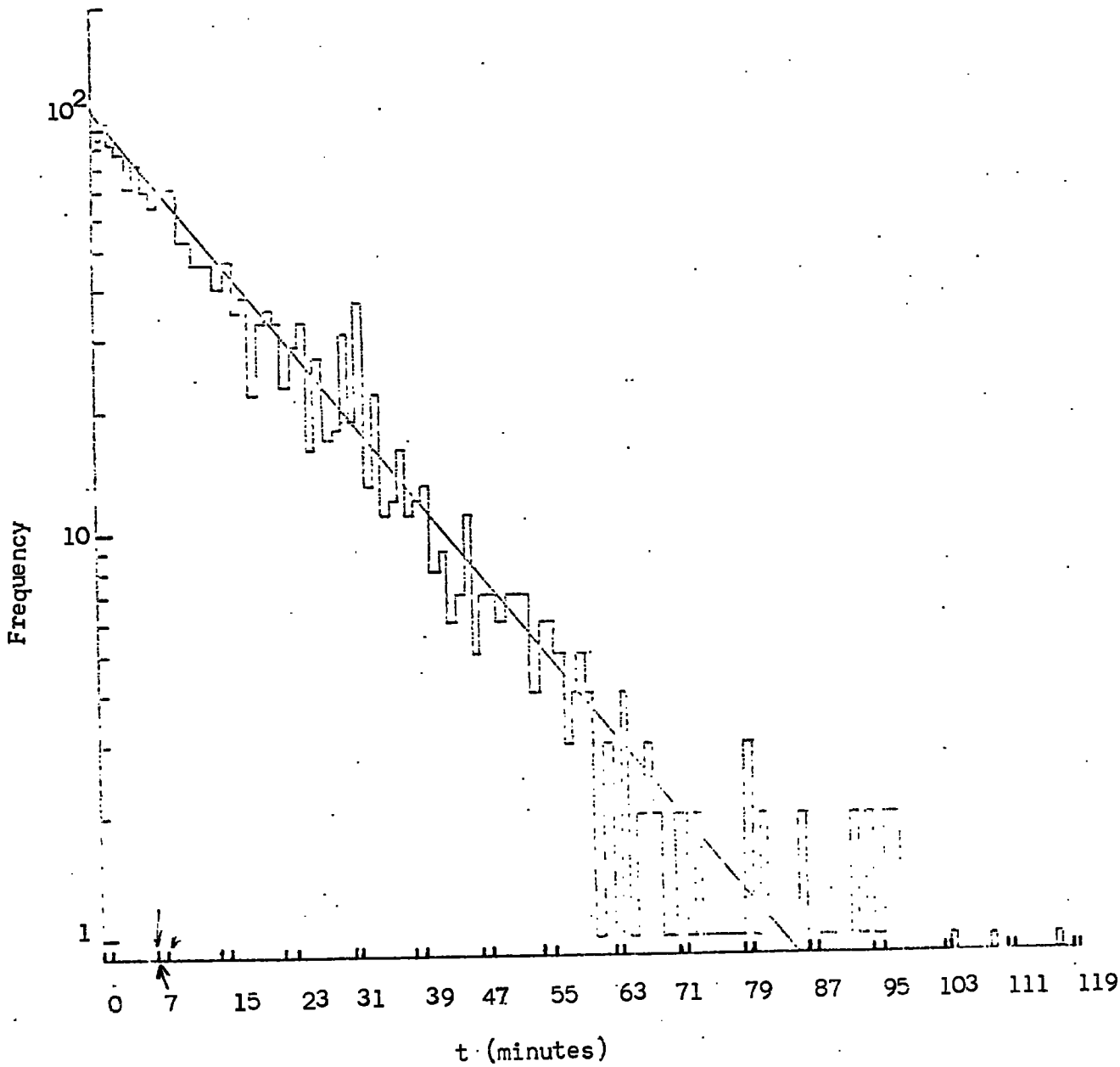

Figure 3.17. The time separation of showers triggering the flash tube chamber. ADC cells are 1 minute wide.

3.10 The angular distribution of accepted particles

The distribution of the projected zenith angle in the front view of the chamber was drawn for all measured air shower triggered tracks and is shown in figure 3.18. In this case a symmetrical distribution about zero angle was obtained and a maximum zenith angle which can be measured for a track passing the top of F1B and the bottom of F4A and produce at least one flashed tube in them is 37^{o}.

A single event E38-98 has been observed during the shower run showing horizontal EAS triggering the chamber and this made an angle about 78^{o} to the vertical.

One can expect an increase in efficiency for tracks of increasing zenith angle, because of the increased track length of the particle in the flash tubes, but this effect is small.

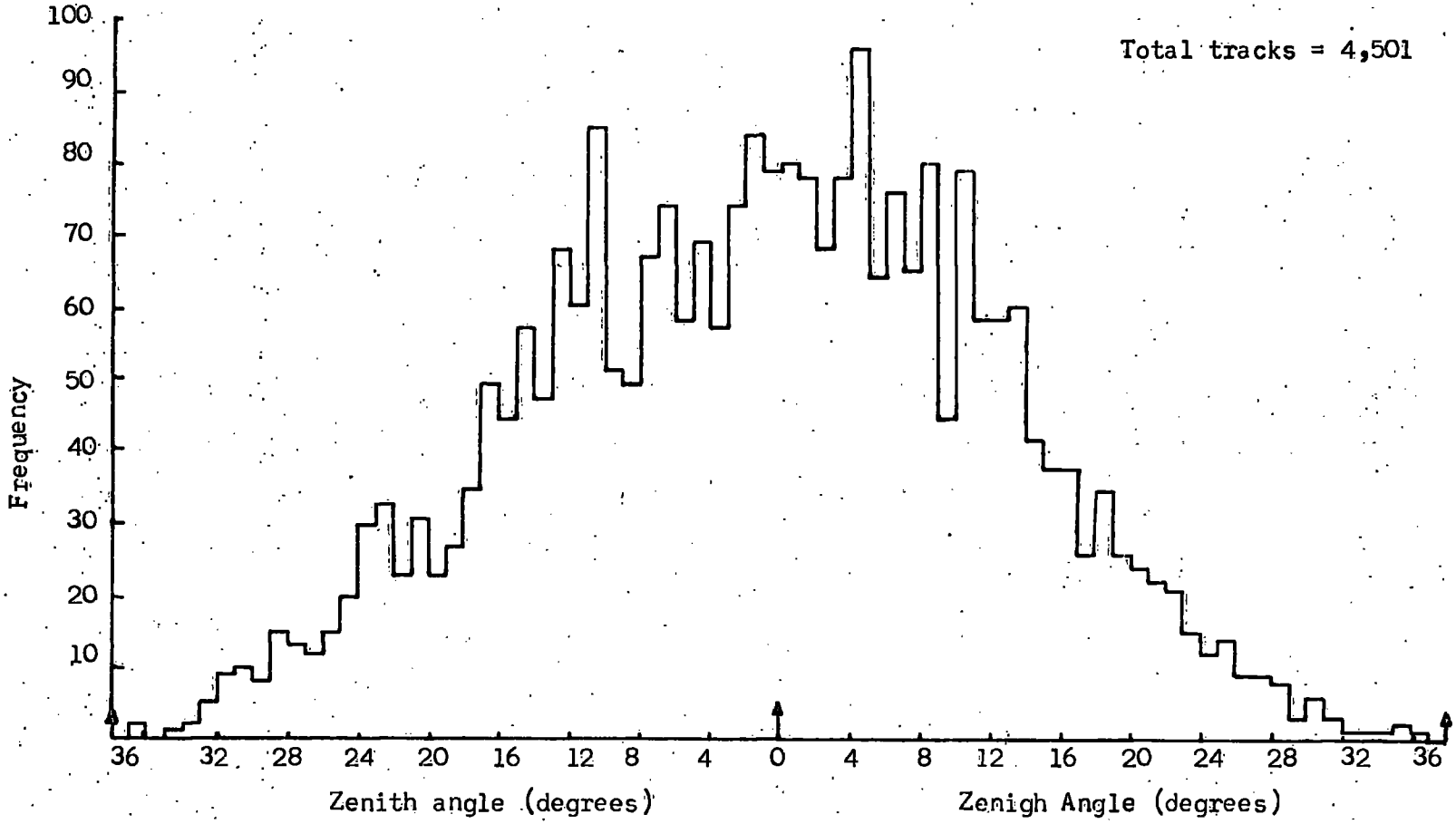

Figure 3.18. The distribution in the ~~project zonigh~~ projected zenith angle for all measured air shower tracks.

CHAPTER FOUR

The Characteristic Interactions of Incoherent Particles in Cosmic Rays Observed in the Flash Tube Chamber

4.1. Introduction

The flash tube chamber is a powerful visual technique for studying the properties of cosmic ray particles. The types of interaction when the incoherent component of cosmic rays at sea level traverses the chamber have been measured and studied. The incoherent muons, muons which arrive at the sea level with neither electronic or muonic accompaniment, are selected by a two-fold coincidence between scintillators A and B with resolving time 0.1μs. As the measured two fold rate was 11.5 $\pm$ 0.4 sec^{-1} a dead time of one minute was imposed between coincidences that triggered the chamber. All the single particle calibration runs, 5,283 single particle events were taken with time delay of 20μs between the occurrence of the single particle and the application of the high voltage pulse to the chamber.

4.2. Classification of the observed events

The interactions produced by incoherent cosmic ray particles traversing the chamber are classified and their frequency of occurrence given. The different types of event observed are shown in figure 4.1 and their frequency of occurrence are shown in table 4.1. It is seen from the table that the most frequent type of events are recoil electron production 37% and significant multiple scattering in F2 and F3 6%.The event types shown in figures 4.1.1, 4.1.2 and 4.1.3 have been studied in detail (next-sections) and the remaining event types except those shown in figures 4.1.5 4.1.6 and 4.1.12 can be understood in terms of either the electro-magnetic interactions of muons or nuclear active particles. The

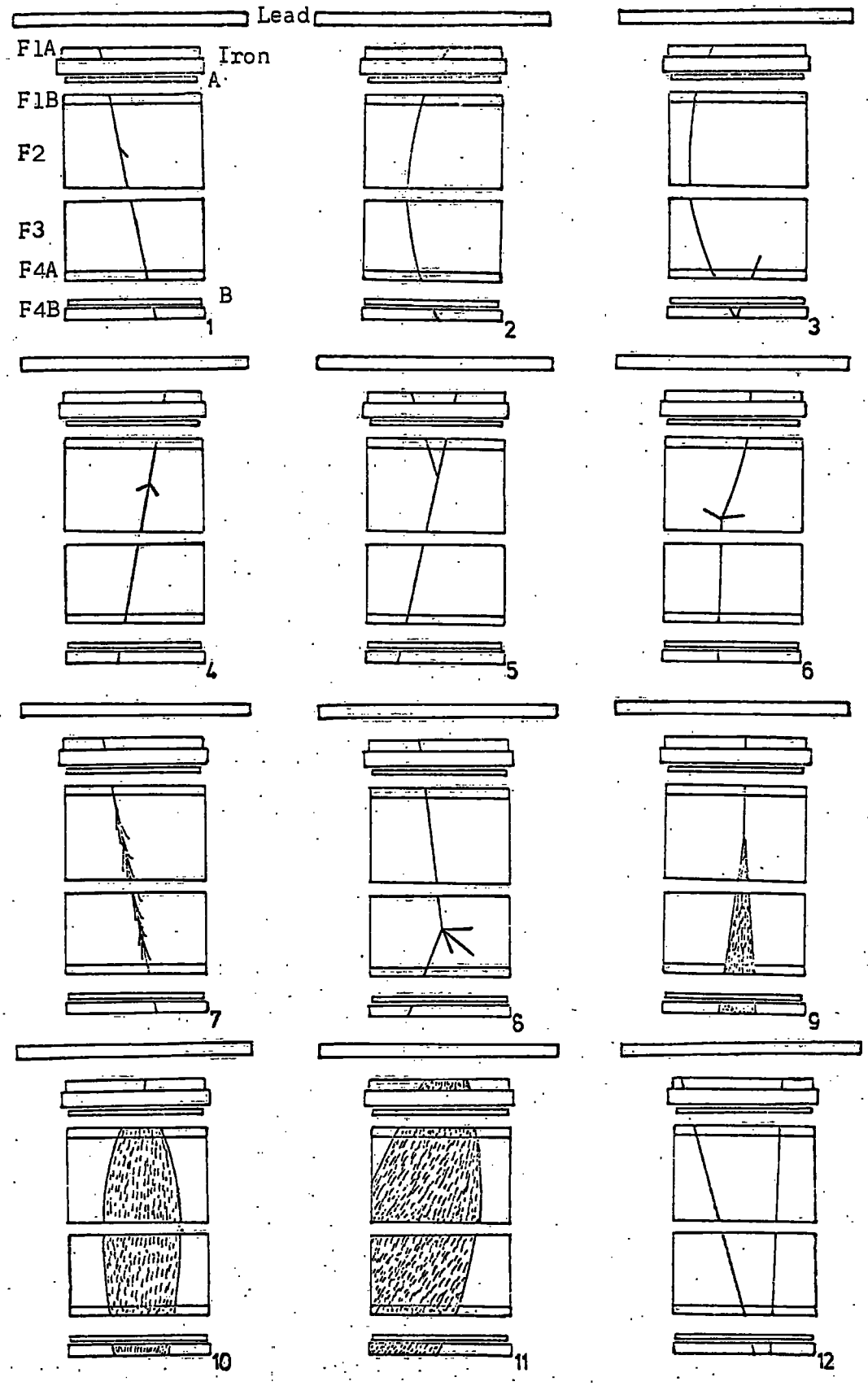

Figure 4.1 Typical interaction of incoherent cosmic ray particles in traversing the flash tube chamber.

Event type (see fig. 4.1)	Description	No. of events observed	No. of photos scanned	% of photos showing event type
1	Straight track with recoil electron of energy > 3 MeV (3 flash tubes)	388	1,046	37%
2	C shaped multiple scattering in traversing F2 and F3 (3.28 radiation lengths) with sagitta > 2cm	330	5,283	6%
	S shaped multiple scattering in traversing F2 and F3 with sagittas > 1 cm	3	5,283	∿0.06%
3	Multiply scattered μ with decay electron in F4	27	5,283	0.5%
4	Interaction in flash tubes from which 2 secondaries emerge from same point.	25	5,283	0.5%
5	Penetrating particle which produces single backward secondary of range > 5 flash tubes	27	5,283	0.5%
	Penetrating particle produces single backward secondary which penetrates 15 cm iron	2	5,283	∿0.04%
6	Stopping particle produces 3 charged secondaries	0	5,283	-
7	Track with close electron accompaniment	4	5,283	∿0.08%
8	Nuclear interaction in flash tubes	13	5,283	0.25%
9	Narrow angle cascade developing from interaction in flash tubes	17	5,283	0.3%
10	Interaction in iron (15 cm thick)	17	5,283	0.3%
11	Interaction in lead (15 cm thick)	7	5,283	0.1%
12	Two penetrating particles. These events include genuine two time coincident particles (resolving time 0.1μs) and events in which a single muon produced the trigger and a background muon traversed the chamber in its sensitive time (∿150μs)	18	1,046	1.7%

TABLE 4.1 The observed frequency of events of the type illustrated in figure 4.1.

event types shown in figure 4.1.5 are probably produced by muon electroproduction of a nuclear resonance followed by decay to the ground state in which a backward pion is emitted, the overall reaction being $\mu p \rightarrow \mu n \pi^+$. 27 events of this type were observed in which the range of the secondary was >5 flash tubes. Two events C9-111 and C14-95 of this type show that the penetrating particle produces a single backward secondary which penetrates 15 cm iron.

No events of the type shown in figure 4.1.6 have been observed in the present work. Only one event of this type has been observed in the previous work (J. King, 1970, Ph.D Thesis) from 1,000 single particles measured. This event shows a stopping particle which produces 3 charged secondaries. This type of event is possibly $K^{\pm} \rightarrow \pi^{\pm} + \pi^+ + \pi^-$ with branching ratio 6%.

Figure 4.1.12 shows two penetrating particles in which a single muon produced the trigger and a second muon traversed the chamber in its sensitive time $\sim$150μs. The track with higher efficiency was presumably the trigger particle and the less efficient one a background track. The mean number of flashed tubes on these 18 tracks was 69.4 in F2 and F3 compared with the triggered particles which have a mean of 74.77 in F2 and F3.

4.3. Knock-on electrons

The interaction of μ-mesons in the glass of the flash tubes producing a knock-on electron with sufficient energy to traverse into the gas of the flash tube was observed. It was assumed that the collision takes place in the centre of the glass which has a mean thickness 0.32 cm. The high energy knock-on electron is ejected at a very small angle to the primary, and in consequence both the primary and the knock-on electron travel together for a relatively large distance. As the energy of the knock-on electron is reduced its angle of ejection and its scattering increase.

The differential collision probability for a particle of mass, m, and spin $\frac{1}{2}$ has been calculated by Bhabha (1938) and by Massey and Corben (1939), and is as follows:

$$\phi_{coll}(E,E')\,dE' = \frac{2\,C\,m_e\,c^2}{\beta^2}\,\frac{dE'}{(E')^2}\left[1 - \frac{\beta^2 E'}{E'_m} + \tfrac{1}{2}\left(\frac{E'}{E+mc^2}\right)^2\right], g^{-1}cm^2$$

where $C = 0.15\ Z/A$

β is the velocity of the incident particle of energy E

$m_e c^2$ is the rest mass of the electron

E' is the energy of the recoil electron.

E'_m is the maximum transferable energy to the electron by a primary particle.

The probability of production of a knock-on of kinetic energy in the range from E' minimum to E' maximum by a muon of energy E is given by:

$$\phi_{coll}(E, > E'_{min}) = \int_{E'_{min}}^{E'_m}\left\{\frac{2C\,m_e c^2}{\beta^2}\,\frac{1}{(E')^2}\left(1 - \frac{\beta^2 E'}{E'_m} + \tfrac{1}{2}\left[\frac{E'}{E+mc^2}\right]^2\right)\right\}dE'$$

The kinetic energy of knock-ons were estimated by the number of flash tubes and electrodes they traversed in F2 and F3. The plot of projected recoil angle as a function of range for a sample of recoil tracks of range > 3 flash tubes is shown in figure 4.2 and the observed range has been converted into electron energy assuming an energy loss of 1 MeV per flash tube and 0.6 MeV per electrode traversed. In this figure, only the knock-ons which have at least 3 flashed tubes on knock-on track are plotted. The expected spatial recoil angles for different electron energies calculated from the kinematics of μe collision for different muon energies is also shown in figure 4.2.

If α is the angle of emission of the electron with respect to the primary and E' the electron kinetic energy produced by a muon of momentum p (Kannangara and Zivkovic, 1953), then,

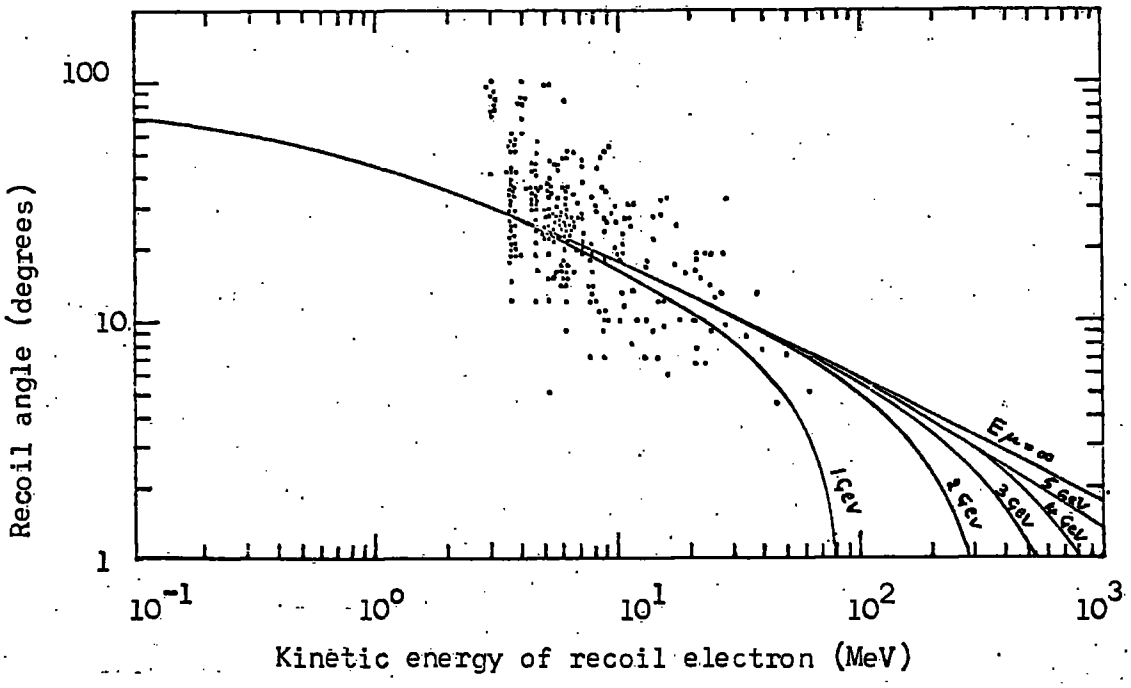

Figure 4.2 Scatter plot showing the correlation between the electron recoil angleand the electron energy for a sample of 295 events of the type shown in figure 4.1.1

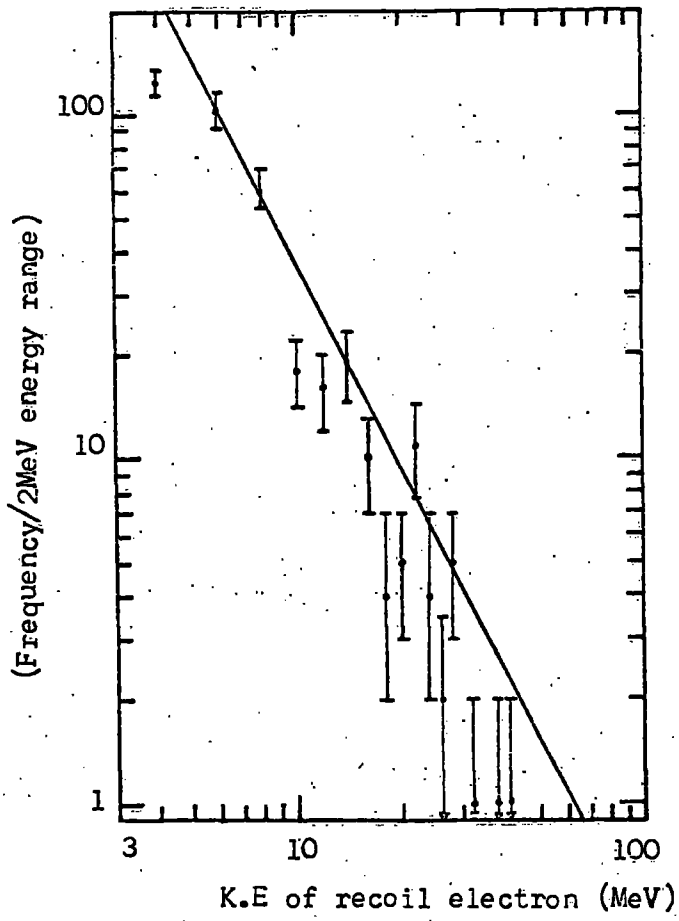

Figure 4.3 The differential energy spectrum of 388 knock on electron tracks observed in F2 and F3 on the passage of 1046 incoherent muons.

$$E' = \frac{2m_e p^2 \cos^2\alpha}{(m_e + \sqrt{p^2+m_\mu^2})^2 - p^2 \cos^2\alpha}$$

for a given primary energy. E' is a maximum when $\alpha = 0$. The maximum transferable energy for a muon of median energy 2.1 GeV is 300 MeV.

It is seen in figure 4.2 that about half the events are consistent with μe collision dynamics but that about half also lie above the curve corresponding to infinite energy muons. This can be understood in terms of the strong multiple scattering of low energy electrons in the flash tubes. At low energies 3-6 MeV, more events lie above the curve than below it and this is attributed to low energy electrons recoiling close to the forward direction not being resolvable from the track itself.

The differential energy spectrum of all the knock-on electron tracks of energy >3 MeV (3 flash tube) were observed in F2 and F3 on the passage of 1046 muons is shown in figure 4.3. The full line shows a fit corresponding to a law of the form $N(E')dE' \propto dE'/(E')^2$.

The histogram of the differential energy spectrum of the 388 knock-on electrons of energy >3 MeV were observed in F2 and F3 ($93\ g\ cm^{-2}$) is shown in figure 4.4. The dotted curve corresponds to the fit using the probability of production of a knock-on of a kinetic energy in the range E' minimum - E' maximum per single particle track.

A normalization to the theoretical curve was made at the total number of knock-on electrons observed and it may be seen that the agreement between experiment and theory is good.

A typical measured knock-on electron ejected by a single charged particle, muon, is shown in figure 4.1.1 and plate 4.1.

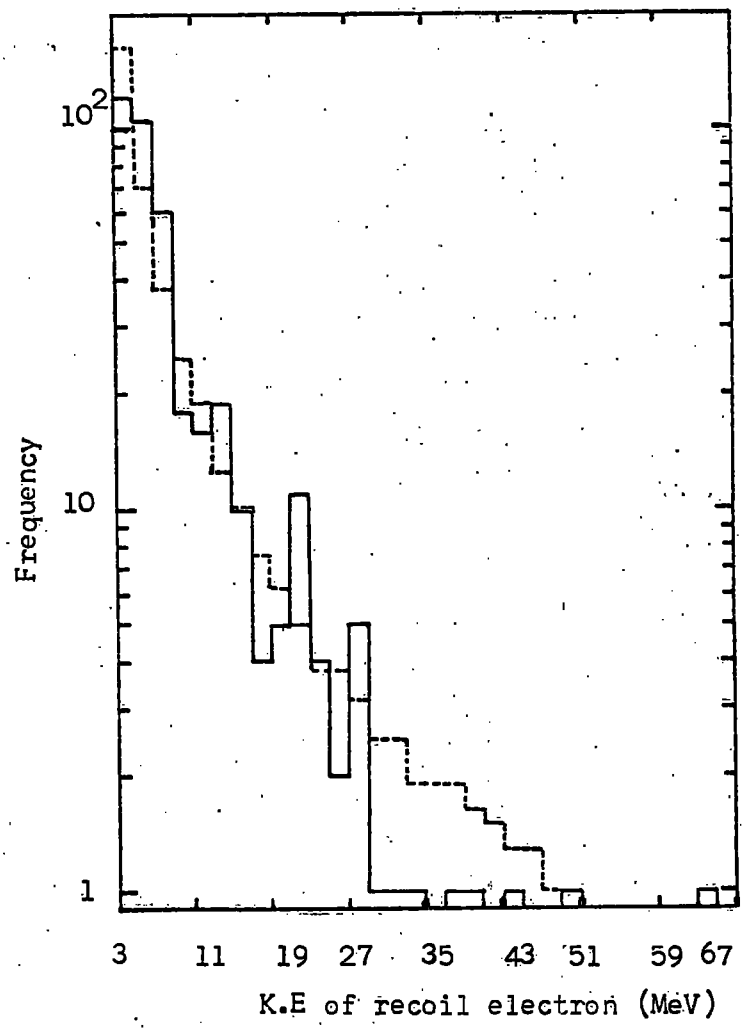

Figure 4.4 The differential energy spectrum of 388 knock-on electrons observed in the regions F2 and F3 of the chamber on the passage of 1046 incoherent muons. The dotted curve represents the theoretical fit to the probability of production of a K.O of energy between E'_{min}, and E'_{max} and assuming the primary particle is a muon of kinetic energy 3 GeV. 3 GeV is the median energy of incoherent muons traversing the chamber at the centre of F2 and F3.

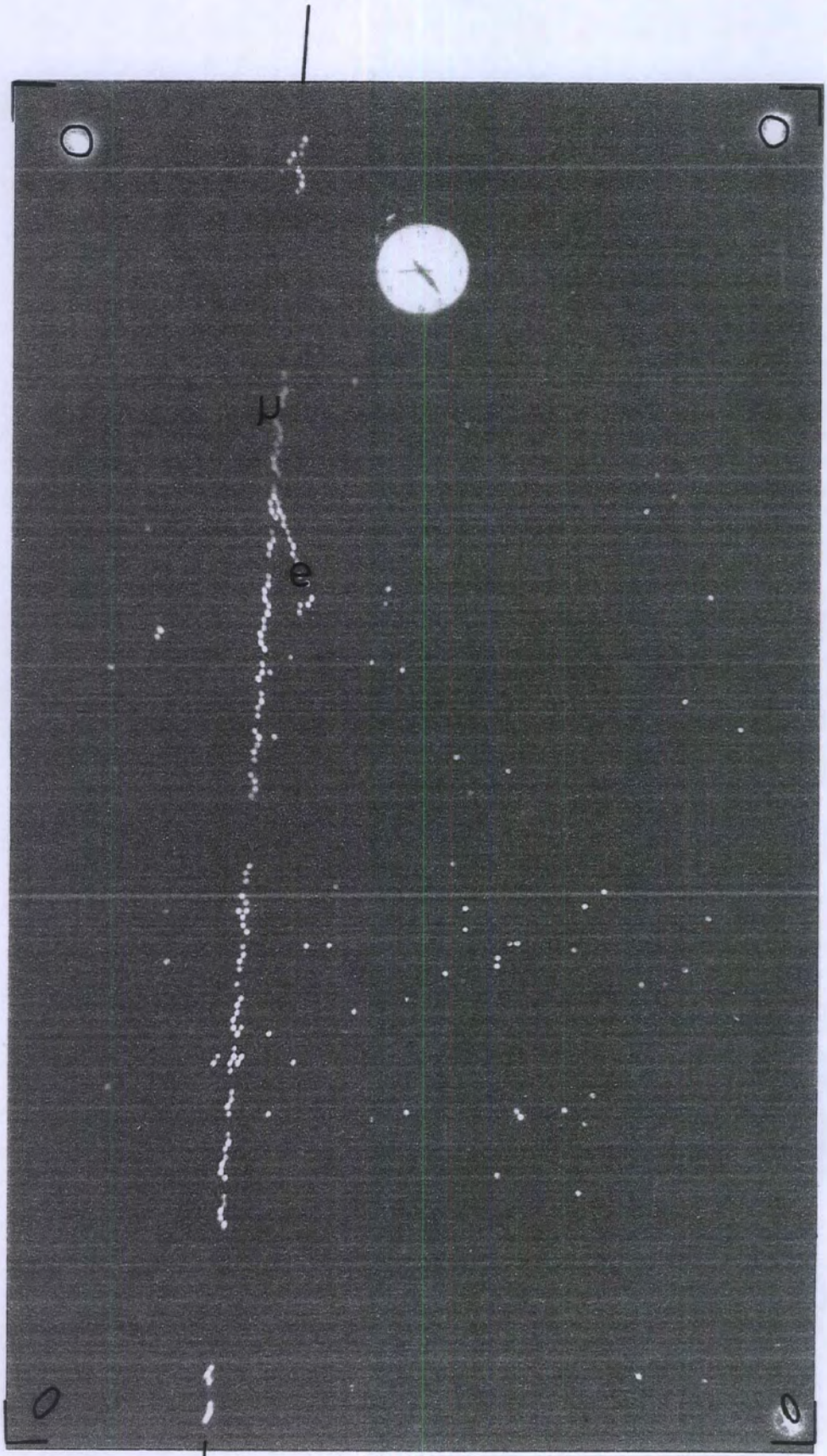

Plate 4.1 Event (C5-29)

A knock-on electron of about 22 MeV kinetic energy is produced by a single particle traversing the flash tube chamber.

4.4. The Multiply Scattered particles

It was noticed during the single particle calibration run that 6% of the observed 5,283 single calibration particles showed C - shape multiple scattering in traversing the chamber (sagitta $\Delta > 2$ cm). The events measured were of the type shown in figure 4.1.2. The sagitta Δ cm was measured as a maximum perpendicular distance from the chord formed by the line joining the points where the trajectory crossed the top of F2 and the bottom of F3 to the scattered trajectory. The integral scattering distribution for 5,283 penetrating particles in the chamber is shown in figure 4.5. The expected multiple scattering distribution of single muons was calculated assuming the rms projected angle of scatter of a particle in traversing t radiation length is: $\langle\theta\rangle = \frac{1}{\sqrt{2}} \frac{K t^{\frac{1}{2}}}{p\beta c}$, where K = 21 MeV. If ℓ is the linear distance between the top of F2 and the bottom of F3 then $\langle\Delta\rangle = \ell/8 \langle\theta\rangle$ and (Rossi 1952),

$$p(\Delta)\, d(\Delta) = \frac{1}{\sqrt{2\pi}\langle\Delta\rangle} \exp - \left(\frac{\Delta^2}{2\langle\Delta^2\rangle} \right) d\Delta$$

for a particle of a given $p\beta c$.

Identifying $p\beta c$ with the value at the center of F2 and F3 the above expression has been weighted over the momentum spectrum of muons in the middle of the chamber and capable of production coincidences and the final result which has been broadened for an rms error in measuring Δ of 1.1 cm is shown also in figure 4.5. Three events were observed during the scanning showing S-shape multiple scattering in traversing F2 and F3 with sagittas $\Delta > 1$ cm. ~~These events might be due to a large angle scattering which changed the direction of the trajectory of a C-shape multiple scattering particle.~~

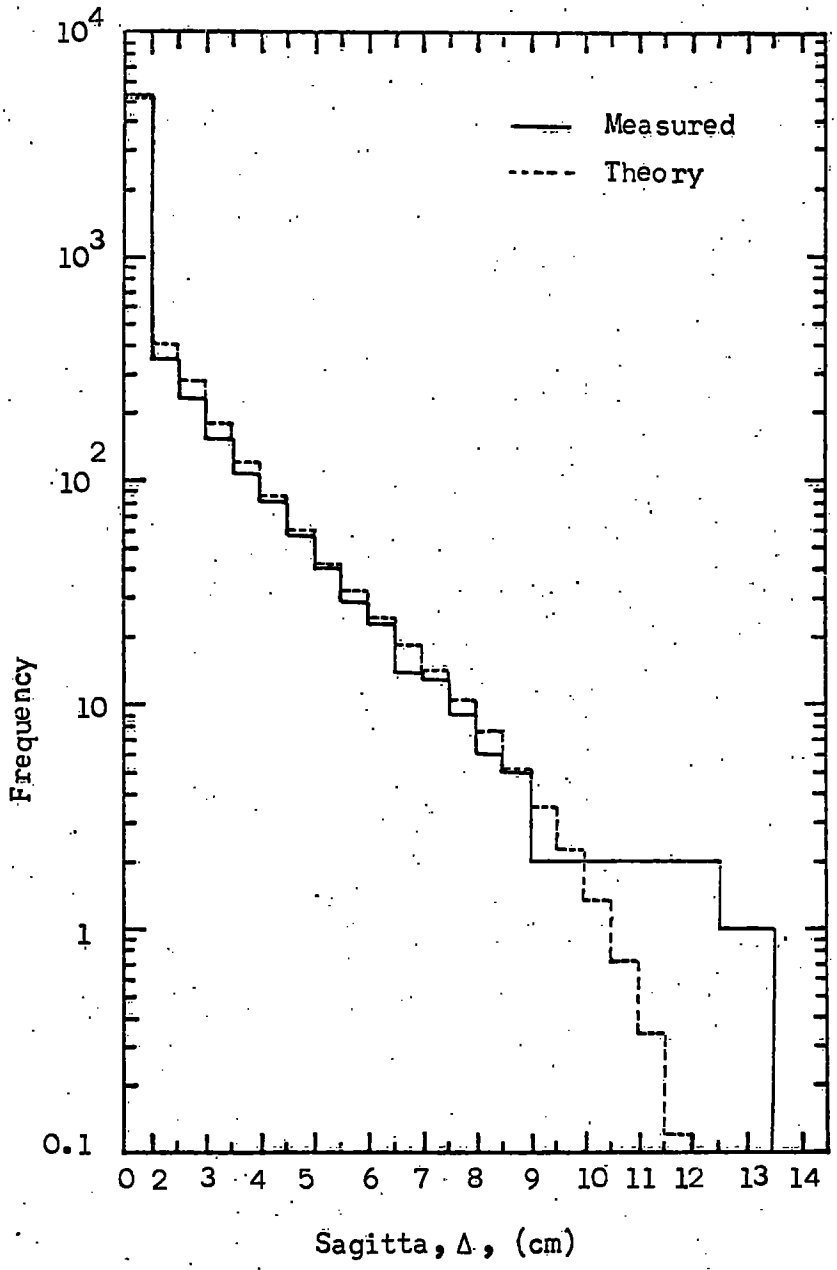

Figure 4.5 Integral scattering distribution for 5,283 penetrating particles in traversing the regions F2 and F3 of the chamber. (Note the change of scale after the first cell).

4.5 The Mass Estimation of Stopping Incoherent Particles

4.5.1. Introduction

From measuring the multiple scattering and residual ranges of the particles that stop in a flash tube chamber mass estimates of stopping particleshave been made. In a sample of 5,283 photographs of incoherent cosmic ray particles traversing the chamber, 27 photographs showed a significantly scattered stopping muon with a decay electron produced at the end of its range. The same method which has been described in section 3.6 was applied to determine the momentum at the mid point of the trajectory and the mass of the stopping particle.

4.5.2. The mass distribtuion

The scatter plot of the range R as a function of the momentum $p\beta c$ for 27 stopping single particle is shown in figure 4.6. The curves of muon, pion, kaon, and proton are calculated from Serre (1967) range-energy tables. The curves for 10 m_e and 10m_p are calculated from Rossi (1952). The maximum value of $p\beta c$ which can be measured was 710 MeV and this corresponds to a sagitta Δ cm measured (precision 1 cm) for the trajectory from the top of F2 to the bottom of F3.

Thus once $R/ p\beta c$ is measured β can be found from the curve which has been shown in figure 3.10 and M (mass) can be found:

$$Mc^2 = p\beta c\ (1 - \beta^2)^{\frac{1}{2}}/\beta^2$$

The mass distribution for the 27 scattered stopping muons in the chamber with an electron produced at the end of its range is shown in figure 4.7.

A typical μ-e decay is shown in figure 4.1.3 and plate 4.2.

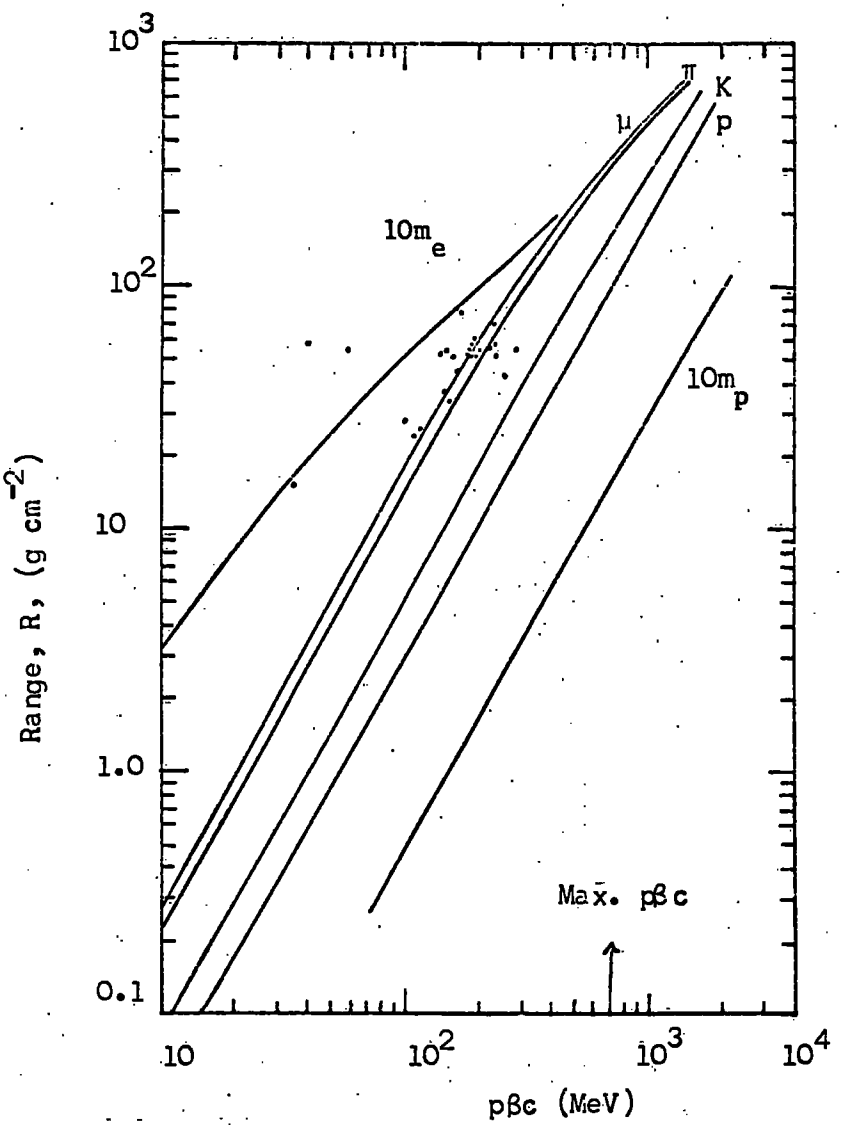

Figure 4.6 The scatter plot for 27 stopping incoherent cosmic ray particles in the flash tube chamber.

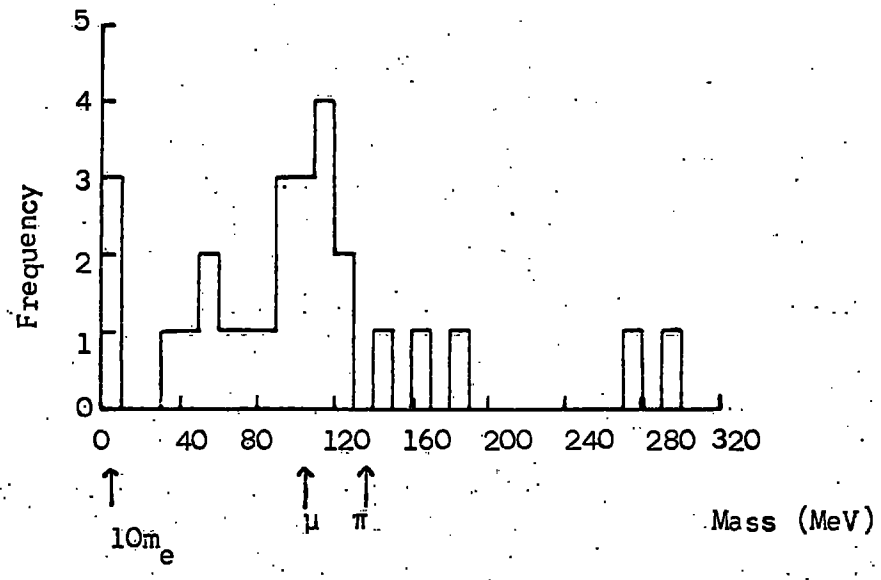

Figure 4.7 The mass distribution of 27 stopping incoherent cosmic ray particles obtained from measuring multiple scattering and residual range.

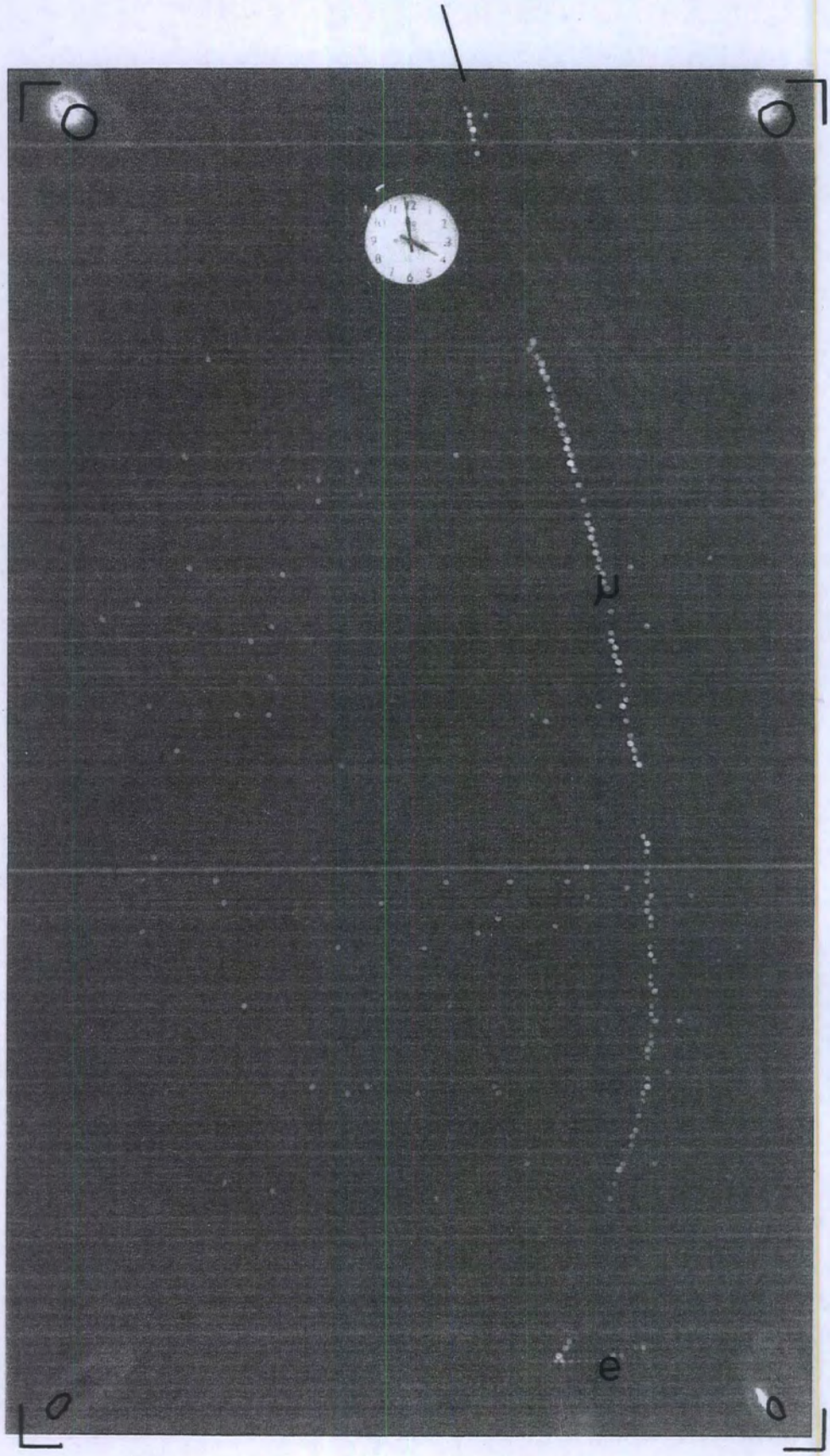

Plate 4.2 Event (C8-178)

Typical μ -e decay

4.5.3 Discussion

It is seen from the mass distribution that the most probable mass is consistent with the muon mass as expected. Of the 27 events, 4 events stopped at the bottom of F3 or $F4_A$ and the decay electron traversed scintillator B producing the necessary coincidence and the remaining 23 events stopped in either scintillator B or $F4_B$. It is noticed that fewer decay events are observed to stop at the bottom of F3 or in F4A than in scintillator B or $F4_B$ in spite of the fact that there is more stopping material at the bottom of F3 and in F4A. The reason is that a resolving time of 0.1μs for the coincidence time between A and B scintillators was used, so only 4.6% of muons stopping at the bottom of F3 and in F4A produced a decay electron in time to satisfy the coincidence requirement.

Three events were observed with low mass value $< 10m_e$. These events can be explained as due to π^+ mesons which would suffer nuclear as well as Coulomb scattering and this effect would underestimate $p\beta c$ and give a low mass value.

CHAPTER FIVE

CONCLUSION

The theory of the possible existence of three elementary particles (quarks) arose from an attempt to understand the observed multiplet structure of elementary particles. To date there is no strong positive experimental evidence for the existence of quarks and its well known that a considerable number of attempts have been made to detect the production of quarks at high energy accelerators. In cosmic rays, there is a wide variety of experimental techniques that have been used to search for quarks and of the searches so far reported, most have used the fractional charge as the identifying feature. However, some charge-independent searches have been conducted.

In this work flash tubes have been used as a visual detector to search for quarks and study the characteristics of cosmic ray particles at sea level. The flash tube depends for its operation on the ionisation left by an ionising particle. The position of the quark charges e/3, 2e/3 and the charge e particle on the ionisation curve was calculated. The experiment was run for 2,570 hours using as a master trigger EAS producing a local electron density $> 40 m^{-2}$. Two candidates were observed in the ionisation region expected for e/3 quarks and they satisfied all the conditions applied . However the most likely explanation is that they are background incoherent muons. Charge 2e/3 quarks will not be distinquished from charge e particles in the flash tube chamber.

The upper limit to the flux of e/3 quarks, based on two possible events is $< 1.4\ 10^{-11} cm^{-2} sec^{-1} st^{-1}$. Assuming a quark-nucleon inelastic

cross-section of $\frac{1}{3}$ the nucleon-nucleon inelastic cross-section the probability of a quark traversing the chamber without interacting has been calculated to be 0.165.

Taking this effect into account raises the upper limit to $<8.0.10^{-11}$ $cm^{-2}sec^{-1}st^{-1}$.

In future there is a plan to modify the chamber by increasing the number of plastic scintillators so as to cover the whole sensitive area of flash tubes. Figure 5.1. shows a side view of the flash tube chamber with this proposed modification. A previous particle indicator will be used to detect whether incoherent muons traverse the chamber sensitive volume in the 200μs period preceeding the occurrence of the master air shower trigger thus eliminating the background problem completely.

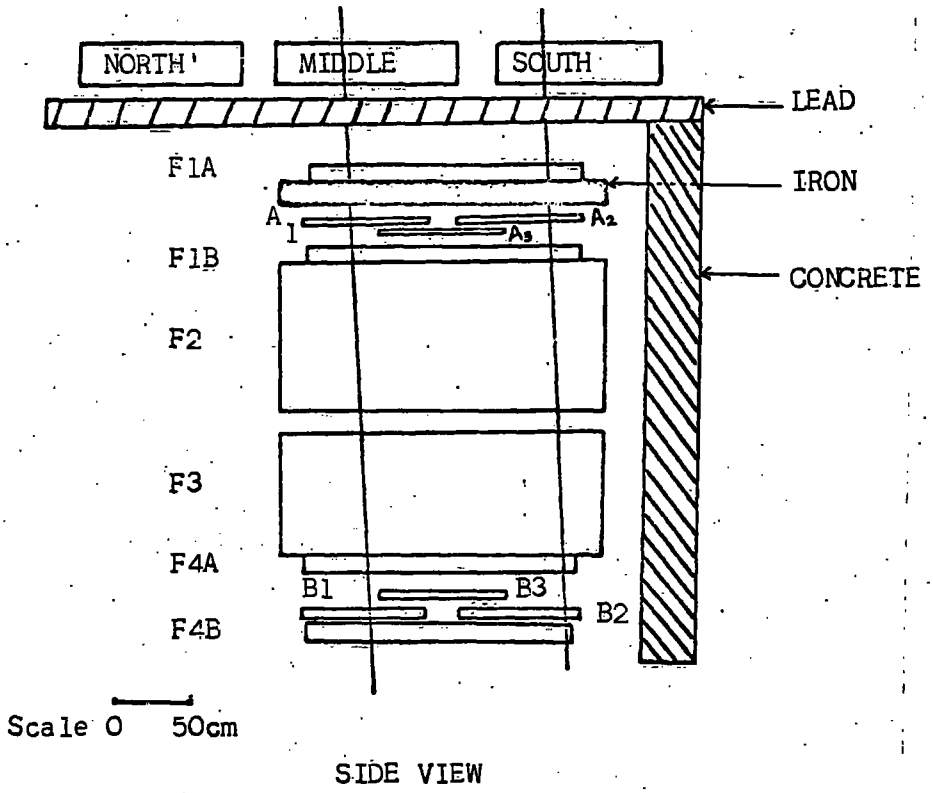

SIDE VIEW

Figure 5.1 The flash tube chamber showing the new position of scintillators A_1, A_2, A_3 and B_1, B_2, B_3. Muon showers of density $> 1\ m^{-2}$ will be selected by a twofold coincidence between, A_1 B_1 and A_2 B_2.

ACKNOWLEDGEMENTS

The author wishes to thank Professor G.D. Rochester F.R.S. for the provision of the facilities for this work, and for his interest and support.

He is particularly grateful to his supervisor, Dr. F. Ashton for his willing guidance and invaluable help through the work. The author would also like to thank Professor A.W. Wolfendale for his interest in this work, and for his freely given advice. Members of the Cosmic Ray Research Group are thanked for helpful discussion and especially Mr. D.A. Cooper and Mr. A. Parvaresh are thanked for their friendly assistance.

The technical staff of the physics department, in particular Mr. M. Lee is thanked for his willing help. The author is grateful to Mrs. D.A. Anson for her patient work in typing this thesis.

Finally, all his family and the British Council are thanked for their financial help during the work.

REFERENCES

Adair, R.K., Barge, D.A., Chu, W.T., and Leipuner, L.B., 1964, Proc. Coral Gables Conf., pp. 36-44.

Adair, R.K., and Kasha, H., 1969, Phys. Rev. Lett., 23, 1355.

Allision, W.W.M., Derrick, M., Hunt, G.P., Simpson, J.D. and Voyvodic, L., 1970, Phys. Rev. Lett., 25, 550.

Ashton, F., Coats, R.B., Holyoak, B., Simpson, D.A. and Thompson, M.G., 1965a, Nuc. Instrum. and Methods, 37, 181.

Ashton, F., Breare, J.M., Holroyd, F.W., Tsuji, K., and Wolfendale, A.W., 1971, Letter Al. Nuovo Cim., 2, 707.

Ashton, F., Cooper, D.A., Parvaresh, A., Saleh, A.J., 1973, J. Phys. A., 6, 577.

Bacry, H., Nuyts, J., and van Hove, L., 1964, Phys. Letters, 9, 279.

Bhabha, H.J., 1938, Proc. Roy. Soc. A, 164, 257.

Cairns, I., McGusker, C.B.A., Peak, L.A., and Wcolcott, R.L.S., 1969, Phys. Rev., 186, 1394.

Chu, W.T., Kim. Y.S., Beam, W.J. and Kwak, N., 1970, Phys. Rev. Lett., 24, 917.

Coxell, H. and Wolfendale, A.W., 1960, Proc. Phys. Soc., 75, 378.

Cocconi, G., 1961, Handbuch der physik, vol. XLVI/I, 215.

Dardo, M., Navarra, G., Penengo, P., and Sitte, K., 1972. Nuovo Cim., 9A, 319.

Frauenfelder, H., Kruse, U.E., and Sard, R.D., 1970, Phys. Rev. Lett., 24, 33.

Gell-Mann, M., 1964, Phys. Letters, 8, 214.

Greisen, K., 1960, Ann. Rev. Nuc. Sci., 10, 63-108.

Galbraith, W., 1958, "Extensive Air Showers" Published by Butterworths Scientific Publication.

Han. M.Y., and Nambu, Y., 1965, Phys. Rev., 139, B1006.

Jones, L., 1970 "Symmetries and Quark Model", Edited by R. Chand, Gordon and Breach.

Jones, L., 1971, Proc. Int. Conf. Cosmic Rays (Hobart), Rapporteur paper (unpublished).

Kannangara, M.L.T., and Zivkovic, M., 1953, Phil. Mag., 44, 797.

King, J., 1970, Ph.D Thesis, Durham University.

Kiraly, P. and Wolfendale, A.W., 1970, Phys. Lett., 31B, 410.

Kokkedee, J.J.J., 1969, "The Quark Model", Published by Benjamin.

Lattes, C.M.G., Muirhead, H., Occhialini, G.P.S., and Powell, C.F., 1947, Nature, 159, 694.

Lee, T.D., 1965, Nuovo Cim., 35, 933.

Lloyd, J.L., 1960, Proc. Phys. Soc., 75, 387.

Massey, H.S.W., and Corben, H.C., 1939, Proc. Camb. Phil. Soc., 35, 84.

McCusker, C.B.A., andCairns, I., 1969, Phys. Rev. Lett., 23, 658.

Oxford, Kinematical Tables, 1961, published by the National Institute for Research in Nuclear Science, Rutherford High Energy Laboratory, Harwell, Didcot, Berkshire. England.

Rahm, D.C., and Sternheimer, R.N., 1969, Brockhaven prepring, BNL 14072.

Rahm, D.C., and Louttit, R.I., 1970, Phys. Rev, Lett., 24, 279.

Rossi, B., 1952, "High Energy Particles", published by Prentice Hall.

Serre, C., 1967, CERN Report, 67-5.

Sitte, K., 1970, Supp. Nuovo Cim., 6, 866.

Tonwar, S.C., Naranan, S., and Sreekantan, B.V., 1971a, Proc. Int. Conf. Cosmic Rays, (Hobart), 3, 1171.

Wilson, J.G., 1970, Nature, 225, 1238.

Yukawa, H., 1935, Proc. Phys. Math. Soc., Japan, 17, 48.

Zwieg, G., 1964, CERN preprints TH401 and TH412, (unpublished).

APPENDIX

The Mass Ratio of Two Body Elastic Collisions in the Non-relativistic Approximation

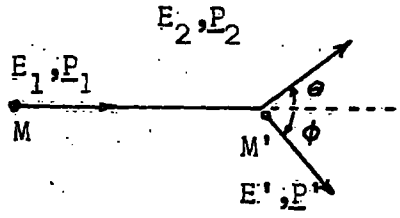

A derivation of the general formula used in section 3.5 for determining the mass ratio of two body elastic collisions in the non-relativistic approximation is given below.

Consider a particle of mass M with kinetic energy E_1 and momentum p_1 scattered through an angle θ in an elastic collision with a particle of mass M', assumed to be initially at rest, and suppose the particle recoils making an angle ϕ with respect to the incident particle direction.

Let (E_2, p_2), (E', p') be the energy and the momentum of the scattered and recoil particles respectively after the collision.

In an elastic collision the total energies and momenta of a particle will be conserved:

$$Mc^2 + E_1 = E_2 + E' \qquad (1)$$

$$\underline{p}_1 = \underline{p}_2 + \underline{p}' \qquad (2)$$

The momentum can be written in form:

$$p' \sin\phi = p_2 \sin\theta \qquad (3)$$

$$p_1 = p_2 \cos\theta + p' \cos\phi \qquad (4)$$

Assume the kinetic energy of the incident particle is $E_1 = Mc^2(\gamma-1)$ and the particle in non-relativistic region (this approximation is valid when θ is finite and measurable).

Thus equation (1) can be written:

$$\frac{p_1^2}{2M} = \frac{p_2^2}{2M} + E'$$

or $$\frac{1}{2M}(p_1-p_2)(p_1+p_2) = E' \qquad (5)$$

From equation (3) we have:

$$p_2 = \frac{p' \sin \phi}{\sin \theta} \qquad (6)$$

Substituting this into equation (4) we get:

$$p_1 = \frac{p' \sin \phi \cos \theta}{\sin \theta} + p' \cos \phi \qquad (7)$$

By simple calculation, assuming $p_1 \tilde{-} p_2$ for heavy mass particles, we obtain from equations (5), (6) and (7):

$$\frac{1}{2M}\left[p' \left(\frac{\sin \phi \cos \theta}{\sin \theta} + \cos \phi - \frac{\sin \phi}{\sin \theta} \right)\right]\left[2 \frac{p' \sin \phi}{\sin \theta}\right] = E'$$

or $$\frac{p'^2}{M}\left[\frac{\sin \phi \cos \theta}{\sin \theta} + \cos \phi - \frac{\sin \phi}{\sin \theta}\right]\left[\frac{\sin \phi}{\sin \theta}\right] = E' \qquad (8)$$

However, if the recoil particle is also non-relativistic then:

$$E' = \frac{p'^2}{2M'}$$

Substituting this into equation (8), we get:

$$\frac{M}{M'} = 2\left[\frac{\sin \phi \cos \theta}{\sin \theta} + \cos \phi - \frac{\sin \phi}{\sin \theta}\right]\left[\frac{\sin \phi}{\sin \theta}\right] \qquad (9)$$

Equation (9) shows that in the non-relativisitic approximation the ratio between the mass of incident particle and recoil particle (M/M') depends only on the scattering angle θ and the recoil angle ϕ.